INTERNATIONAL ATOMIC ENERGY AGENCY
UNITED NATIONS EDUCATIONAL, SCIENTIFIC AND CULTURAL ORGANIZATION

INTERNATIONAL CENTRE FOR THEORETICAL PHYSICS
34100 TRIESTE (ITALY) - P.O.B. 586 - MIRAMARE - STRADA COSTIERA 11 - TELEPHONE: 2240-1
CABLE: CENTRATOM - TELEX 460392 - I

H4.SMR/204 - 10

WINTER COLLEGE ON

ATOMIC AND MOLECULAR PHYSICS

(9 March - 3 April 1987)

(ANALYTICAL LASER SPECTROSCOPY 1)

Double-Resonance Fluorescence, Single-and Double-Resonance Excitation-Ionization, Ionization Yield, Diagnostic and Analytical Applications of Laser Enhanced Ionization

N. OMENETTO

Joint Research Centre
Ispra (Va), Italy

ICTP WINTER COLLEGE ON ATOMIC AND MOLECULAR PHYSICS

TRIESTE , March 1987

"ANALYTICAL LASER SPECTROSCOPY 1"

Lecturer : N. OMENETTO

Joint Research Centre

Ispra (Va) , Italy

VI.

- Double-Resonance Fluorescence
- Single- and Double-Resonance Excitation-Ionization
- Ionization Yield
- Diagnostic and Analytical Applications of Laser Enhanced Ionization

Spectrochimica Acta, Vol. 40B, Nos 10–12, pp. 1411–1422, 1985.
Printed in Great Britain.

0584-8547/85 $3.00 + .00

Laser induced double-resonance ionic fluorescence in an inductively coupled plasma

N. OMENETTO, B. W. SMITH,* L. P. HART,* P. CAVALLI and G. ROSSI
Joint Research Centre, Chemistry Division, Ispra, Varese, Italy

(*Received* 18 *April* 1985; *in revised form* 24 *June* 1985)

Abstract—Two pulsed dye lasers pumped by an excimer laser are simultaneously directed into the analytical zone of an inductively coupled argon plasma. When the two beams are tuned to the appropriate ionic transitions, highly excited ionic levels can be efficiently populated in saturated conditions, the resulting fluorescence being then spectrally isolated with a monochromator and measured. A theoretical outline of this technique, variously called double-resonance fluorescence or two-step fluorescence, is given. The experimental results obtained with the alkaline-earth metals Ca, Sr, Ba and Mg show that the technique does provide excellent sensitivity, freedom from scattering problems and unprecedented spectral selectivity. The laser characteristics, the time overlap between the pulses and the spectral characteristics of the transitions used are discussed. Finally, ionic fluorescence in the plasma is the most suitable analytical application of such double-resonance technique since its use in flame atomic fluorescence suffers from the strong depletion of the excited levels due to collisionally assisted ionization.

1. INTRODUCTION

THE LITERATURE concerning laser excited fluorescence spectroscopy in flames and plasmas describes the characteristics of the atomic or ionic fluorescence transitions obtained after selective laser excitation of one excited level which is then followed by direct radiative deactivation from that level or from collisionally populated nearby levels [1]. The excitation of the selected level is achieved with a single laser tuned at the particular transition frequency. This technique can therefore be referred to as "single-resonance atomic (ionic) fluorescence spectroscopy".

Higher excitation levels can be effectively populated when a second laser, coincident in time and space with the first one, is tuned to a transition starting from the level reached by the first laser or from collisionally populated nearby levels. In this case, the resulting fluorescence can be named "double-resonance atomic (ionic) fluorescence" or "two-step atomic (ionic) fluorescence". To our knowledge, double-resonance fluorescence has not yet been exploited analytically in flames and plasmas, but has been discussed by MIZIOLEK and WILLIS [2] in the determination of lead by electrothermal atomisation and recently by GOLDSMITH [3, 4] in the imaging of hydrogen in a laminar hydrogen–air diffusion flame. On the other hand, double-resonance (two-step excitation) schemes have been used for lifetime determinations [5] and especially in laser enhanced ionization spectroscopy [6–10] and in high resolution molecular spectroscopy [11].

This paper is dedicated to Professor V. A. Fassel.

*On leave from: Department of Chemistry, University of Florida, Gainesville, FL, U.S.A.

[1] N. OMENETTO and J. D. WINEFORDNER, *Prog. Anal. Atom. Spectrosc.* 2 (1/2) (1979).
[2] A. W. MIZIOLEK and R. J. WILLIS, *Opt. Lett.* 6, 528 (1981).
[3] J. E. M. GOLDSMITH, *Opt. Lett.* 10 (March 1985).
[4] J. E. M. GOLDSMITH and R. J. M. ANDERSON, *Appl. Opt.* 24, 607 (1985).
[5] W. GOBNIK, *Z. Physik* A283, 231 (1977).
[6] J. C. TRAVIS, G. C. TURK, J. R. DEVOE, P. K. SCHENCK and C. A. VAN DIJK, *Prog. Anal. Atom. Spectrosc.* 7, 199 (1984).
[7] G. C. TURK, J. R. DEVOE and J. C. TRAVIS, *Anal. Chem.* 54, 643 (1982).
[8] V. S. LETOKHOV in *Chemical and Biochemical Applications of Lasers*, Ed. B. MOORE. Academic Press, New York (1980).
[9] P. CAMUS, Ed., International Colloquium on Optogalvanic Spectroscopy and its Applications, *J. de Physique*, Tome 44, Colloque No. 7, Suppl. 11 (1983).
[10] N. OMENETTO, T. BERTHOUD, P. CAVALLI and G. ROSSI, *Anal. Chem.* 57, 1256 (1985).
[11] W. DEMTROEDER, *Laser Spectroscopy*, Springer Berlin (1981).

The aim of this work is to examine the analytical potential of this technique for the determination of trace elements in conventional atomizers such as flames, graphite furnaces and inductively coupled plasmas. Experimental results obtained for the alkaline-earth ions in an inductively coupled argon plasma are presented. Finally the double-resonance fluorescence technique is compared with that of single-resonance in terms of sensitivity, selectivity and interferences.

2. Theoretical Considerations

In order to illustrate the analytical potential of the double-resonance fluorescence technique, it is assumed, for the sake of simplicity, that the atom (ion) can be treated as a three level system with levels 1, 2 and 3 arranged in increasing order of energy. The first laser is tuned to transition $1 \rightarrow 2$ and the second to transition $2 \rightarrow 3$. Resonance fluorescence is then observed from level 3 down to level 2. The levels are also coupled by collisions, but collisional excitation is neglected in comparison to downwards deexcitation (quenching). In order to interact with all the absorbing atoms, the lasers are assumed to be spectrally much larger than the absorption profile of the atoms (ions) in the flame or plasma. In addition, a steplike temporal excitation function is assumed and self-absorption is absent.

By defining as R_{ij} the rate coefficients (s^{-1}) for the radiative as well as collisional coupling between levels i and j, we then have the following terms:

$$\begin{aligned} R_{12} &= B_{12}\rho_\lambda(\lambda_{12}) \\ R_{23} &= B_{23}\rho_\lambda(\lambda_{23}) \\ R_{13} &= 0 \\ R_{21} &= A_{21} + B_{21}\rho_\lambda(\lambda_{12}) + k_{21} \\ R_{32} &= A_{32} + B_{32}\rho_\lambda(\lambda_{23}) + k_{32} \\ R_{31} &= k_{31} \end{aligned} \tag{1}$$

here, B_{ij} ($J^{-1}\,cm^3\,nm\,s^{-1}$) is the Einstein coefficient for stimulated absorption ($i < j$) or emission ($i > j$), A_{ij} is the Einstein coefficient for spontaneous emission, k_{ij} is the quenching rate coefficient and $\rho_\lambda(\lambda_{ij})$ is the spatially homogeneous spectral energy density ($J\,cm^{-3}\,nm^{-1}$) of the laser.

By solving the rate equations for the population of level 3 [1], under stationary conditions, i.e. for $(dn_3/dt) = 0$, we have

$$(n_3)^{DR} = \frac{B_{12}\rho_\lambda(\lambda_{12})B_{23}\rho_\lambda(\lambda_{23})n_T}{B_{12}\rho_\lambda(\lambda_{12})B_{23}\rho_\lambda(\lambda_{23})\left(\frac{g_1+g_2+g_3}{g_3}\right) + (A_{32}+k_{32}+k_{31})} \cdot \frac{1}{\left[A_{21}+k_{21}+B_{12}\rho_\lambda(\lambda_{12})\left(1+\frac{g_1}{g_2}\right)\right] + B_{32}\rho_\lambda(\lambda_{23})\left(A_{21}+k_{21}+k_{31}\frac{g_3}{g_2}\right)} \tag{2}$$

where the superscript DR stands for double-resonance. In deriving this expression, use has been made of the relationship between the B coefficients, i.e., $B_{ij}g_i = B_{ji}g_j$.

From Eqn (2), it is easy to see that, in the limiting case where both lasers are able to saturate the transitions $1 \rightarrow 2$ and $2 \rightarrow 3$ respectively, i.e. when $B_{12}\rho_\lambda(\lambda_{12})$ and $B_{23}\rho_\lambda(\lambda_{23})$ are much greater than A's + k's, the maximum population of level 3 is reached and is given by

$$(n_3)^{DR}_{max} = n_T\left(\frac{g_3}{g_1+g_2+g_3}\right). \tag{3}$$

This result is expected because of the assumptions made, i.e. level 3 is coupled only with levels 2 and 1 and therefore no losses such as enhanced chemistry or ionization out of level 3 occur. Therefore, if the statistical weights of the three levels are the same, level 3 will share one third of the total atom (ion) population. For the single-resonance case (superscript SR), i.e. when

fluorescence at λ_{21} is measured with excitation by a single laser tuned at λ_{12} and $\rho_\lambda(\lambda_{23}) = 0$, similarly, in saturation, n_2 is given by

$$(n_2)^{SR}_{max} = n_T\left(\frac{g_2}{g_1+g_2}\right). \tag{4}$$

The maximal fluorescence radiance obtained for the single-resonance and the double-resonance excitations is given by the expressions

$$(B_F)^{SR}_{max} = (n_2)^{SR}_{max} h\nu_{21} A_{21}\left(\frac{l}{4\pi}\right) \tag{5}$$

and

$$(B_F)^{DR}_{max} = (n_3)^{DR}_{max} h\nu_{32} A_{32}\left(\frac{l}{4\pi}\right) \tag{6}$$

where l is the fluorescence depth of observation towards the detector.

The ratio of the fluorescence radiances is then

$$\frac{(B_F)^{DR}_{max}}{(B_F)^{SR}_{max}} = \left(\frac{A_{32}}{A_{21}}\right)\left(\frac{\lambda_{21}}{\lambda_{32}}\right)\left(\frac{g_3}{g_2}\right)\left(\frac{g_1+g_2}{g_1+g_2+g_3}\right). \tag{7}$$

The main outcome of Eqn (7) is that no loss of sensitivity is expected for the double-resonance fluorescence compared to the single-resonance case if both transitions are saturated, the level has a large statistical weight and a line with a high transition probability for spontaneous emission is chosen. Indeed, many highly excited levels have large A values. In addition, as pointed out by Miziolek and Willis [2], the second laser can probe an energy region where the number of states is higher and therefore many more fluorescence transitions can be selected either from the directly pumped level or from nearby levels. The single resonance fluorescence technique is already spectrally very selective. The addition of a second excitation step combined with the increased choice of fluorescence wavelengths results in unprecedented spectral selectivity.

The double-resonance fluorescence technique is subject to scattering problems in much the same way as the single-resonance technique if either laser is within the bandpass of the monochromator. In fact, scattering will be *overcome* in either technique if fluorescence is measured at a wavelength different from λ_{32} or λ_{21}, i.e. non-resonance fluorescence. Double-resonance fluorescence offers a unique and simple way of *correcting* for scattering when measuring resonance fluorescence (λ_{32}). In fact, since the signal measured at λ_{32} would essentially be zero when the first laser, tuned at λ_{12}, is not present because of the negligible thermal population of level 2, any residual signal observed in these conditions will be due only to scattering. The true fluorescence signal is then difference between the signals measured at λ_{32} with and without $\rho_\lambda(\lambda_{12})$.

In the single-resonance fluorescence technique with conventional excitation sources, the limiting noise is generally due to background emission from the atomizer [1, 12]. This also holds in the case of laser excitation provided that source induced noise can be minimized. The effect of laser intensity variations is reduced by operating under saturation conditions. Scattering noise can be eliminated by measuring non-resonance fluorescence, in which case the limiting noise is again background emission noise. The double-resonance fluorescence signal, however, can in principle be located in a spectral region where the atomizer emission noise is reduced. This was for example the case of lead [2] where fluorescence could be monitored at a wavelength substantially shorter than either one of the lasers used for excitation.

Finally, the above considerations have been made for an optically thin system i.e. in the absence of self-absorption and self-reversal. Self-absorption is absent with either technique in saturation conditions. However, it is clear that when the double-resonance fluorescence transitions terminate in a level which lies from about 2 to 4 eV above the ground state (post-

[12] H. G. C. Human, N. Omenetto, P. Cavalli and G. Rossi, *Spectrochim. Acta* 39B, 1345 (1984).

filter) self-reversal should not play any significant role. As a result, the linear dynamic range of the technique will be improved.

3. EXPERIMENTAL

The experimental set-up used in this work is schematically shown in Fig. 1. The output from an excimer laser (Lambda Physik, Model EMG-102, Göttingen, Germany) operated with XeCl at 308 nm and 10 Hz is split so to pump simultaneously two dye lasers (Jobin–Yvon, Longjumeau, France). The tunable outputs from the dye lasers are then directed with mirrors into a flame or the inductively coupled plasma. As shown in Fig. 1, a prism is used as a retroreflector for beam 1. The prism can be moved along a ~ 1.5 m optical rail. In this way, the pulse from dye laser 1 can be optically delayed in order to make it temporally coincident with that of dye laser 2. To check such coincidence a beam splitter directs both beams to a fast photodiode (Electro-optical Products Division ITT, Fort Wayne, Ind., U.S.A., Type F-4000, S-5 response, typical rise time 0.5 ns) placed near the plasma or the flame. The signals are fed into a boxcar integrator system (Stanford Research Corp., Palo Alto, California, U.S.A.) equipped with a sampling unit (SR 255, 100 ps gate width) whose output is digitized and then processed by a computer (HP Model 9816 S, Hewlett Packard, San Diego, California, U.S.A.). When the retroreflector is at the extreme positions of the rail, dye laser 1 leads or lags the other by 3.4 and 4.6 ns, respectively. The corresponding variation of the fluorescence signal did not exceed 60% of the maximum.

The air–acetylene flame was supported on a Meker type burner head fitted on a conventional premix chamber with pneumatic nebulization. The inductively coupled plasma was a standard commercial unit (Plasma-Therm, Kresson, N.J. U.S.A., Model 2500) operating at 27 MHz with a cross-flow nebulizer (Labtest, Ratingen, Germany) fed by a peristaltic pump. The fluorescence from the ICP was collected with a 1.29-m grating monochromator (Spex Model 1269 Metuchen, N.J., U.S.A.) and from the flame with a high luminosity monochromator (Model H-10, Jobin Yvon, Longjumeau, France). In both cases, a photomultiplier (Hamamatsu Corporation, Japan, Model R 9285) wired for fast response was used and the signals fed into the boxcar integrator.

The characteristics of the components have been given in detail in a previous paper [12].

4. RESULTS

4.1. *General*

There are several ways to tune the laser output in resonance with the atomic (ionic) transitions. In our case, the monochromator was set at the desired fluorescence wavelength(s) and the laser scanned across the line(s) until a signal was obtained or the single-resonance

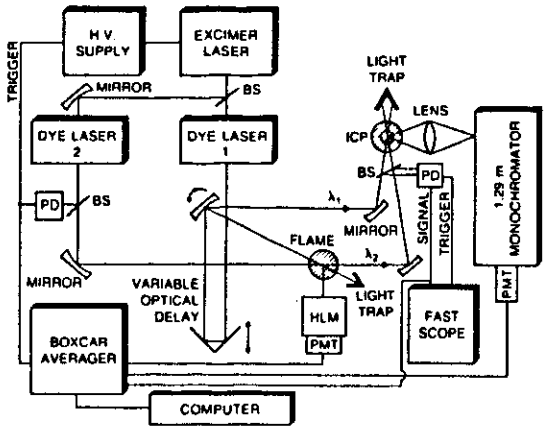

Fig. 1. Schematics of the experimental set-up used. BS: beam splitter; PD: photodiode; PMT: photomultiplier tube; HLM, high luminosity monochromator.

fluorescence resulting from the primary excitation step was monitored while scanning the second laser. This procedure is clearly illustrated in Fig. 2. Here, λ_1 is fixed and the resulting λ_F is monitored. By scanning the second laser, a decrease in the fluorescence signal will be observed whenever a transition exists at λ_2 which is resonant with a higher excitation level. The optical delay line is then varied until the maximum decrease in the single-resonance fluorescence is observed. The spatial overlapping of the two beams in the atomizer is carefully optimized by the micrometric adjustments on the mirrors.

4.2. *Double-resonance fluorescence of the alkaline-earth metals*

The elements investigated are Ca, Sr, Ba and Mg. Among these, only Mg was studied both in the flame (atomic fluorescence) and in the ICP (ionic fluorescence). For the others, only ionic fluorescence in the plasma was investigated as reported below.

4.2.1. *Calcium.* The simplified energy scheme pertinent to the calcium ion transitions investigated is illustrated in Fig. 3. The shape of the excitation pulses and their timing relationship are illustrated in Fig. 4. The duration of the pulse (FWHM) is 4 ns for the 370.603 nm line and 4.5 ns for the 396.847 line. Also, the pulses appear to have identical rise times. From the statistical weight of the levels and the values of the transition probabilities published by WIESE *et al.* [13], one can conclude that double resonance fluorescence does not offer a sensitivity advantage over the single-resonance case (see Eqn (7)). In fact, the results collected in Table 1 confirm this prediction for the wavelength pair 396.847 and 370.603 nm. Clearly, these results should be considered qualitative since the model assumes steady state conditions and a temporally constant, spatially homogeneous spectral energy density. A quantitative comparison requires detailed treatment of the temporal and spatial spectrum characteristics.

Even with laser energies of few hundreds microjoules, a non linear behavior of the

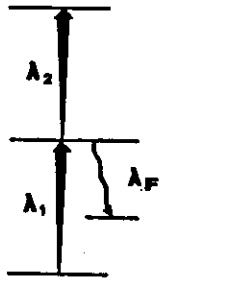

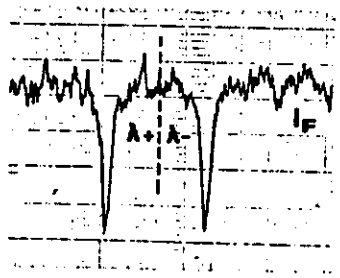

Fig. 2. Recorder tracing of the decrease (~ 35%) in the single resonance fluorescence signal (I_F) indicated in the figure as the second laser (λ_2) is scanned in forward ($\lambda+$) and backwards ($\lambda-$) directions.

[13] W. L. WIESE, M. W. SMITH and B. M. MILES, *Atomic Transition Probabilities*, Vol. II, *Sodium through Calcium*. NSRDS-NBS 2., Washington, D.C. (1969).

Ca II

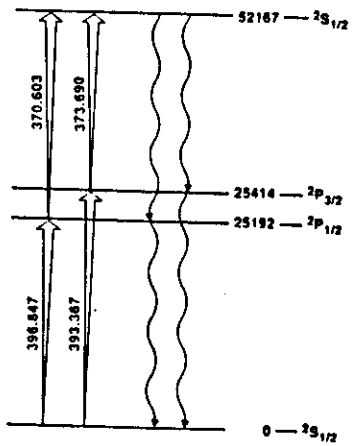

Fig. 3. Simplified partial energy level diagram for the calcium ion transitions investigated in this work. The energy of each level (in cm^{-1}) is also indicated.

Ca II

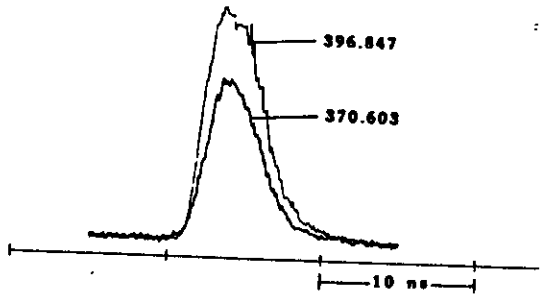

Fig. 4. Experimental laser pulse shapes and their timing relationship for the excitation of calcium fluorescence.

fluorescence signal versus laser energies at either λ_1 or λ_2 could be observed because of the high quantum efficiency of the ICP. Similar results were obtained with the other pair of transitions at 393.367 and 373.690 nm. Figure 5 shows an excitation spectrum obtained by keeping one laser fixed at λ_{23}, i.e. 370.603 nm, and scanning the lower transition (λ_{12}) while the fluorescence wavelength was monitored at 373.690 nm (see Fig. 3). The resonance transition at 396.847 nm gives a stronger signal compared to that at 393.367 since it reaches the $^2P_{1/2}$ level which is directly coupled with the second excitation step (370.603 nm). This Figure illustrates the versatility and selectivity of the technique and also the signal-to-noise ratio obtained at the 10 ng/ml level.

Table 1. Single-resonance and double-resonance fluorescence signals for 1 μg/ml of calcium*

Excitation wavelength (nm)	Laser† energy (μJ/pulse)	Fluorescence wavelength (nm)	Fluorescence signal (arbitrary units)	DR/SR ratio‖ calculated	DR/SR ratio‖ found
396.847	158	396.847	28		
		370.603	N.D.‡		
		373.690	N.D.		
370.603	136	370.603	N.D.		
		373.690	N.D.		
396.847 + 370.603		370.603	8	0.41	0.28
		373.690	15	0.80	0.53

*ICP conditions: 850 W, 25 mm above coil. The signals are not corrected for the response of the monochromator/detector.
†Measured at the ICP.
‡ND = not detectable.
‖Double-resonance/single-resonance ratio. Calculated values obtained from Eqn (7). The transition probability values were taken from WIESE *et al.* [13].

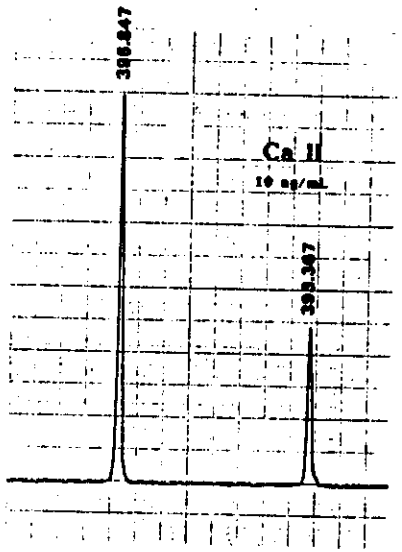

Fig. 5. Double-resonance fluorescence excitation spectrum of calcium ion. Fluorescence monochromator set at 373.690 nm. One laser wavelength is fixed at 370.603 nm while the other laser is scanned.

4.2.2. *Strontium and barium.* Figures 6 and 7 show the energy levels for the strontium and barium ions with the laser excitation transitions used and the fluorescence lines measured. The trend is similar to that observed for the calcium ion. In the case of strontium (Fig. 6), collisional population of the "S" level, situated approx. 0.7 eV above the level reached with the second laser, resulted in the emission of a weak fluorescence signal at 346.446 nm. This signal was however 2% of that obtained at 430.545 nm and ~4% of that at 416.180 nm.

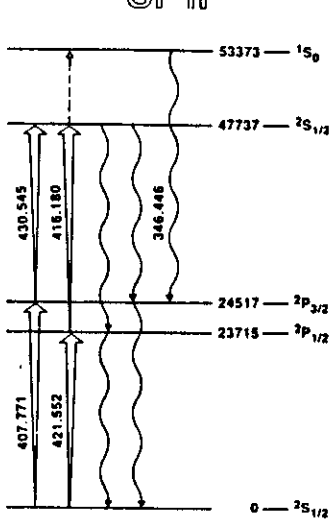

Fig. 6. Simplified partial energy level diagram for the strontium ion transitions investigated in this work. The energy of each level (in cm^{-1}) is also indicated.

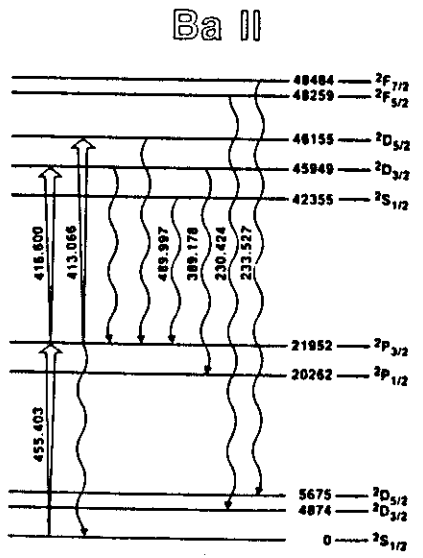

Fig. 7. Simplified partial energy level diagram for the barium ion transitions investigated in this work. The energy of each level (in cm^{-1}) is also indicated.

In the case of barium (Fig. 7) the double-resonance signals at 413.066 and 389.178 nm were 1.3 times and 0.5 times the single-resonance signal at 455.403 nm. The signal at 489.997 nm was 0.33 times that at 455.403 nm. Ultraviolet fluorescence from the collisionally assisted F levels was 1–2% of the signal at 413.066.

4.2.3. *Magnesium.* With this element, both atomic fluorescence in the flame and ionic fluorescence in the plasma were studied. One important advantage of double-resonance excitation is that it allows one to reach energy levels normally unaccessible to thermal excitation in the flame. This opens the way to the evaluation of excited state dynamics, which is important in combustion diagnostics. On the other hand, from an analytical point of view, atomic fluorescence might be less attractive because of the potential ionization losses from the excited level. This important consideration can now be pointed out with reference to Fig. 8. In this figure, two double-resonance excitation schemes are shown. In scheme A, the level reached by radiative pumping lies 1.893 eV below the ionization potential of the atom while in scheme B the final excited level is 0.665 eV below the ionization level. Assuming that thermal ionization proceeds via a single level collision, it can be calculated that the probability of loosing atoms from the pumped level to the ionization continuum is more than two orders of magnitude larger in case B when compared with scheme A [6]. Consequently, the double-resonance fluorescence signal can be much larger with scheme A. This prediction was clearly borne out experimentally by comparing the fluorescence monitored at ~ 383 nm with that monitored at ~ 278 nm. The former fluorescence signal was about one order of magnitude larger, despite the fact that the spontaneous transition probabilities for the lines of scheme B are similar to those pertinent to the lines of scheme A [13].

On the basis of these theoretical considerations and of the experimental results obtained for magnesium, double-resonance atomic fluorescence in flames will very often suffer from ionization losses, which will be more severe the nearer the final excitation level is to the ionization continuum. In the double-resonance ionic fluorescence in the ICP, however, the second ionization potential of the ion is usually much larger than the energy of the excited level reached by the simultaneous radiative pumping and the fluorescence technique can therefore be fully exploited. This is shown in the energy level diagram of the magnesium ion reported in Fig. 9. Here, the excitation process reaches a level which lies 6.2 eV below the ionization potential of the ion.

4.2.4. *Detection limits in aqueous solutions in the ICP.* Table 2 collects the detection limits obtained for the four elements, together with the transitions used and the laser energies measured at the plasma location. In all cases the fluorescence signal was monitored at a wavelength different from the second pumping transition. (In the conventional fluorescence terminology fluorescence at a wavelength different from that absorbed is generally called non resonance fluorescence. Here, instead of the rather confusing name "double-resonance non-resonance fluorescence", the terminology "two-step non-resonance fluorescence" seems more appropriate). Therefore, scattering problems due to the second laser are overcome.

The detection limits are similar to those obtained with the single-resonance technique [1], since the limiting noise was essentially the same in both cases and was due to the ICP emission background.

It is worth noting that this experimental system was designed primarily for diagnostics studies in the ICP by laser induced fluorescence [14]. Here, the spatial resolution required was achieved by making both laser beams parallel with folding mirrors and then focussing both beams into the plasma with a single lens. Therefore, for analytical purposes, this system, which uses 5 mirrors and 4 apertures can be greatly simplified with the result that higher laser powers (closer approach to saturation) and lower detection limits can be obtained.

4.2.5. *Spectral selectivity.* The spectral selectivity of the double-resonance fluorescence is demonstrated using the well known Cd/As interference. As shown in Fig. 10, arsenic atoms in the thermally populated level (1.35 eV above the ground state) absorb the radiation at 288.812 nm which differs by 0.01 nm from the wavelength of the resonance line of cadmium. Because of the relatively large spectral bandwidth of our laser (~ 0.02 nm) and the significant

[14] N. OMENETTO, Lecture given at the Winter Conference on Plasma Spectrochemistry, Leysin, Switzerland (January 1985), to be submitted for publication.

Table 2. Detection limits (ng/ml) for aqueous solutions of Ca, Sr, Ba and Mg obtained by double-resonance ionic fluorescence

Element	Excitation transitions (nm)	Laser energy (μJ/pulse)	Fluorescence transition (nm)	Detection* limit (S/N = 2)
Ca	λ_1 = 396.847	158	373.690	0.007
	λ_2 = 370.603	136		
Sr	λ_1 = 407.771	140	416.180	1
	λ_2 = 430.545	260		
Ba	λ_1 = 455.403	340	389.178	1
	λ_2 = 416.600	360		
Mg†	λ_1 = 279.553	23	279.079	0.05
	λ_2 = 279.806	12		

*ICP conditions: 850 W, 25 mm above load coil. Fluorescence monochromator slit width adjusted to isolate the transition indicated in the Table. Laser repetition frequency: 10 Hz. For all elements, 10 pulses were averaged by the boxcar integrator.

†Frequency doubling, with ~ 10% conversion efficiency, was used.

population of the arsenic absorbing level in the ICP, both atomic species are excited and fluorescence then results at the same wavelength. Since cadmium has only this resonance fluorescence line, its determination at trace levels in the presence of significant amounts of arsenic is plagued by spectral interference. For our experimental conditions, 1000 μg/ml of arsenic in the solution gave a signal equivalent to 0.66 μg/ml of cadmium. Figure 10 illustrates how double-resonance excitation can be used to completely overcome this interference. Here,

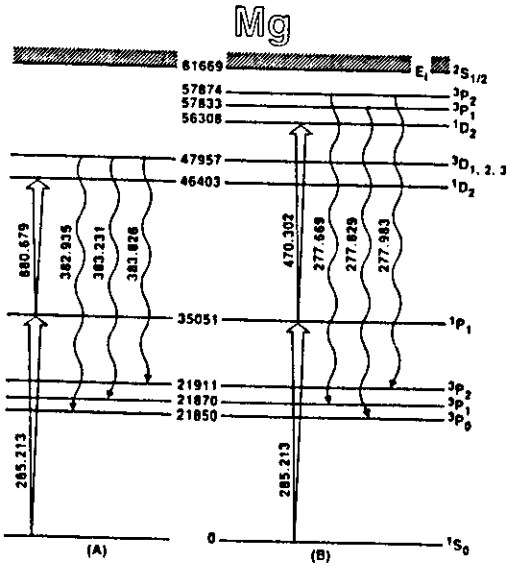

Fig. 8. Simplified partial energy level for the magnesium atom. (A) and (B) represent two different excitation schemes intended to demonstrate the different ionization losses occurring (see text for discussion).

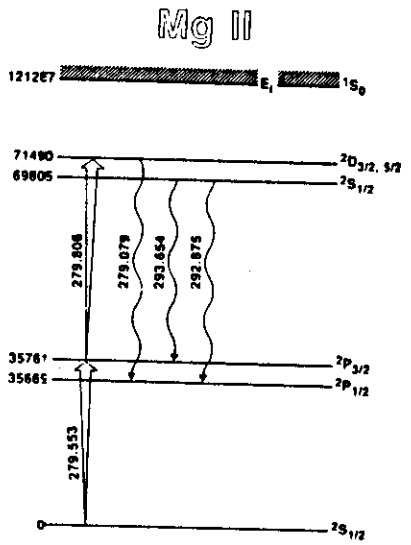

Fig. 9. Simplified partial energy level diagram for the magnesium ion transitions investigated in this work. The energy of each level (in cm^{-1}) is also indicated.

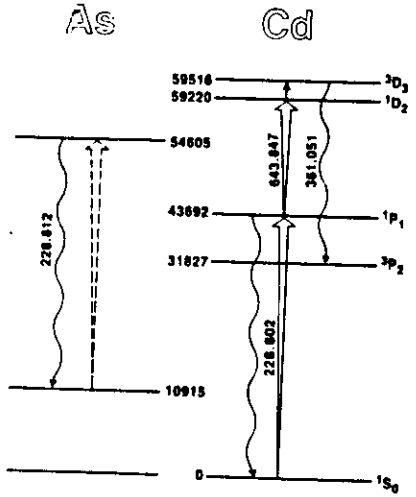

Fig. 10. Simplified energy level schemes pertinent to the description of the spectral interference As/Cd. In the cadmium scheme the two laser excitation wavelengths and the monitored fluorescence wavelength are indicated. The energy of each level (in cm^{-1}) is also indicated.

the cadmium fluorescence is measured at 361.051 nm after radiative excitation by two lasers to the $^1D_2$ level and collisional excitation to the fluorescing $^3D_3$ level. In this way, 1000 μg/ml of arsenic had no detectable effect on the fluorescence signal of 1 μg/ml of Cd.

5. Conclusions

The main purpose of the research described in this paper was to examine some features of the technique of double-resonance or two-step fluorescence in an inductively coupled plasma. Although the number of elements investigated was rather limited, it is felt that some considerations can be summarized as follows:

(i) The double-resonance fluorescence technique can indeed result in a viable analytical technique, the more so if both absorption transitions are saturated, a level of high statistical weight is reached and the transition probability of the resulting fluorescence line is high, and the ionization limit is well-removed from the highest laser-populated state (see (iv)).

(ii) Compared with the conventional single-resonance fluorescence technique, the new technique offers higher spectral selectivity and a larger choice of fluorescence transitions. If the conditions outlined in item (i) are met, then it may also provide better signal-to-noise ratios and therefore better detection limits.

(iii) In contrast with the conventional single-resonance fluorescence, the new technique offers a unique way of correcting any scattering signal, if present, by simply blocking the first excitation transition. Scattering noise, of course, will still be present. To overcome the scatter, a two-step non resonance fluorescence line can be measured in the same way as in the single-resonance technique.

(iv) Double-resonance atomic fluorescence in a flame atomizer is not expected to be a generally applicable sensitive analytical tool due to the unavoidable ionization losses which proceeds very rapidly by collisions from the excited level. This loss will be more pronounced the nearer the final level is to the ionization continuum. Indeed, two-step ionization spectroscopy in flames is capable of extremely high detection sensitivities [6–10, 15].

(v) In view of the considerations outlined in item (iv), a much better analytical approach is to use double-resonance ionic fluorescence in an inductively coupled plasma, due to the large value of the ionization potential of the ion (sometimes just referred to as the second ionization potential).

(vi) For diagnostic purposes, the new technique offers the possibility of monitoring high lying states, which are not accessible in conventional emission spectroscopy and offers high spatial resolution due to fact that the signal is generated only at the intersection of the two laser beams

(vii) The technique is obviously complex since two lasers are needed and care is required in order to achieve temporal as well as spatial coincidence of the two beams in the atomizer.

Acknowledgements—B. W. SMITH and L. P. HART would like to thank the Joint Research Centre authorities and in particular the Education Training Service for the grant of visiting scientist fellowships.

[15] L. P. HART, B. W. SMITH and N. OMENETTO, *Spectrochim. Acta B*, in press.

Laser induced fluorescence and ionization spectroscopy: Theoretical and analytical considerations for pulsed sources*

N. Omenetto, B. W. Smith, and L. P. Hart****

Commission of the European Communities, Joint Research Centre – Ispra Establishment, Chemistry Division, I-21020 Ispra (VA), Italy

Laserinduzierte Fluorescenz- und Ionisationsspektroskopie: Theoretische und analytische Betrachtungen über gepulste Quellen

Zusammenfassung. Es werden verschiedene theoretische Betrachtungen über die Einfach- und Doppelresonanzverfahren der Fluorescenz- und Ionisationsspektroskopie in Flammen und Plasmen (über Ein- bzw. Stufenprozeß) mit Anregung durch gepulste durchstimmbare Farbstofflaser vorgestellt. Für Laserimpulse von mehreren Nanosekunden Dauer kann die Einstufenanregung (Laseranregung mit nachfolgender Stoßionisation) vom analytischen Standpunkt durchaus nützlich sein, auch wenn die Ionisierungsausbeuten aufgrund der kurzen Bestrahlungszeit gering sind. Der Wirkungsgrad der Ionisierung kann beträchtlich erhöht werden, wenn zwei Laser, die auf miteinander gekoppelte atomare Übergänge abgestimmt wurden, in der Atomisierungszelle räumlich und zeitlich zusammentreffen; hierdurch wird das Verfahren äußerst empfindlich, bis in den pg/ml-Bereich.

Die Einbußen, die die Atomfluorescenz aufgrund solcher Ionisationsprozesse erleidet, sind dabei um so größer, je näher der angeregte Endzustand zum Ionisationskontinuum liegt. Wie weiterhin gezeigt wird, ist es für eine hohe Empfindlichkeit zweckmäßiger, Doppelresonanz-Ionenfluorescenz in einem induktiv gekoppelten Plasma anzuregen. Die experimentellen Ergebnisse wurden mit einem Excimerlaser (XeCl) erhalten, der gleichzeitig zwei Farbstofflaser pumpte. Fluorescenz- und Ionisationsverfahren werden auch im Hinblick auf mögliche Interferenzen verglichen, die bei der Analyse realer Proben zu erwarten sind.

Summary. Several theoretical considerations are presented for the single resonance (single step) and double resonance (double step) techniques of fluorescence and ionization spectroscopy in flames and plasmas with tunable pulsed dye laser excitation. For short (several nanoseconds) laser pulses, single step excitation with one laser beam followed by collisional ionization can be useful from an analytical point of view even though ionization yields are low because of the short irradiation time. When two lasers, tuned to two connected atomic transitions, are spatially and temporally coincident in the atom cell, the ionization efficiency is greatly enhanced making the technique extremely sensitive, down to pg/ml levels. Atomic fluorescence suffers from losses due to such enhanced ionization process, the losses being more severe the closer the final excited level is to the ionization continuum. It is then shown that double resonance ionic fluorescence in an inductively coupled plasma is more suitable if high sensitivity needs to be achieved. The experimental results were obtained with an excimer laser (XeCl) which simultaneously pumped two dye lasers. The fluorescence and ionization techniques are also compared in terms of the potential interferences expected in the analysis of real samples.

1. Introduction

When a pulsed, tunable dye laser traversing a flame or a plasma, is tuned to an appropriate atomic transition, efficient excitation occurs in a time scale which can be essentially given by the reciprocal of the product of the Einstein coefficient of stimulated absorption and the spectral energy density of the laser field, considered to be a quasicontinuum since its spectral width exceeds the width of the atomic absorption profile [1, 22]. The fate of the excited atoms can be described by several pathways, namely:

i) radiative deexcitation (fluorescence);

ii) downwards collisional deexcitation (quenching);

iii) upwards collisional excitation including ionization; and

iv) chemical reactions.

Because of the high spectral energy density of the laser beam, the population of the excited state is greatly enhanced with respect to the thermal population existing prior to irradiation by the laser; indeed, if the laser spectral energy density is sufficiently high, the transition will be satured, i.e. the populations of the two levels will be locked together in the ratio of their respective degeneracies [1, 22].

The relative importance of the above deexcitation processes depends upon many parameters including the probability of spontaneous emission from the level considered, the type of collision partners in the flame or plasma which greatly affects the quenching process and the energy difference between the excited level and the ionization continuum (the activation energy) which has a very high influence on the probability of collisional ionization [32].

When two laser beams tuned at two different absorption transitions are made spatially and temporally coincident in the flame or plasma, high lying atomic levels can be

* This paper is an extension of the lecture given by one of the authors (N.O.) at the XXIV. Colloquium Spectroscopicum Internationale

** *On leave from:* Department of Chemistry, University of Florida, Gainesville, Florida 32611, USA

Offprint requests to: N. Omenetto

Fresenius Z Anal Chem (1986) 324 : 60 – 69
© Springer-Verlag 1986

efficiently populated. Fluorescence resulting from the directly pumped level or from collisionally coupled levels can then result and can be utilized for analytical purposes. The activation energy, however, decreases considerably, thereby enhancing the probability of atom losses due to collisionally assisted ionization. The resulting ionization signal can, therefore, be monitored with a corresponding increase in the detection sensitivity.

A large body of literature exists describing the basic principles and the experimental apparatus of the fluorescence and the ionization techniques; the reader is referred to the articles by Omenetto and Winefordner [22] reviewing atomic fluorescence spectroscopy, by Travis et al. [32] for laser enhanced ionization in flames and to the monography by Camus [6] dealing with a more general approach to ionization spectroscopy.

In the scientific literature dealing with the subject of ionization spectroscopy in flames, many papers have appeared in the past few years, from the NBS group as well as from other research teams, describing in detail several theoretical and experimental aspects of the technique [2, 4, 8, 9, 12, 13, 15–18, 32, 40, 41]. A major effort was directed towards the understanding of the (complex) electrical field distribution and the mechanism of electron/ion collection, towards the study of the electron pulse shape, towards the assessment of the so-called electrical interferences and towards the evaluation of various electrode shapes and positions in the flame. The mechanism of electron/ion formation following single-step and two-step laser excitation has also been described, although to a minor extent compared with the above mentioned studies.

The ionization counterpart of fluorescence following two-step excitation has been shown to be very sensitive and selective, but the two-step excited atomic fluorescence technique has not yet received much attention in the analytical literature, apart from a study on lead atomized in a graphite furnace [21] and an experimental mapping of the hydrogen spatial distribution in a laminar air-hydrogen diffusion flame [11].

In our laboratory the fluorescence and the ionization techniques have been used for diagnostic and analytical purposes. Single-step excitation and two-step excitation provided by two pulsed tunable dye lasers were utilized. In the application of the ionization technique, advantage was taken of the excellent work carried out by the research team of the National Bureau of Standards [26–39] where the extremely high analytical potential of the technique was first sensed and subsequently demonstrated experimentally.

The aim of this paper is twofold. Firstly, it gives an extensive but rather simple theoretical evaluation of the primary excitation mechanisms leading to the ionization of the metal atoms in flames, showing the competition between the fluorescence and the ionization processes. Only pulsed laser excitation is considered and single-step excitation is compared with two-step excitation in terms of the expected ionization yields. Secondly, several experimental results are discussed for the ionization and fluorescence in an air acetylene flame and in an inductively coupled argon plasma and the two techniques are compared for potential interferences.

Some of the conclusions derived here are indeed identical to those already stressed by Travis et al. [32] when similar assumptions hold. It is felt that the systematic approach followed here, which considers one and two lasers for the excitation and both linearity and saturation for the interaction process between the radiation field and the atoms, will be on the one hand useful for the non-initiated readers and on the other hand will help elucidating the different roles played by the various parameters in a unified manner.

2. Theoretical considerations

As shown in Fig. 1, six levels are indicated. Among these, one is the ionization continuum and two, labelled as 2′ and 3′, are not directly coupled with the laser field, and can be considered as losses for the overall upwards radiative plus collisional ionization process. The time-dependent population of each level is found by solving a system of five differential equations, which can be done numerically with a computer. However, it is possible to reduce the number of levels to three, as explained below, and thereby obtain a relatively simple relationship for the population of the levels and, more importantly, an expression showing the role played by the predominant parameters in the fluorescence and ionization processes. The rate equations approach is considered to be valid here since it is assumed that the relaxation rates in atmospheric pressure atomizers are very fast and, in addition, the excitation field is far from being monochromatic, which further relaxes the need to consider coherence effects [1, 22]. Nevertheless, the outcome should not be trusted for extremely short irradiation times, i.e. much less than a nanosecond.

The collisional and radiative rate coefficients (s^{-1}) between lower (l) and upper (u) levels are indicated as k_{lu}, $B_{lu}\varrho_\lambda(\lambda_{lu})$, $B_{ul}\varrho_\lambda(\lambda_{lu})$, k_{ul}, A_{ul}, B_{lu}, B_{ul} and A_{ul} are the Einstein coefficients of stimulated absorption, emission, and spontaneous emission, respectively, and $\varrho_\lambda(\lambda)$ is the spectral energy density of the laser. The laser is assumed to be a spectral continuum with regard to the atomic absorption profile and its temporal behaviour is idealized as having a rectangular shape, of duration Δt_l. Also, the irradiance of the beam is taken to be spatially homogeneous and the atomic population density is low so that radiation trapping does not need to be considered. Finally, because of the short laser pulses considered here, neither enhanced chemical reactions nor recombination between the ions and the electrons are considered, there processes occurring in a time scale much longer than 5–10 ns. Recombination was not considered by Axner et al. [2] in their steady-state derivation. Also, multiphoton ionization processes are not considered to play a major role and are disregarded, as well as thermal ionization from the ground state.

2.1 Single step excitation — collisional ionization

In this case, only one laser beam, tuned at $\lambda_{1\to 2}$ is present and collisions must then transfer the atoms from the excited level 2 to the ionization continuum. The three levels considered here are, therefore, level 1, level 2 and the continuum, with number densities (cm^{-3}) n_1, n_2 and n_i, with $n_1 + n_2 + n_i = n_T$, the total atomic population.

The rate equations are:

$$\frac{dn_i}{dt} = R_{2i}n_2 \tag{1a}$$

$$\frac{dn_2}{dt} = R_{12}n_1 - n_2(R_{2i} + R_{21}) \tag{1b}$$

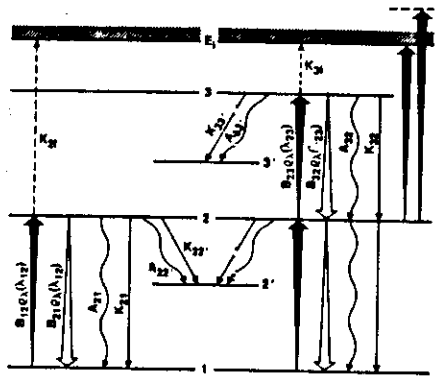

Fig. 1. Simplified picture of the various excitation-ionization processes described in the text. The levels are coupled by radiation and collisions, as indicated. E_i represents the ionization continuum. Refer to the text for the explanation of the symbols used

where

$$R_{12} = B_{12}\varrho_\lambda(\lambda_{12}) + k_{12} \tag{2a}$$

$$R_{2i} = k_{2i} \tag{2b}$$

$$R_{21} = A_{21} + k_{21} + B_{21}\varrho_\lambda(\lambda_{12}). \tag{2c}$$

Expressing n_i in Eq. (1b) as a function of n_T and using standard methods for the solution of differential equations, with D being the differential operator, we get

$$(D + R_{12} + R_{2i} + R_{21})n_2 = R_{12}n_T - R_{12}n_i \tag{3a}$$

$$\frac{Dn_i}{R_{2i}} = n_2 \tag{3b}$$

$$n_i[D^2 + D(R_{12} + R_{2i} + R_{21}) + R_{12}R_{2i}] = R_{12}R_{2i}n_T. \tag{3c}$$

The quadratic equation in D can be solved giving the roots

$$D = \frac{-X \pm \sqrt{X^2 - 4Y}}{2} \tag{4a}$$

where

$$X \equiv R_{12} + R_{21} + R_{2i} \tag{4b}$$

$$Y \equiv R_{12}R_{2i}. \tag{4c}$$

The general solution for $n_i(t)$ is then given by

$$n_i(t) = C_1e^{-\alpha_1 t} + C_2e^{-\alpha_2 t} + C_0 \tag{5a}$$

where C_1, C_2 and C_0 are integration constants and

$$\alpha_2 = \frac{X - \sqrt{X^2 - 4Y}}{2} \tag{5b}$$

$$\alpha_3 = \frac{X + \sqrt{X^2 - 4Y}}{2}. \tag{5c}$$

An expression can, therefore, be written for $n_2(t)$, by using Eqs. (3b) and (5a), as follows

$$n_2(t) = -\frac{1}{R_{2i}}(\alpha_2C_1e^{-\alpha_2 t} + \alpha_3C_2e^{-\alpha_3 t}). \tag{6}$$

With the boundary conditions that $n_i(t) = n_2(t) = 0$ for $t = 0$, we have that $C_1 + C_2 = -C_0$ and therefore, after some simple algebra,

$$C_1 = C_0\frac{\alpha_3}{\alpha_2 - \alpha_3} \tag{7a}$$

$$C_2 = -C_0\frac{\alpha_2}{\alpha_2 - \alpha_3} \tag{7c}$$

and

$$C_0 = n_T. \tag{7c}$$

Equation (7c) is the trivial solution of the differential equation or the steady-state value reached when t grows to infinity [and $D = 0$ in Eq. (3c)]. The final expressions for the time behaviour of n_i and n_2 are

$$n_i(t) = n_T\left(1 + \frac{\alpha_3}{\alpha_2 - \alpha_3}e^{-\alpha_2 t} - \frac{\alpha_2}{\alpha_2 - \alpha_3}e^{-\alpha_3 t}\right) \tag{8}$$

and

$$n_2(t) = n_T\frac{\alpha_2\alpha_3}{R_{2i}(\alpha_2 - \alpha_3)}(e^{-\alpha_2 t} - e^{-\alpha_3 t}). \tag{9}$$

The limiting cases for these equations can be checked with the assumptions made at the beginning, i.e. for $t = 0$, both $n_i(t)$ and $n_2(t) = 0$, while for $t = \infty$ $n_2(t) = 0$ and $n_i(t) = n_T$.

The number of ions created during the laser pulse will be given by the integral of the collisional rate R_{2i} times $n_2(t)$, i.e.

$$n_i = \int_0^{\Delta t_l} R_{2i}n_2(t)dt. \tag{10}$$

If a unity efficiency of charge collection is assumed then the signal will reproduce the number of ions formed. This number can then be found by integrating Eq. (9) and is given by

$$n_i = \frac{n_T}{\alpha_3 - \alpha_2}[\alpha_3(1 - e^{-\alpha_2\Delta t_l}) - \alpha_2(1 - e^{-\alpha_3\Delta t_l})]. \tag{11}$$

This equation can now be discussed for both linear and non-linear interaction between the atoms and the radiation. Firstly, α_3 and α_2 can be written, after expansion of the square root in Eqs. (5), as

$$\alpha_3 = X - \frac{Y}{X} \qquad \alpha_2 = \frac{Y}{X} \tag{12}$$

where, according to Eqs. (2) and (4), X and Y are given by the expressions

$$X = B_{12}\varrho_\lambda(\lambda_{12}) + k_{12} + k_{2i} + B_{21}\varrho_\lambda(\lambda_{12}) + A_{21} + k_{21} \tag{13}$$

$$Y = [B_{12}\varrho_\lambda(\lambda_{12}) + k_{12}]k_{2i}.$$

2.1.1 Linear interaction

In this case, the spontaneous radiative rate coefficient, A_{21}, and the quenching rate coefficient, k_{21}, are considered to be much greater than the radiative pumping rate $B_{12}\varrho_\lambda(\lambda_{12})$, which is in turn considered to be much greater than k_{12}. For example, for a pulsed laser, attenuated with neutral density filters to avoid optical saturation, and an air acetylene flame at atmospheric pressure ($T \sim 2500$ K), order of magnitude estimates of these coefficients would be $B_{12}\varrho_\lambda(\lambda_{12}) \sim 10^5 \div 10^6$, $k_{21} \sim 10^8$, $A_{21} \sim 10^7 \div 10^8$, $k_{12} \sim 10^3 \div 10^4$.

Then α_1 and α_2 can be simplified as

$$x_1 = A_{21} + k_{21} + k_{2i}$$

$$x_2 = \frac{B_{12}\varrho_\lambda(\lambda_{12})k_{2i}}{A_{21} + k_{21} + k_{2i}} \qquad (14)$$

$$x_1 - \alpha_2 \cong x_1.$$

When these values are substituted in Eq. (11) we obtain after some algebraic manipulation

$$n_i = n_1\left[1 - \exp\left(-\frac{B_{12}\varrho_\lambda(\lambda_{12})k_{2i}}{A_{21} + k_{21} + k_{2i}}\,\Delta t_l\right)\right]. \qquad (15)$$

This equation clearly shows that the ionization yield, i.e. the ratio between number of ions formed and the total atomic population, is governed by the values of the collisional ionization rate coefficient, k_{2i}, and the duration of the laser excitation pulse, Δt_l. The value of k_{2i} depends upon how close level 2 is to the ionization continuum. However, even if k_{2i} is much greater than $(A_{21} + k_{21})$, the product $B_{12}\varrho_\lambda(\lambda_{12})\Delta t_l$ will still be exceedingly small, e.g. ~0.01 for a 10 nanosecond laser pulse

It can, therefore, be concluded that single-step, *linear excitation with nanosecond laser pulses in flame is not expected to produce any significant ionization yield.* As shown here, if the level reached by the laser is close to the ionization potential of the atom (which requires uv lasers) *and* the duration of the laser pulse is long, e.g. microsecond, then the ionization yield increases considerably. When a cw laser is considered, Δt_l in the expression should be replaced by the residence time of the atoms in the excitation beam. However, recombination of ions and electrons needs to be considered and the rate equations given here do not hold.

2.1.2 Optical saturation

The treatment here follows closely that given in the previous paragraph, with the assumption that now $B_{12}\varrho_\lambda(\lambda_{12}) \gg A_{21} + k_{21} + k_{2i}$). We then have

$$x_1 = B_{12}\varrho_\lambda(\lambda_{12}) + B_{21}\varrho_\lambda(\lambda_{12})$$

$$x_2 = \frac{B_{12}\varrho_\lambda(\lambda_{12})k_{2i}}{B_{12}\varrho_\lambda(\lambda_{12}) + B_{21}\varrho_\lambda(\lambda_{12})} \qquad (16)$$

$$x_1 - \alpha_2 \cong x_1.$$

Substituting these values into Eq. (11) and remembering that $B_{lu}g_l = B_{ul}g_u$, we obtain

$$n_i = n_T\left\{1 - \exp\left[-\left(\frac{g_2}{g_1 + g_2}\right)k_{2i}\Delta t_l\right]\right\}. \qquad (17)$$

Similar considerations as those given for Eq. (15) apply here. The ionization yield will depend on the product $k_{2i}\Delta t_l$, i.e. again on the value of k_{2i} and on the duration of the interaction between the atoms and the radiation. Indeed, as reported by Travis et al. [31], a useful rule of thumb for pulse length requirements, put forth by C. A. van Dijk, is that unity ionization yield may be approached with an optically saturating laser pulse whose duration significantly exceeds the reciprocal of the effective ionization rate of the laser populated excited state. The *effective* rate is described here by the coefficient k_{2i}, which is believed to be much lower than the radiative and quenching rates when level 2 is some eV below the ionization continuum.

From these considerations it can be concluded that *single step, saturated excitation with nanosecond laser pulses in a flame is not expected to give a significant ionization yield,* unless excited levels are reached very near to the ionization potential. However, *for longer laser pulses* (up to the limit where ion-electron recombination needs to be considered) the *ionization can indeed be significant.*

These conclusions are important when the technique of laser saturated fluorescence is used for flame and plasma diagnostics to evaluate the total number density of the atoms or ions in a selected excitation volume, since ionization occurring during the laser pulse is usually neglected.

2.1.3 Optical saturation – Radiation and collisional losses from the excited level

Although the theoretical treatment of paragraphs 2.1.1 and 2.1.2 shows the role played by the essential parameters of the single-step, collisionally assisted ionization process, in many cases the excited level 2 is coupled with an intermediate energy level such as that indicated as 2′ in Fig. 1. Level 2′ can be, for example, a metastable level, as in the case of Tl and Pb. If recycling of atoms between level 2′ and levels 1 and 2 is not fast, level 2′ is a trap. Therefore, losses from 2 cannot be neglected as there will be a direct competition between these losses and the ionization rate described by the effective rate coefficient k_{2i}. If the interaction between the laser and the atoms is linear, we should deal with a four level system, i.e. with levels 1, 2, 2′ and the ionization continuum. However, we can proceed as done by Hurst et al. [20] by considering that, if the laser is able to saturate the optical transition $1 \rightarrow 2$, the populations of the two levels will be maintained in the ratio of their respective degeneracies during the laser pulse and this "locked" population will decay away due to both losses to level 2′ and to the ionization continuum. We can, therefore, treat the system again as a 3-level system.

With these premises, we have

$$n_1(t) + n_2(t) = n_{12}(t) \qquad (18a)$$

$$n_2(t) = \frac{g_2}{g_1}n_1(t) = \left(\frac{g_2}{g_1 + g_2}\right)n_{12}(t) \qquad (18b)$$

$$n_{12} + n_{2'} + n_i = n_T \qquad (18c)$$

where $n_{12}(t)$ is the total population of levels 1 and 2, locked together for the entire duration of the laser pulse.

The rate equations for the system then are

$$\frac{dn_i}{dt} = k_{2i}n_2 \qquad (19a)$$

$$\frac{dn_{12}}{dt} = -[k_{2i} + A_{22'} + k_{22'}]n_2. \qquad (19b)$$

Making use of Eq. (18), we obtain

$$\frac{dn_{12}}{dt} = -(k_{2i} + A_{22'} + k_{22'})\left(\frac{g_2}{g_1 + g_2}\right)n_{12}. \qquad (20)$$

Solution of Eq. (20), with the boundary conditions that $n_{12}(t) = n_1$, at $t = 0$, i.e. before the laser irradiation, gives

$$n_{12}(t) = n_1 \exp\left[-(k_{2i} + A_{22'} + k_{22'})\left(\frac{g_2}{g_2 + g_1}\right)t\right]. \qquad (21)$$

Assuming, as before, unity collection efficiency of the ions formed, the number of ions during the laser pulse will be given by

$$n_i = \int_0^{\Delta t_l} k_{2i}n\,(t)dt = \int_0^{\Delta t_l} k_{2i}\left(\frac{g_2}{g_1 + g_2}\right)n_{12}(t)dt \qquad (22a)$$

whose solution is

$$n_i = \frac{n_T k_{2i}}{k_{2i} + A_{22'} + k_{22'}}\left\{1 - \exp\left[-\left(\frac{g_2}{g_1 + g_2}\right)\left(k_{2i} + A_{22'} + k_{22'}\right)\Delta t_l\right]\right\}. \qquad (22b)$$

The important new outcome of this relationship, in addition to those already discussed in Eq. (17), is that, even if the laser is able to saturate the transition, the effective ionization rate has to be much faster than the loss rate from level 2. This shows that, for several atomic species in the flame, single step excitation with nanosecond laser pulses will result in even lower ionization yields than those predicted by Eq. (17).

2.2 Two-step excitation with saturation of first step – collisional ionization

By referring to Fig. 1, the atoms are now excited stepwise by two lasers tuned at λ_{12} and λ_{23}, respectively. Since the two excitation transitions share a common level, temporal coincidence should be ensured and is assumed here, as well as spatial coincidence in the flame. The duration of both laser pulses is the same, and the effective rate of collisional ionization is k_{3i}. In order to reduce the number of differential equations, transition $1 \rightarrow 2$ is saturated and, therefore, at any time during the excitation pulse, n_1 and n_2 are related to each other and to n_{12}, as shown in Eq. (18).

The rate equations are

$$\frac{dn_i}{dt} = k_{3i}n_3$$

$$\frac{dn_3}{dt} = n_2B_{23}\varrho_\lambda(\lambda_{23}) - n_3 \cdot [B_{32}\varrho_\lambda(\lambda_{23}) + A_{32} + k_{32} + k_{3i}] \qquad (23)$$

$$n_{12} + n_3 + n_i = n_T.$$

By proceeding as in Section 2.1.1, X and Y will now be given by the following expressions

$$X \equiv \left(\frac{g_2}{g_3}\right) \cdot \left(\frac{g_1 + g_2 + g_3}{g_1 - g_2}\right)B_{23}\varrho_\lambda(\lambda_{23}) + A_{32} + k_{23} + k_{3i} \qquad (24a)$$

and

$$Y \equiv \left(\frac{g_2}{g_1 + g_2}\right)B_{23}\varrho_\lambda(\lambda_{23})k_{3i}. \qquad (24b)$$

By using Eq. (12) for α_2 and α_3 and Eq. (11), the number of ions produced during the laser pulses can be derived in a straightforward manner. Two cases are then again distinguished:

2.2.1 Linear interaction in the second step

This occurs when the downward relative and quenching rate coefficients, A_{32} and k_{32}, are much greater than $B_{23}\varrho_\lambda(\lambda_{23})$. In this case

$$n_i = n_T\left\{1 - \exp\left[-\frac{B_{23}\varrho_\lambda(\lambda_{23})k_{3i}}{A_{32} + k_{32} + k_{3i}}\left(\frac{g_2}{g_1 + g_2}\right)\Delta t_l\right]\right\}. \qquad (25)$$

This equation has to be compared with Eq. (15). The important difference is that, even when $A_{32} + k_{32} \sim A_{21} + k_{21}$ and $B_{12}\varrho_\lambda(\lambda_{12}) = B_{23}\varrho_\lambda(\lambda_{23})$, k_{3i} can be *several orders of magnitude greater than* k_{2i} due to the exponential dependence of the ionization probability on the energy difference between the excited level and the ionization continuum. Therefore, two step, linear excitation with nanosecond laser pulses in a flame can result in a higher degree of ionization because the level reached by the second step is closer to the continuum.

In the limiting case where k_{3i} is greater than $(A_{32} + k_{32})$,

$$n_i = n_T\left\{1 - \exp\left[-\left(\frac{g_2}{g_1 + g_2}\right)B_{23}\varrho_\lambda(\lambda_{23})\Delta t_l\right]\right\} \qquad (25a)$$

similar to the limiting case of $k_{2i} \gg (A_{21} + k_{21})$ in Eq. (15).

2.2.2 Optical saturation of the second step

This is obviously a much more interesting situation since in this case the induced radiative rates dominate over the term $(A_{32} + k_{32})$. If $B_{23}\varrho_\lambda(\lambda_{23})$ is also much greater than k_{3i}, the number of ions is given by

$$n_i = n_T\left[\left\{1 - \exp\left[-\left(\frac{g_3}{g_1 + g_2 + g_3}\right)k_{3i}\Delta t_l\right]\right\}\right]. \qquad (26)$$

As before, this equation should be compared with Eq. (17). The comparison shows that the ionization yield, in the two cases, for equal laser pulses, is strictly governed by the ratio k_{3i}/k_{2i}, as expected. It can be concluded that *two-step saturated excitation with nanosecond laser pulses in a flame is likely to result in significant ion production,* the more so if level 3 is close to the ionization continuum.

As before, when k_{3i} is greater than $B_{23}\varrho_\lambda(\lambda_{23})$, Eq. (25a) results, but now $B_{23}\varrho_\lambda(\lambda_{23})$ is several orders of magnitude larger giving a significantly higher ionization yield.

2.2.3 Optical saturation of both steps – radiation and collisional losses from the level excited by the second step

In this case, we proceed as in paragraph 1.3, i.e. in order to simplify the treatment, both transitions are assumed to be saturated so that the populations of levels 1, 2 and 3 are locked together. Collisional losses from level 3 need to be considered when level 3 is not close to the ionization continuum. It is easy to anticipate that the number of ions formed will depend upon the ratio of the rate coefficients for ionization and the total loss coefficients from level 3 to level 3′, as indicated in Fig. 1.

To derive the final equation, it is firstly recalled that

$$n_{123} = n_1 + n_2 + n_3 \qquad (27a)$$

$$n_3 = \left(\frac{g_3}{g_1 + g_2 + g_3}\right)n_{123} \qquad (27b)$$

$$\frac{dn_{123}}{dt} = -(k_{3i} + A_{33'} + k_{33'})\left(\frac{g_3}{g_1 + g_2 + g_3}\right)n_{123}. \qquad (27c)$$

With the same procedure as done before, we obtain

$$n_i = \frac{n_i k_{3i}}{k_{3i} + A_{33'} + k_{33'}}\left\{1 - \exp\left[-\left(\frac{g_3}{g_1 + g_2 + g_3}\right)\cdot\left(k_{3i} + A_{33'} + k_{33'}\right)\Delta t_i\right]\right\}. \tag{28}$$

Similar conclusions can be derived from this equation, as was done after Eq. (22b). In addition, because of the assumptions made here and in paragraph 2.1.3, it can be seen from Eqs. (22b) and (28) that, even when the expression within brackets in the right hand side of both equations is much larger than unity, the fraction of the total atomic population which will be ionized approaches a value which can be negligibly small or significant depending upon the rate of accumulation of atoms in the two traps, which are level 2′ (or 3′) and the ionization continuum.

2.3 Two-step ionization

Two-step ionization is distinguished from two-step excitation-collisional ionization since the second laser step can either directly ionize the atom or reach a level whose energy defect with the ionization potential is so low that collisional ionization proceeds instantaneously. In this case, the system can again be reduced to a 3 level system and the effects of saturation of either both transitions on the time dependent populations examined.

2.3.1 Two-step ionization without radiative and collisional losses from level 2

In this case losses to level 2′ are not considered and ionization proceeds directly via the pumping processes $1 \rightarrow 2$ and $2 \rightarrow 3$. With the assumptions given, $(dn_2/dt) \cong (dn_i/dt)$.

The procedure followed is that of section 2.1.1, and Eqs. (4b) and (4c) are now given by the expressions

$$X \equiv B_{12}\varrho_\lambda(\lambda_{12}) + B_{21}\varrho_\lambda(\lambda_{21}) + B_{23}\varrho_\lambda(\lambda_{23}) + A_{21} + k_{21} \tag{29a}$$

and

$$Y \equiv B_{12}\varrho_\lambda(\lambda_{12})B_{23}\varrho_\lambda(\lambda_{23}). \tag{29b}$$

Four cases can be sorted out:

2.3.1.1 Linear interaction for both steps. Since $B\varrho$ is much less than $(A + k)$, α_3 and α_2 are given by

$$\alpha_3 = A_{21} + k_{21} \tag{30a}$$

$$\alpha_2 = \frac{B_{12}\varrho_\lambda(\lambda_{12})B_{23}\varrho_\lambda(\lambda_{23})}{A_{21} + k_{21}} \tag{30b}$$

$$\alpha_3 - \alpha_2 \cong \alpha_3 \tag{30c}$$

and, from Eq. (11)

$$n_i = n_1\left\{1 - \exp\left[-\frac{B_{12}\varrho_\lambda(\lambda_{12})B_{23}\varrho_\lambda(\lambda_{23})}{A_{21} + k_{21}}\right]\Delta t_i\right\}. \tag{31}$$

2.3.1.2 Linear interaction for step 1, optical saturation for step 2. In this case, we obtain

$$\alpha_3 = B_{23}\varrho_\lambda(\lambda_{23}) \tag{32a}$$

$$\alpha_2 = B_{12}\varrho_\lambda(\lambda_{12}) \tag{32b}$$

$$\alpha_3 - \alpha_2 \cong \alpha_3 \tag{32c}$$

and from Eq. (11)

$$n_i = n_1\left\{1 - \exp\left[-B_{12}\varrho_\lambda(\lambda_{12})\Delta t_i\right]\right\}. \tag{33}$$

2.3.1.3 Optical saturation for step 1, linear interaction for step 2. In this case, we obtain

$$\alpha_3 = \left(1 + \frac{g_1}{g_2}\right)B_{12}\varrho_\lambda(\lambda_{12}) \tag{34a}$$

$$\alpha_2 = \left(\frac{g_2}{g_1 + g_2}\right)B_{23}\varrho_\lambda(\lambda_{23}) \tag{34b}$$

$$\alpha_3 - \alpha_2 \cong \alpha_3 \tag{34c}$$

and from Eq. (11)

$$n_i = n_1\left\{1 - \exp\left[-\left(\frac{g_2}{g_1 + g_2}\right)B_{23}\varrho_\lambda(\lambda_{23})\Delta t_i\right]\right\}. \tag{35}$$

2.3.1.4 Optical saturation for both steps. In this case, we have

$$\alpha_3 = B_{12}\varrho_\lambda(\lambda_{12})\left(g + a - \frac{a}{g + a}\right) \tag{36a}$$

$$\alpha_2 = \left(\frac{a}{g + a}\right)B_{12}\varrho_\lambda(\lambda_{12}) \tag{36b}$$

$$\alpha_3 - \alpha_2 = B_{12}\varrho_\lambda(\lambda_{12})\left(g + a - \frac{2a}{g + a}\right) \tag{36c}$$

where $B_{12}\varrho_\lambda(\lambda_{12})$ has been chosen as a reference for the saturating radiation rate coefficient and g and a are given by

$$g \equiv \left(1 + \frac{g_1}{g_2}\right) \tag{37a}$$

$$a \equiv \frac{B_{23}\varrho_\lambda(\lambda_{23})}{B_{12}\varrho_\lambda(\lambda_{12})}. \tag{37b}$$

If we identify for simplicity the numerical factors of Eqs. (36a) and (36b) as G and G', respectively, Eq. (11) gives

$$n_i = \frac{n_T}{B_{12}\varrho_\lambda(\lambda_{12})(G - G')}\{B_{12}\varrho_\lambda(\lambda_{12}) \cdot G(1 - e^{-G'B_{12}\varrho_\lambda(\lambda_{12})\Delta t_i}) - G'B_{12}\varrho_\lambda(\lambda_{12})(1 - e^{-GB_{12}\varrho_\lambda(\lambda_{12})\Delta t_i})\}. \tag{38}$$

By inspecting the equations derived in the previous paragraphs (2.3.1.1–2.3.1.4), the following considerations can be outlined:

i) Compared to the single-step excitation collisional ionization cases treated in section 2, k_{2i} has been replaced here by $B_{23}\varrho_\lambda(\lambda_{23})$. Therefore, Eqs. (15) and (17) are directly comparable with Eqs. (31) and (35). It can be seen that the ionization yield of the two techniques are governed by the ratio $[B_{23}\varrho_\lambda(\lambda_{23})/k_{2i}]$, as expected.

ii) When the two steps are optically satured, the only parameter governing the ionization yield is the product $B\varrho\Delta t_i$. If this product is much greater than unity, *all the atoms in the interaction volume will undergo ionization.*

2.3.2 Two-step ionization including radiative and collisional losses from level 2

This case is exactly equivalent to that discussed under paragraph 2.1.3 of section 2, the only difference being that now k_{2i} has to be replaced by $B_{23}\varrho_\lambda(\lambda_{23})$. By proceeding as before, the final expression for the number of ions formed is [see Eq. (22b)]:

$$n_i = \frac{n_i B_{23}\varrho_\lambda(\lambda_{23})}{B_{23}\varrho_\lambda(\lambda_{23}) + A_{22'} + k_{22'}}\cdot\left\{1 - e^{-\left(\frac{g_2}{g_1 + g_2}\right)\{B_{23}\varrho_\lambda(\lambda_{23}) + A_{22'} + k_{22'}\}\Delta t_i}\right\}. \tag{39}$$

Equation (39) once again stresses the importance of the *product* $B\varrho\Delta t_i$. Indeed, saturation of both transitions will dominate the losses towards level 2′ but a low ionization yield will still result if $B\varrho\Delta t_i$ is less than unity.

2.4 Signal enhancement due to the second step

In a two-step excitation scheme, the "ionization enhancement" (IE) is defined as the ratio between the ionization signal measured with steps 1 + 2 and that of step 1 only. It is not easy to predict theoretically what the enhancement factor will be. However, it is easy to compare the theoretical equations derived to show which are, under the assumptions given, the parameters governing that factor.

2.4.1 Single-step excitation (collisional ionization) versus two-step excitation (collisional ionization)

2.4.1.1 Final laser steps linear. Here, the radiative step populating the collisionally ionized level does not result in optical saturation of the transition. If the exponentials of Eqs. (15) and (25) are then expanded in series, and we assume that the pulse duration of the two lasers is the same, we obtain

$$IE = \left[\frac{B_{23}\varrho_\lambda(\lambda_{23})k_{3i}}{B_{12}\varrho_\lambda(\lambda_{12})k_{2i}}\right]\left(\frac{A_{21} + k_{21} + k_{2i}}{A_{32} + k_{32} + k_{3i}}\right)\left(\frac{g_2}{g_1 + g_2}\right). \tag{40}$$

2.4.1.2 All laser steps saturating. From Eqs. (17) and (26) a similar comparison in optically saturated conditions gives

$$IE = \left(\frac{k_{3i}}{k_{2i}}\right)\left(\frac{g_3}{g_2}\right)\left(\frac{g_1 + g_2}{g_1 + g_2 + g_3}\right). \tag{41}$$

It can be seen that it is not justified a priori to consider the enhancement as simply given by the probability of ionization of the level reached in the optical excitation step, i.e. solely by the "effective" ionization rate. This will only be the case when both transitions are saturated. When collisional and radiative losses are in competition with the ionization process [Eqs. (22b) and (28)], and all optical steps are saturated, Eq. (41) is again obtained.

2.4.2 Single-step excitation (collisional ionization) versus two-step ionization

With two-step ionization, a unity ionization yield may be achieved and, therefore, the enhancement is expected to be maximum. Several cases follow from the theoretical expressions derived before.

2.4.1.2 Both laser steps linear. In this case, Eqs. (15) and (31) apply, giving

$$IE = \frac{B_{23}\varrho_\lambda(\lambda_{23})}{k_{2i}}. \tag{42}$$

2.4.2.2 Step 1 linear, step 2 saturating. Comparison here should be made of Eqs. (15) and (33) with the following result

$$IE = \frac{A_{21} + k_{2i}}{k_{2i}}. \tag{43}$$

2.4.2.3 Step 1 saturating, step 2 linear. Equations (17) and (35) combined result in expression

$$IE = \frac{B_{23}\varrho_\lambda(\lambda_{23})}{k_{2i}} \tag{44}$$

which is identical to Eq. (42).

2.4.2.4 Both steps saturating. This is the case of maximum enhancement. In fact, when the product $B\varrho\Delta t_i$ is greater than unity, rationing Eqs. (38) and (17) gives

$$IE = \left(\frac{g_1 + g_2}{g_2}\right)\left(\frac{1}{k_{2i}\Delta t_i}\right). \tag{45}$$

2.5 Saturation absorption rate considerations

The ionization signal measured after one step or two step excitation should grow linearly with the spectral irradiance of the laser and then saturate, i.e. it becomes independent upon the laser power. It is interesting to note that in ionization experiments with nanosecond laser pulses, if the rate of recombination, k_{i1}, between the electrons and the ions to regenerate neutral atoms is negligible, the ionization continuum is a trap. This has consequences on the value of the saturation parameter for the transition involving the first excitation step. In addition, when the second excitation step is present, the value of the saturation parameter can modify considerably, as seen from the following *qualitative* considerations.

It is known that the radiative absorption rate between levels 1 and 2 can be expressed as [1, 22]

$$R_{12} = \frac{g_2}{g_1}A_{21}\frac{\lambda^3}{8\pi hc}E_\nu(\nu_{12}) \tag{46a}$$

where h is the Planck constant, c the velocity of light and $E_\nu(\nu_{12})$ is the spectral irradiance of the laser and is related to $\varrho_\nu(\nu_{12})$ by the expression

$$E_\nu(\nu_{12}) = c\varrho_\nu(\nu_{12}) \tag{46b}$$

where the energy density is given in terms of frequency rather than wavelength.

The saturation spectral irradiance for a 3-level system, where the levels 1, 2 and i are considered and where radiative excitation couples levels 1 and 2, is given by the following relationship [1, 22]

$$E_\nu^s(\nu_{12}) = \left(\frac{g_1}{g_2}\right)\left(\frac{cA_{21}}{B_{21}Y_{21}}\right)\left[\frac{1}{1 + \frac{g_1}{g_2} + \frac{k_{2i}}{k_{i1}}}\right] \tag{47a}$$

or, by making use of the relation between B_{21} and A_{21} and of the definition of the quantum efficiency, Y_{21}, as

$$Y_{21} = \frac{A_{21}}{A_{21} + k_{21} + k_{2i}}. \tag{47b}$$

Equation (47) becomes

$$E_1^*(\nu_{12}) = \left(\frac{8\pi h\nu^3}{c^3}\right)\left(\frac{A_{21} + k_{21} + k_{2i}}{A_{21}}\right) \cdot \left[\frac{1}{1 + \left(\frac{g_2}{g_1}\right)\left(\frac{k_{i1} + k_{2i}}{k_{i1}}\right)}\right]. \tag{47c}$$

By substituting Eq. (47c) into Eq. (46a), the *saturation absorption rate* will be given by

$$R_{12}^* = \frac{A_{21} + k_{21} + k_{2i}}{1 + \frac{g_1}{g_2} + \frac{k_{2i}}{k_{i1}}}. \tag{48}$$

Equation (48) refers to single step excitation. When the second excitation step is used and we assume that either collisional ionization from the level reached is fast or the second laser transition directly ionizes the atom, it is easy to see that the same procedure leads to the expression

$$(R_{12}^*)_{2\text{-step}} = \frac{A_{21} + k_{21} + B_{2i}\varrho_\nu(\nu_{2i})}{1 + \frac{g_1}{g_2} + \frac{B_{2i}\varrho_\nu(\nu_{2i})}{k_{i1}}}. \tag{49}$$

Rationing Eqs. (49) and (48) then gives

$$\frac{(R_{12}^*)_{1\text{-step}}}{(R_{12}^*)_{2\text{-step}}} = \frac{k_{2i}[A_{21} + k_{21} + B_{2i}\varrho_\nu(\nu_{2i})]}{B_{2i}\varrho_\nu(\nu_{2i})(A_{21} + k_{21} + k_{2i})}. \tag{50}$$

If the second step is saturated, then $B_{2i}\varrho_\nu(\nu_{2i})$ will be much greater than $(A_{21} + k_{21})$, and Eq. (50) will reduce to

$$\frac{(R_{12}^*)_{1\text{-step}}}{(R_{12}^*)_{2\text{-step}}} = \frac{k_{2i}}{A_{21} + k_{21} + k_{2i}}. \tag{51}$$

When k_{2i} is (much) less than $(A_{21} + k_{21})$, these equations show that the saturation rate of the first optical excitation step *decreases when the second step is also present*. This result is similar to that obtained for atomic fluorescence in 3-level systems where the third level is a long-lived, metastable level (e.g. thallium and lead) [22].

2.6 *Fluorescence versus ionization*

In the previous discussions, the emphasis has been on the degree of ionization obtained under various excitation conditions. For those cases in which the limit is a high degree of ionization, the fluorescence is decreased significantly by the ionization process, which fact has not been repetitively reiterated through the discussion.

By referring to the theoretical expressions derived, it is now a simple matter to compare the temporal evolution of the fluorescence and ionization signals. One only needs to remember that the fluorescence radiance, in conditions of negligible selfabsorption, is given by

$$B_F(t) = n_2(t) \cdot h\nu_{21}A_{21}(l/4\pi) \tag{52}$$

where B_F ($Js^{-1} \cdot cm^{-2} \cdot sr^{-1}$) is the fluorescence radiance, $h\nu_{21}$ is the energy of the emitted photon, l is the fluorescence depth (towards the detector) and 4π accounts for the isotropicity of the fluorescence process. The fluorescence temporal behaviour is, therefore, given by Eq. (9) in the case of single-step excitation-collisional ionization and by a similar expression for $n_3(t)$ when two-step excitation is considered (see paragraph 2.2).

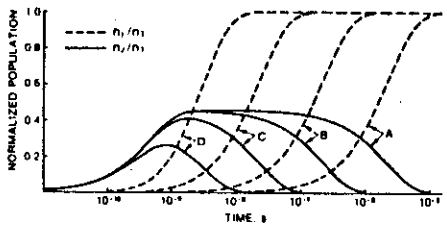

Fig. 2. Temporal behaviour of the normalized populations of the ions and of the fluorescing atoms in the single-step excitation, collisional ionization scheme. See text for discussion. *A*: $k_{2i} = 10^6\ s^{-1}$; *B*: $k_{2i} = 10^7\ s^{-1}$; *C*: $k_{2i} = 10^8\ s^{-1}$; *D*: $k_{2i} = 10^9\ s^{-1}$

It is, therefore, easy to realize that, under the assumption of saturation conditions, the relative magnitude of k_{2i} (and k_{3i}) with respect to $A_{21} + A_{22}$ (and $A_{32} + A_{33}$) will govern the fluorescence and ionization signals. Some typical situations are shown in Fig. 2 where the normalized populations of level 2 and the number of ions are plotted as a function of time by using the general Eqs. (8) and (9). The spontaneous transition probabilities, and the quenching coefficients, are kept constant at $10^8\ s^{-1}$ while the laser pumping rates are assumed to be $10^9\ s^{-1}$. The four curves shown in Fig. 2 refer to values of k_{2i} ranging from $10^6\ s^{-1}$ to $10^9\ s^{-1}$. As pointed out before, these results have to be taken mainly for illustrative purposes rather than on a rigorous quantitative basis. Indeed, the rate equations approach is not expected to be accurate at the very beginning of the interaction (where coherence effects might play and thus need to be considered), and recombination between the ions and the electrons has to be taken into account for interaction times longer than, say, 100 ns or a microsecond. The curves do, however, represent the expected behaviour of the fluorescence and ionization signals in the case of single-step and two-step excitation characterized by short (several nanoseconds) laser pulses showing that even for such short interaction times, the fraction of atoms lost as ions can indeed be significant if the effective collisional ionization rate is comparable to the other radiative and collisional (quenching) rates. As a result, in double-resonance fluorescence experiments in flames where the level reached by the second laser is close to the ionization potential, the analytical sensitivity of the technique is adversely affected [24]. On the other hand, for strong, single resonance transitions in the visible and near-ultraviolet, if the level reached is not close to the ionization potential, the peak of the time-resolved, saturated fluorescence signal will accurately reflect the total number of atoms and the ionization loss will be negligible.

3. Experimental

The experimental set-up, similar to that used previously [24], is shown in Fig. 3; details of the components are given in

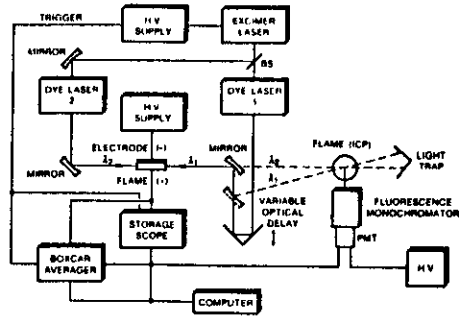

Fig. 3. Experimental set-up used in the fluorescence and ionization experiments. *H.V.* High voltage; *BS* Beam splitter; *PMT* Photomultiplier tube

Table 1. As shown in the figure, the excimer laser beam is split in order to simultaneously pump two dye lasers. In the ionization experiments, the two beams counterpropagate colinearly along the flame axis, while for the fluorescence measurements, the mirrors are adjusted so to provide maximum spatial overlap of the two beams in the flame or plasma. In order to make the two laser pulses temporally coincident, one laser pulse is delayed with respect to the other by sliding a retroreflector along an optical rail. The time behaviour was checked with a beam splitter which directed the beams to a fast photodiode placed at the flame (plasma) position. As seen from the traces of Fig. 4, when the retroreflector is at the extreme positions of the rail, one laser leads or lags the other by 3.4 ns and 4.6 ns, respectively. When the retroreflector is carefully adjusted, the two pulses can be made to overlap. A typical example is represented in Fig. 5 where the two pulses shown were used for the excitation of the double-resonance ionic fluorescence of strontium in the inductively coupled plasma [24].

Table 1. Instrumental components and operating parameters

Excimer laser

Model EMG-102 (Lambda Physik, Göttingen, FRG). The laser is operated with XeCl, has a pulse energy of ~130 mJ and a pulse width of ~12 ns. The repetition rate can be varied up to 100 Hz.

Dye lasers

The dye lasers are manufactured by Jobin Yvon (Instruments S.A., Division Jobin-Yvon, Longjumeau, France). One laser consists of the eight cell oscillator-amplifier system described by Bos [5] and the other is the standard one-cell configuration. Six frequency doubling crystals (3 KDP and KPB) allow the wavelength range from 217 to 360 nm to be covered. The fundamental output of the dye laser has a pulse energy ranging from 1 mJ to 7 mJ, depending on the dye, and a pulse width of ~4–5 ns

Flames

For the ionization experiments, the air-acetylene flame is supported on a three-slot burner head. For the fluorescence experiments, the air-acetylene flame is supported on a circular burner (Meker-type) and is shielded by a flow of argon

Inductively coupled plasma (ICP)

The plasma is a standard commercial model (Plasma Therm, Kresson, NJ, USA, Model 2500) operating at 27 MHz with a cross flow nebulizer (Labtest, Ratingen, FRG) fed by a peristaltic pump. Typical operating parameters: power 0.8–1 kW; plasma coolant gas flow 12 l · min^{-1}; auxiliary gas 0.2–0.8 l · min^{-1}; carrier gas 0.8–1.2 l · min^{-1}. The height of observation is fixed at 25 mm above the coil

Monochromators and associated optics

For flame work, the monochromator is the high luminosity model H-10 (Jobin Yvon, Longjumeau, France) and for ICP work the 1.29 m grating monochromator (model 1269, Spex, Metuchen, NJ, USA). No optics are used between the flame and the monochromator for the fluorescence experiments while the ICP is imaged by a lens-mirrors arrangement into the entrance slit of the SPEX monochromator. A quartz prism (Jobin Yvon, Longjumeau, France) is used as a retroreflector to optically delay one laser beam with respect to the other

Ionization system

Molybdenum electrode, water cooled, immersed in the air-acetylene flame [37]. The high voltage is applied between the electrode and the burner body. The signal is processed by a combination of a current and a voltage amplifier. The system is manufactured by SOPRA (Bois Colombes, France).

Detectors and data processing

Hamamatsu type R928S photomultiplier, wired for fast response (Hamamatsu Corporation, Japan). Box-car integrator (Stanford Research Corporation, Palo Alto, CA, USA) equipped with a sampling unit (SR 255) whose output is digitized and processed by a computer (HP Model 9816 S, Hewlett Packard, San Diego, CA, USA). Fast photodiode: Type F-4000, S-5 response, typical rise time 0.5 ns (Electrooptical Products Division ITT, Fort Wayne, IN, USA). Storage oscilloscope: Model 468 (Tektronix, Beaverton, NJ, USA). Fast oscilloscope: Model 7904 (Tektronix, Beaverton, NJ, USA).

Dyes

The dyes are manufactured by Exciton (Dayton, Ohio, USA) and are dissolved in spectroscopically pure solvents (Merck, Darmstadt, FRG).

Energy meters

Model ED-500 Joulemeter (Lambda Physik, Göttingen, FRG). Volume absorbing disc calorimeter (Model 38-0101, Scientech, Boulder, CO, USA).

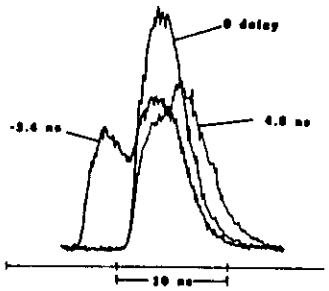

Fig. 4. Experimental waveforms obtained for the two laser pulses used in the double resonance experiments when the optical delay shown in Fig. 3 is moved along the rail. The pulses are measured with a fast photodiode

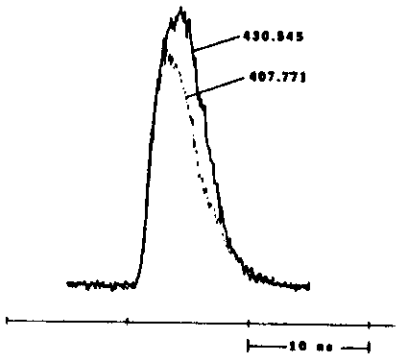

Fig. 5. Experimental waveforms obtained for the two laser pulses used in the double resonance ionic fluorescene of strontium nebulized in the inductively coupled plasma. Excitation wavelengths (nm) are also indicated

4. Results and discussion

4.1 Fluorescence

The analytical results obtained in our laboratory by single-step and two-step laser excitation in an inductively coupled argon plasma and in an air-acetylene flame have been already described in the literature in a detailed manner [19, 24]. It has been shown that the use of two-step excitation results in a much greater spectral selectivity and provides a unique way of correcting for scattering problems in resonance fluorescence experiments. The loss of atoms expected in the flame because of collisionally assisted ionization (see paragraph 2.2) was demonstrated experimentally for the magnesium atom. It was, therefore, concluded that the analytical utility of the double-resonance fluorescence technique could best be exploited in the case of ionic fluorescence excited in an inductively coupled plasma since in that case the energy difference between the level reached by two-step excitation and the second ionization potential of the ions is usually very large (i.e. k_{3i} in the theoretical considerations of paragraph 2.2 should be very small). The excellent results

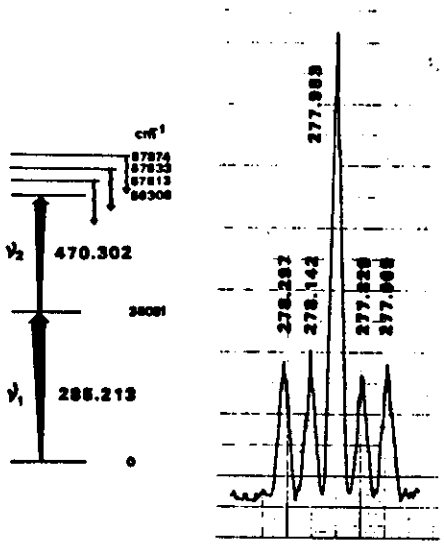

Fig. 6. Partial double resonance fluorescence spectrum of the magnesium atom nebulized in the inductively coupled plasma. The excitation scheme is shown to the left of the figure. The wavelengths are indicated in nanometers. Mg concentration: 1 μg/ml

obtained for the double-resonance ionic fluorescence of alkaline earth elements in the plasma is documented in Table 2 which collects the detection limits obtained [24].

The double-resonance fluorescence technique allows direct access to highly excited levels ($\gtrsim$7 eV above the ground state) whose thermal population is negligible at the flame temperature. These levels are collisionally coupled with nearby levels from which fluorescence is observed and several parameters of interest (temperature, collision cross sections, lifetime) can then be evaluated.

A partial double-resonance fluorescence spectrum of the magnesium atom is shown in Fig. 6. In this case, laser excitation populates a level located 6.98 eV above the ground state and 0.66 eV below the ionization potential of the atom. The five lines shown are due to non-resonance fluorescence transitions (of the anti Stokes type, since the fluorescence emission terminates into a manifold of levels lying approximately 22,000 cm^{-1} above the ground state) and their relative intensities can be compared using published values of radiative transition probabilities [42] to check for the lack of thermal equilibrium.

The relevance of these measurements in the field of combustion diagnostics is evident. For example, the excitation temperature in an inductively coupled argon plasma is known to increase with the excitation energy of the levels involved and a common temperature describes the population of a manifold of levels with similar energy separation from the ground state [10]. In this way, atomic energy levels close to the ionization continuum are in "thermal equilibrium" with ground state ions, leading to the concept of a two-temperature local thermal equilibrium, where high

energy levels couple to the ground state through one temperature but equilibrate with nearby levels through another (lower) temperature [10]. The possibility of evaluating the plasma temperature by means of laser excited fluorescence has been amply described in the literature [43]. Two-step excitation is, therefore, expected to become another important tool in the study of the excitation dynamics in flames and plasmas.

4.2 Ionization

Pure aqueous solutions of several elements were nebulized in order to evaluate the analytical sensitivity of the two-step excitation, collisional ionization technique. The laser beams were simply made to overlap as much as possible along the flame axis, parallel to the electrode. No beam expanders nor spatial filtering were used. As in our previous study [25], the limiting noise of the technique was found to be radio-frequency noise induced by the firing of the excimer laser. The distance between the electrode and the burner was fixed at 2.6 cm; thus, its influence on the analytical signal was not investigated. The laser beam was located approximately 5 mm below the electrode. In the case of a matrix solution containing an easily ionizable element, it is well known that such distance needs to be considerably reduced to avoid the so-called electrical interferences [37].

From the experimental data obtained, which are reported below for each element investigated, some considerations are worth being stressed:

i) As expected from the theoretical considerations outlined in the previous section and as also reported experimentally by others [7, 8, 9, 38], two-step excitation *always results* in (much) larger ionization signals and improved detection limits compared to single-step excitation; this holds when the two-step transitions reach a higher lying energy level than the single-step and the laser spectral energy densities are comparable.

ii) As can be seen from section 2.4, the enhancement factors will vary significantly from element to element, depending on parameters such as collisional cross sections and transition probabilities. For the same element, the enhancement factor varies with laser power and energy of the level reached in the second step. The enhancement factors observed varied from 32 in the case of strontium to 375 for lead.

iii) A combination of the ionization yield (n_i/n_T) and the enhancement factor enables the determination of the collisional rate coefficients, k_{2i} and k_{3i}, for a specific excitation scheme and experimental conditions. This was investigated by simultaneous absorption, fluorescence and ionization measurements for the lithium atom under accurately controlled experimental conditions (i.e. flame geometry, homogeneous laser excitation volume, calibrated detection system). The complete experiment is reported in detail elsewhere [27]. The ionization yield with single-step excitation was found to be 0.26%, increasing to 58% with two-step excitation. k_{2i} and k_{3i} were then calculated and found to be $0.8 \cdot 10^6$ and $3.5 \cdot 10^8$ s^{-1}, respectively [27].

iv) Molecular species can also be detected and their ionization spectrum easily observed when the laser is tuned to a molecular absorption band.

v) Even if only in a qualitative way, the dependence of the ionization signal upon the laser power has been studied for strontium.

Table 2. Detection limits (S/N = 2) for several elements in aqueous solutions by two-step laser enhanced ionization and two-step non resonance fluorescence

Element	Excitation wavelengths (nm)	Atomizer	Technique[a]	Detection limit (ng/ml)
Ag I	λ_1 = 328.068 λ_2 = 421.094	Flame	LEI	0.05[b]
Li I	λ_1 = 670.784 λ_2 = 460.286	Flame	LEI	0.0002
Na I	λ_1 = 588.995 λ_2 = 568.266	Flame	LEI	0.002[b]
Pb I	λ_1 = 283.306 λ_2 = 600.193	Flame	LEI	0.2[b]
Sr I	λ_1 = 460.733 λ_2 = 554.336	Flame	LEI	0.2
Sr II[c]	λ_1 = 407.771 λ_2 = 430.545	ICP	LIF	1
Ca II[c]	λ_1 = 396.847 λ_2 = 370.603	ICP	LIF	0.007
Ba II[c]	λ_1 = 455.403 λ_2 = 416.600	ICP	LIF	1
Mg II[c]	λ_1 = 279.553 λ_2 = 279.806	ICP	LIF	0.05

[a] *LEI* Laser Enhanced Ionization; *LIF* Laser Induced Fluorescence
[b] Contamination was the limiting factor, producing high blank values. In the case of lead, this could probably be caused by prolonged aspiration of a 1% lead solution for the analysis of traces of thallium in lead samples [25]
[c] From Reference [24]

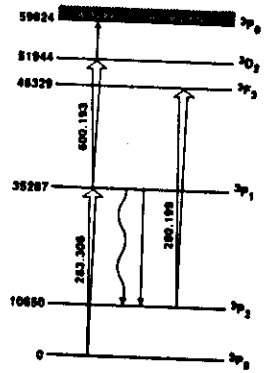

Fig. 7. Partial energy level scheme for atomic lead. Laser excitation transitions are indicated in nanometers. Fluorescence (*wavy line*) and quenching are also indicated

The detection limits obtained for the elements studied are collected in Table 2. Additional information is itemized by element.

4.2.1 Lead

The transitions investigated for lead are shown in Fig. 7. The best detection limit (0.2 ng/ml) was obtained with the

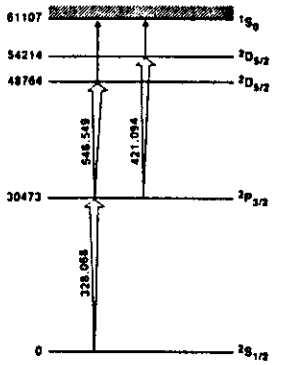

Fig. 8. Partial energy level scheme for atomic silver. Laser excitation transitions are indicated in nanometers

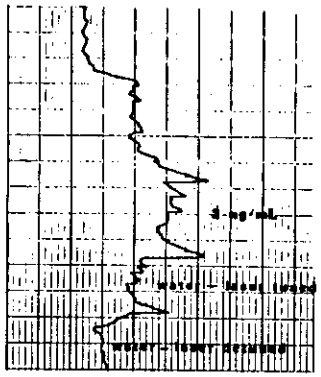

Fig. 9. Memory effects are blank ionization signals for low concentrations of silver nebulized in the air-acetylene flame. The spikes and the water signals shown disappear when the laser is detuned

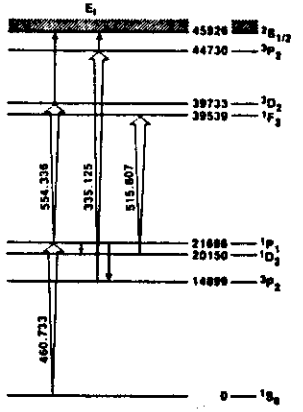

Fig. 10. Partial energy level scheme for atomic strontium. Laser excitation transitions are indicated in nanometers

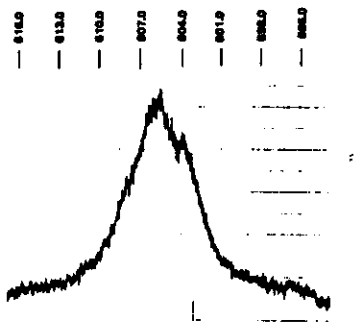

Fig. 11. Molecular ionization spectrum due to SrOH (5 mg/l) in the air-acetylene flame. The laser spectral scan (nm) is indicated

two exciting transitions sharing a common level, i.e. 283.306 nm and 600.193 nm. The measured laser energy was 60 μJ for the uv line and 650 μJ for the second excitation step. In these conditions, an enhancement factor of 375 was measured. Another scheme, also shown in Fig. 7, involves at first the indirect enhancement of the population of the $^3P_2$ level due to radiative and collisional deactivation from the $^3P_1$ level reached with the first laser step, followed by excitation to the $^3F_3$ level achieved with the second laser tuned at 280.199 nm. This scheme has been used to evaluate the lifetime of the $^3P_2$ metastable level [23].

4.2.2 Silver

Two schemes were used for silver and are shown in Fig. 8. The best combination was given by the lines 328.068 nm and 421.094 nm, resulting in a detection limit of 0.05 ng/mL A curious combination of contamination and memory effects was sometimes noted at low silver concentrations and is shown in Fig. 9. It can be seen from this figure that the water used in the experiment contained about 2 ng/ml of silver. Indeed, no signal and no spikes due to memory effects could be observed when the second laser was detuned from the 421.094 nm line. Such effect was not investigated any further.

4.2.3 Strontium

The energy scheme pertinent to the strontium atom is shown in Fig. 10. The greatest enhancement factor of 46 was measured with the lines at 460.733 nm and 554.336 nm. Similar results were also achieved by tuning the second laser to

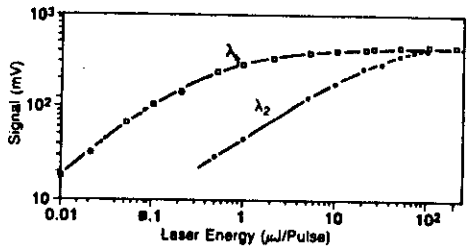

Fig. 12. Power dependence of the ionization signal for the strontium atom in the air-acetylene flame. □ second laser: 100 μJ/pulse, energy of first laser varied with neutral density filters; ● first laser: 210 μJ/pulse, energy of second laser varied with neutral density filters

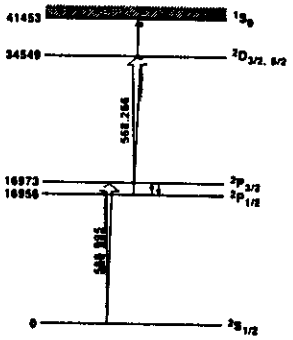

Fig. 13. Partial energy level scheme for atomic sodium. Laser excitation transitions are indicated in nanometers

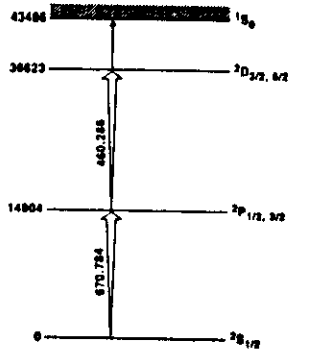

Fig. 14. Partial energy level scheme for atomic lithium. Laser excitation transitions are indicated in nanometers

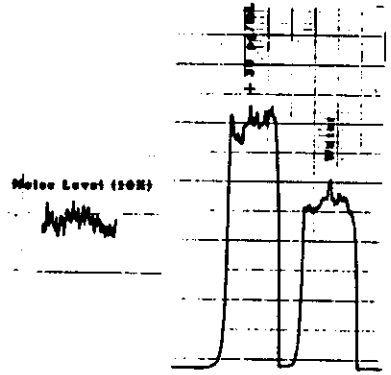

Fig. 15. Recorder tracings of the two-step ionization signals obtained by nebuling water and a solution containing 30 pg/ml of lithium. The noise in the baseline is shown (10× expanded) to the left of the figure

515.607 nm. With these combinations, a detection limit of 0.2 ng/ml was calculated. A detection limit of 2 ng/ml resulted from the pair of lines 460.733 nm and 335.125 nm, which do not share a common level. The laser energy measured for the transitions 460.733 nm, 554.336 nm and 335.125 nm was 1200 μJ, 650 μJ and 70 μJ, respectively. As shown in Fig. 11, a partial ionization spectrum of the molecule SrOH could easily be seen by scanning the laser in the region 595.616 nm. This spectrum was not studied in detail nor were other wavelength regions explored.

The dependence of the ionization signal upon the laser power was investigated in the case of strontium with the laser excitations set at 460.733 nm and 554.336 nm. For this experiment, the laser energy was 210 μJ and 100 μJ, respectively. The results are shown in Fig. 12. Here, the curve labelled λ_1 refers to the signals obtained as a function of the energy of the laser tuned to λ_1 *in the presence of the second step* at λ_2. Similarly, the curve labelled λ_2 refers to the signals obtained by decreasing the energy of the laser tuned to λ_2 *in the presence of the first step* at λ_1. In order to verify the theoretical behaviour predicted in section 2.5, the ionization signal needs to be measured at λ_1 *with and without* λ_2 *present*. The results shown in Fig. 12 are not fully explained by the equations derived in section 2.3 as the ionization signal, while varying the energy of λ_1, becomes asymptotic at energy levels ~2 orders of magnitude less than the converse case, while the two cases are expected to be about the same. Work is continuing to more fully characterise such power dependence.

4.2.4 Sodium and lithium

The two-step excitation schemes for these elements are illustrated in Figs. 13 and 14. In the case of sodium,

Table 3. Potential problems caused by the aspiration on a matrix solution (~ 1%wt) and their effect of LIF and LEI techniques

Problem	Physical explanat on and cause		Effect on the analytical signal		Solution*	
	LIF	LEI	LIF	LEI	LIF	LEI
Enhanced radiative background emission Not source induced	Thermal excitation of atomic and molecular species		Severe increase in noise	Negligible increase in noise	Improve spectral discrimination	
Enhanced background signal	Wavelength independent[b] Scattering from unvaporized particles at excitation	Wavelength independent[b] Ionization (possibly multiphoton ionization) by matrix constituents	Increase in the noise level Spurious signal		Scan laser thru absorption profil- if $\delta\lambda_l > \delta\lambda_{abs}$. If the contrary holds, measure at a nearby wavelength	
					Use non resonance fluorescence	Use two-step excitation
Source induced	Atomic and molecular fluorescence	Atomic and molecular ionization	Potential spectral interference		Change excitation wavelength	
					Change fluorescence wavelength	Use two-step excitation
Chemical interferences	Compound formation Decreased atomization efficiency		Significant variation (usually a reduction) of sensitivity		Use standard addition methods	
					Use releasing agents	Use releasing agents only if their ionization potential is higa
Mechanical (physical) interferences	Decreased aspiration efficiency Clogging problems		Reduction of sensitivity		Use standardizing solutions	
		Salt deposition on water-cooled electrode		Memory effects		Frequent cleaning of electrode
Ionization interferences	Shifting of ionization equilibrium in the flame	Severe distortion of the electrical field distribution in the flame	Increase in sensitivity	Severe loss of sensitivity (at limit, complete loss of signal)	Use of ionization buffers	Keep the laser beam as close as possible to the cathode in the flame

* In some cases, the effect can only be reduced
[b] The wavelength independence refers only to a narrow interval in the vicinity of the absorption line

contamination was severe since a signal was often obtained by simply igniting the flame, with no water nebulized into it. In these conditions, the detection limit of 0.002 ng/ml reported in Table 2 has to be considered only indicative, the true value being at least as good as that achieved with lithium.

A typical experimental tracing of the ionization signal and of its base line noise is shown in Fig. 15 for lithium at very low concentration levels in the solution. The water signal observed was due to lithium as demonstrated by its disappearance when the second laser was detuned from the 460.286 nm line (see Fig. 14). In this case, a detection limit of 0.2 pg/ml was calculated.

5. Conclusions

From the theoretical considerations outlined in section 2 and the experimental results obtained with the air-acetylene flame as atomizer and the inductively coupled plasma as atomizer/ionizer, it can be concluded that the ionization and fluorescence techniques are two extremely versatile and sensitive methods of atomic analysis of low traces of several elements in solution. In the case of the ionization technique with short (nanoseconds) excitation pulses, a significantly high fraction of the atoms available will be ionized during the laser pulse when a two-step excitation scheme is used with saturation of both transitions. Because of this loss of atoms, the atomic fluorescence technique resulting from the same excitation scheme in a flame will suffer losses from the competing ionization process. The fluorescence technique, on the other hand, will result in greater spectral selectivity compared to the ionization technique, since, after the excitation process, the signal can still be spectrally isolated by means of a monochromator.

It appears that the goal of achieving in the flame atomizer and with pneumatic nebulization the same, if not better, detection limits as those typical of the atomic absorption technique with electrothermal atomization, is closely approached. Therefore, the future of both the ionization and fluorescence techniques seems to be bright. As stated by

Travis et al. [32], advances in tunable laser technology, specialized sample treatment and new atom reservoirs can greatly extend the applicability of such techniques.

Our theoretical treatment of the various excitation processes leading to ionization is clearly simplified. The *simultaneous measurement of both fluorescence and ionization signals*, now in progress in our laboratory, will certainly help to unambiguously define the excitation process investigated.

Finally, from the practical point of view of the analyst involved in the quantitative detection of traces of various metals in a matrix solution by a flame spectroscopic technique, an attempt was made to outline for both fluorescence and ionization methods the potential interferences which might occur, together with the possible ways to overcome such problems. These considerations are collected in Table 3, in a self explanatory manner. By inspecting this table, one can see that the major differences between the two techniques are found in the different role played by the flame emission background (which is almost irrelevant in the ionization method) and in the effect of the ionization interferences which acts for the two methods in a completely opposite way.

Acknowledgements. B. W. Smith and L. P. Hart would like to thank the Joint Research Centre authorities and in particular the Education Training Service of Ispra, for the grant of visiting scientist fellowships.

References

1. Alkemade CThJ, Hollander Tj, Snelleman W, Zeegers PJTh (1982) Metal vapours in Flames. Pergamon Press, Oxford
2. Axner O, Berglind T, Heully JL, Lindgren IJ, Rubinsztein-Dunlop H (1984) J Appl Phys 55:3215–3225
3. Axner O, Lindgren I, Magnusson I, Rubinsztein-Dunlop H (1985) Anal Chem 57:776–778
4. Berthoud T, Lipinsky J, Camus P, Stehle JL (1983) Anal Chem 55:959–963
5. Bos F (1981) Appl Opt 20:3553–3555
6. Camus P (ed) (1983) International colloquium on optogalvanic spectroscopy and its applications, J. de Physique, 44, Suppl. II
7. Chaplygin VT, Zorov NB, Kuzyakov YuYa (1983) Talanta 30:505–508
8. Curran FM, Van Dijk CA, Crouch SR (1983) Appl Spectrosc 37:385–389
9. Curran FM, Lin KC, Leroi GE, Hunt PM, Crouch SR (1983) Anal Chem 55:2382–2387
10. De Galan L (1984) Spectrochim Acta 39B:537–550
11. Goldsmith JEM, Anderson RJM, (1985) Appl Opt 24:607–609
12. Green RB, Havrilla GJ, Trask TO (1980) Appl Spectrosc 34:561–569
13. Hall JE, Green RB (1983) Anal Chem 55:1811–1814
14. Hart LP, Smith BW, Omenetto N (1985) Spectrochim Acta B: 40B:1637–1649
15. Havrilla GJ, Green RB (1980) Anal Chem 52:2376–2383
16. Havrilla GJ, Green RB (1981) Anal Chem 53:134–135
17. Havrilla GJ, Weeks SJ, Travis JC (1982) Anal Chem 54:2566–2570
18. Havrilla GJ, Schenck PK, Travis JC, Turk GC (1984) Anal Chem 56:186–193
19. Human HGC, Omenetto N, Cavalli P, Rossi G (1984) Spectrochim Acta 39B:1345–1363
20. Hurst GS, Nayfeh MH, Young JP (1977) Phys Rev A15:2283–2292
21. Miziolek AW, Willis RJ (1981) Opt Lett 6:528–530
22. Omenetto N, Winefordner JD (1979) Prog Anal At Spectrosc 2:1–183
23. Omenetto N, Berthoud T, Cavalli P, Rossi G (1985) Appl Spectrosc 39:500–503
24. Omenetto N, Smith BW, Hart LP, Cavalli P, Rossi G (1985) Spectrochim Acta B, 40B:1411–1422
25. Omenetto N, Berthoud T, Cavalli P, Rossi G (1985) Anal Chem 57:1256–1261
26. Schenck PK, Hastie JW (1981) Opt Eng 20:522–528
27. Smith BW, Hart LP, Omenetto N (1985) to be published
28. Smyth KC, Schenck PK, Mallard WG (1980) ACS Symposium Series, No. 134, Laser probes for combustion chemistry, Crosley DR, (ed), Washington DC USA
29. Travis JC, Schenck PK, Turk GC, Mallard WG (1979) Anal Chem 51:1516–1520
30. Travis JC (1982) J Chem Educ 59:909–914
31. Travis JC, Turk GC, Green RB (1982) Anal Chem 54:1006A–1018A
32. Travis JC, Turk GC, De Voe JR, Schenck PK, Van Dijk CA (1984) Prog Anal At Spectrosc 7:199–241
33. Trask TO, Green RB (1983) Spectrochim Acta 38B:503–517
34. Turk GC, Travis JC, De Voe JR, O'Haver TC (1978) Anal Chem 50:817–820
35. Turk GC, Travis JC, De Voe JR, O'Haver TC (1979) Anal Chem 51:1890–1896
36. Turk GC, Mallard WG, Schenck PK, Smyth KC (1979) Anal Chem 51:2408–2410
37. Turk GC (1981) Anal Chem 53:1187–1190
38. Turk GC, De Voe JR, Travis JC (1982) Anal Chem 54:643–645
39. Turk GC, Walters RL Jr (1985) Anal Chem 57:1979–1983
40. Van Dijk CA, Alkemade CThJ (1980) Comb Flame 38:37–49
41. Van Dijk CA, Curran FM, Lin KC, Crouch SR (1981) Anal Chem 53:1275–1279
42. Wiese WL, Smith MW, Miles BM (1969) Atomic transition probabilities, NSRDS-NBS22, Washington DC USA
43. Zizak G, Omenetto N, Winefordner JD (1984) Opt Eng 23:749–755

Received November 1, 1985

Reprinted from Analytical Chemistry, 1985, 57, 1256.

Analytical Laser Enhanced Ionization Studies of Thallium in the Air–Acetylene Flame

Nicolo' Omenetto,* Thierry Berthoud,[1] Paolo Cavalli, and Guglielmo Rossi

Joint Research Centre, Chemistry Division, Ispra (Varese), Italy

Analytical studies are presented for the determination of thallium at ultratrace levels in the air–acetylene flame by means of laser enhanced ionization spectrometry. Two excimer-pumped tunable dye lasers were used. Several transitions were investigated and compared in terms of detection limits. An enhancement factor of 38 was obtained by exciting at 291.832 nm and using a second photon at 377.572 nm or at 276.787 nm to indirectly increase the population of the metastable $^2P_{3/2}$ level. At a repetition frequency of 50 Hz and with optimized filtering, the detection limit was found to be 8 pg/mL, therefore showing that the flame rivals the detection power achievable only by the use of electrothermal atomization. The technique has been applied to the direct determination of sub-microgram-per-gram concentration levels of thallium in three commercial lead samples.

Thermally assisted ionization from excited states occurs in flames at atmospheric pressure whenever a laser tuned at appropriate optical atomic transitions is capable of exciting a significant fraction of atoms into these states. The detection of the resulting current forms the basis of a very sensitive technique for trace analysis variously called "laser enhanced ionization" (LEI), "optogalvanic spectrometry", or simply "laser atomic ionization" (*1–5*). This new method of chemical analysis, in addition to sharing some common advantages of the other flame spectrometric methods, possesses a few unique features such as the complete freedom from any scattering and stray light problems.

The thorough investigation of the analytical potential of this technique, pioneered and carried out at the National Bureau of Standards (*1*), had led to the attainment of very low detection limits, from nanograms per milliliter to picograms per milliliter, the key point being that, for several elements, flame atomization could then rival electrothermal atomization.

The major emphasis in the studies carried out so far in the literature has been directed toward the understanding of the basic principles of the technique, namely, the characterization of the electric field distribution in the flame, the optimization of the electrode(s) geometry, and the evaluation of the so-called electrical interferences which are important whenever an easily ionized concomitant present in the sample solution modifies the field distribution.

A significant improvement in both sensitivity and spectral selectivity was achieved by using the two-color or two-wavelength excitation provided by two lasers tuned at two optical transition sharing a common intermediate level (*6*).

The aim of this paper is 2-fold. First, the LEI technique is characterized for the determination of thallium in the air–acetylene flame by using both one- and two-color excitation provided by two excimer-pumped pulsed dye lasers. Secondly, the technique is applied to the direct determination of this element at the sub-microgram-per-gram level in commercial lead samples.

[1] DCAEA/SEA/SEACC, Fontenay-aux-Roses, France.

THEORETICAL CONSIDERATIONS

The different parameters involved in the excitation of atoms to a specific level and the subsequent formation and collection of charges have been amply described and discussed in the past (*7*) as well as more recent (*8*) literature. The following considerations are therefore not new and are only meant to provide a basis for the understanding of the experimental tests made on the different thallium transitions described later. By referring to Figure 1, we consider two different excitation transitions between lower levels, designated as l′ and l (l′ < l, l′ being not necessarily the ground state of the atom), and two upper levels designated as u′ and u (u′ < u). Although ionization does not simply proceed by a *single* collision transferring atoms from level u to the continuum state i, we assume that there is a fast collisional redistribution among excitation levels lying between u and i and therefore the cross section and rate coefficients given below should be interpreted as *effective* quantities relating to such a multitude of levels (*9*).

The probability, P_i^*, that a given collision will produce ionization from the excited level u is given by

$$P_i^* = \exp[-(E_i - E_u)/kT] \quad (1$$

where E_i and E_u are the ionization and excitation energies (eV or cm^{-1}), respectively; k is the Boltzmann constant (8.62×10^{-5} eV K^{-1} or 0.695 cm^{-1} K^{-1}), and T is the temperature of the air–acetylene flame (~2500 K). It is worth stressing (*1, 2*) that the probability of ionization increases by about 2 orders of magnitude for each electronvolt of excitation.

The rate coefficient, k_{ui} (s^{-1}), for the production of ions from level u by collision with a specific flame constituent j is given by the relationship

$$k_{ui} = \bar{v}\sigma_j n_j P_i^* \quad (2$$

where $\bar{v}$ (cm s^{-1}) is the mean relative velocity of the atom and the colliding species, σ_j (cm^2) is the cross section for the process, and n_j (cm^{-3}) is the number density of the colliding species j.

When the excited levels u′ and u are considered and if it is assumed that σ_j does not change, then the ratio of the ionization rate coefficients will be given by

$$\frac{k_{ui}}{k_{u'i}} = \exp[(E_u - E_{u'})/kT] \quad (3$$

Assuming that the rate of depletion of level u by ionizing collisions is small compared to τ_u^{-1}, where τ_u is the optical lifetime of level u, which includes both radiative and collisional deexcitation, the LEI signal from the upper level u will be obtained by integrating over time the rate of ion production. Such rate is given by the product $n_u k_{ui}$, where n_u is the steady-state atom population density of level u. Such population, in the limit of the two-level approximation, by assuming a broad band laser excitation and equal statistical weights of the lower and upper levels, i.e., $g_l = g_u$, is in turn given by (*5, 10*)

$$n_u = \frac{(n_l + n_u)}{2} \frac{E_s(\nu_{lu})}{E_s(\nu_{lu}) + E_s^*(\nu_{lu})} \quad (4a$$

0003-2700/85/0357-1256$01.50/0

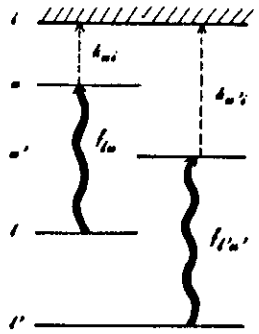

Figure 1. Schematic representation of the energy level scheme used in the theoretical considerations given in the text. See text for the explanation of the symbols.

where $n_l + n_u = n_T$ is the total population of the two levels and can be approximated to n_l^{th}, i.e., to the thermal population of level prior to laser irradiation, $E_s(\nu_{lu})$ is the laser spectral irradiance at ν_{lu} (J s^{-1} cm^{-2} Hz^{-1}), and E_s^* is the saturation parameter of the transition, i.e., it is the value of the laser spectral irradiance producing half of the maximum (saturated) fluorescence signal.

Assuming strict linearity in the interaction, i.e., $E_s(\nu_{lu}) \ll E_s^*(\nu_{lu})$ and making use of the definition of $E_s^*(\nu_{lu})$ (*9, 10*), eq 4 reduces to

$$n_u \propto n_l^{th} E_s(\nu_{lu}) A_{ul} \tau_u \quad (4a)$$

where A_{ul} is the spontaneous transition probability (s^{-1}) and is related to f_{lu}, the absorption oscillator strength of the transition, by the known classical relationship (cgs units) (*9*)

$$f_{lu} = 1.50 \lambda_{ul}^2 A_{ul} \quad (4b)$$

where again the statistical weights of the lower and upper levels are considered to be equal. On other hand, when $E_s(\nu_{lu})$ is (much) greater than $E_s^*(\nu_{lu})$, eq 4 reduces to

$$n_u = \frac{n_l + n_u}{2} \propto \frac{n_l^{th}}{2} \quad (4c)$$

Obviously, the thermal population of different lower levels will scale to each other according to the Boltzmann distribution so that (see Figure 1)

$$\frac{n_l^{th}}{n_{l'}^{th}} = \frac{g_l}{g_{l'}} \exp[-(E_l - E_{l'})/kT] \quad (5)$$

If one then finally considers two excitation transitions starting from two different lower levels and reaching two different upper levels, whose lifetimes are assumed to be the same, the ratio of the ionization signals expected will be given by a straightforward combination of eq 1–5, i.e., for linear interaction, by the relationship

$$\frac{(\mathrm{LEI})\lambda_{lu}}{(\mathrm{LEI})\lambda_{l'u'}} = \left[\frac{f_{lu}\lambda_{ul}^2}{f_{l'u'}\lambda_{u'l'}^2}\right]\left[\frac{E_s(\nu_{lu})}{E_s(\nu_{u'l'})}\right]\left[\frac{g_l}{g_{l'}} e^{-[(E_l - E_{l'})/kT]}\right][e^{(E_u - E_{u'})/kT}] \quad (6)$$

The first factor in the right hand side of eq 6 is the "absorption strength factor" and is an intensive property of the atom considered. The second factor is a "source pumping factor" and depends upon the laser irradiance achievable at the transition investigated. The third factor is a "thermal population factor" which accounts for the population difference of the absorbing level, and the final factor is the "ionization probability factor". It would therefore be a simple matter to use eq 6 in order to predict the best transition to be chosen for single-color laser-enhanced ionization. At saturation, only the last two factors on the right hand side of eq 6 are retained. It is worth remembering, however, that it is easier to saturate a transition characterized by a high value of the absorption oscillator strength.

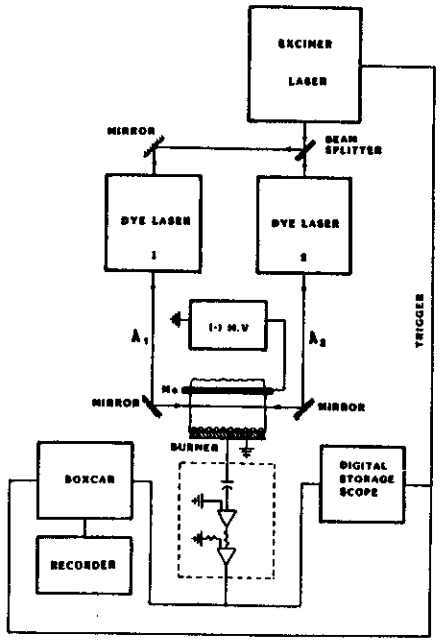

Figure 2. Layout of the experimental setup used.

In the use of two-color ionization, the two transitions usually share a common level, i.e., the second laser photon starts its pumping action from the level reached with the first photon (*6*). In Figure 1, this would mean that u′ = l. In such a case the two beams need to be temporally coincident at the atomizer since the lifetime of the excited levels is usually very short in flames at atmospheric pressure, as indeed observed in ionization experiments with sodium (*11*). The two-wavelength enhancement in the ionization signal as compared to that given by single-wavelength ionization can however be achieved even if u′ ≠ l, provided that the two levels are collisionally and/or radiatively coupled. Therefore, if level u′ is populated with one laser tuned at $\lambda_{l'u'}$ and then atoms can rapidly be transferred to level l, a second laser tuned at λ_{lu} will interact, *within* the lifetime of level l, with an increased atomic population and an enhancement will still be predicted to occur. Indeed, the experimental decay of the enhanced ionization signal observed when the laser photon at λ_{lu} is delayed by various amounts with respect to that at $\lambda_{l'u'}$ can be successfully used to evaluate the lifetime of level l (*12*).

EXPERIMENTAL SECTION

The experimental setup is schematically shown in Figure 2. An excimer laser operated on XeCl at 308 nm (Model EG 102, Lambda Physik, Göttingen, Federal Republic of Germany) was

Table I. Evaluation of the Noise Components in the Experimental Setup Used

excimer laser	dye laser 1	dye laser 2	electrode high voltage	flame	peak-to-peak noise, mV
off	off	off	off	on	a
off	off	off	on	on	1.5
on	off	off	off	on	1.5
on	off	off	on	on	6
on	on	on	on	on	6

[a] Not detectable.

Table II. Effect of Laser Beam Diameter and of Double Passing throughout the Flame

experimental condition	ionization signal,[a] au
without beam expander, single pass	1.50
beam expander (×5), single pass	4.84
beam expander (×5), double pass	9.30

[a] Thallium concentration, 10 ng/mL.

used to pump simultaneously two dye lasers (Jobin Yvon, Longjumeau, France) whose output beams were directed collinearly throughout the flame. The excitation pulses (~5 ns) were provided by the fundamental output of a BBQ dye solution (377.572 nm) and by frequency doubling the outputs of the Rhodamine 590 Chloride and Coumarine 540A dye solutions (291.832 nm and 276.787 nm, respectively). The dyes were supplied by Exciton (Dayton, OH) and dissolved in spectroscopically pure methanol or in an ethanol/toluene mixture (Merck, Darmstadt, Federal Republic of Germany). The laser output power was monitored by a volume absorbing calorimeter (Model 38-0101, Scientech, Boulder, CO). In the experiments using single-wavelength excitation, a beam expander and a mirror behind the flame (not shown in Figure 2) were also used with the purpose of increasing the ionization signal and consequently the power of detection. The LEI apparatus was that described by Berthoud et al. (*11*) and manufactured by SOPRA (Bois Colombes, France), consisting of a water-cooled molybdenum electrode (*13*) immersed in an air–acetylene flame supported on a three-slot burner head. The high voltage (−1600 V) was applied between the electrode and the burner body. Both current and voltage amplifiers were used to extract the signal which was then directly fed into a digital storage oscilloscope (Model 468, Tektronix, Beaverton, NJ) and/or into a boxcar integrator (Model 162-165, Princeton Applied Research, Princeton, NJ), the averaged output being finally displayed on a strip chart recorder.

Standard solutions were prepared by suitable dilution of thallium stock solution (1000 μg/mL in 1 M HNO_3) with high-purity deionized water.

RESULTS AND DISCUSSION

It was felt useful at first to identify the limiting noise of our experimental setup, since ideally this noise should be the shot component of the flame background current. To this purpose, a set of experiments were carried out in a sequence suitable to isolate one noise component from the other. The peak to peak values read on the oscilloscope were then displayed on the strip chart recorder. The results of these experiments are collected in Table I. As one can see, our limiting noise was due to radio frequency pickup from the excimer laser once the high voltage in the flame was switched on. This noise did not increase when both laser beams were tuned at the appropriate thallium lines and water was aspirated into the flame.

The variation in the ionization signal obtained by expanding the laser beam diameter and reflecting it back into the flame is summarized in Table II. As seen here, whenever the electrical field distribution across the flame is not modified

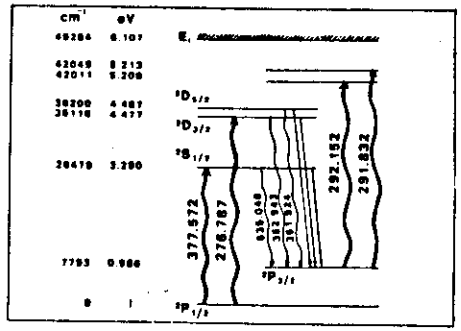

Figure 3. Partial energy level diagram for the thallium atom. Wavelengths are indicated in nanometers. Energies of the levels are indicated in inverse centimeters and electronvolts.

Table III. Comparison of LEI Signals Obtained for Several Single-Wavelength Excitation Schemes[a]

excitation wavelength, nm (energy, μJ)	E_e, eV	$E_i - E_e$, eV	P_i	population factor	LEI signal, au
276.787 (30)	4.477	1.630	5.5×10^{-4}	1	100
291.832 (120)	5.213	0.894	1.6×10^{-2}	2.3×10^{-3}	46.3
377.572 (1000)	3.280	2.827	2.2×10^{-4}	1	12.0
292.152 (120)	5.208	0.899	1.6×10^{-2}	2.3×10^{-3}	10.6

[a] Tl concentration, 5 ng/mL; assumed flame temperature, 2500 K.

by the introduction of the sample solution, a significant improvement is obtained. However, it should be borne in mind that the "electrical interferences" caused by an easily ionizable matrix (*1*) would in fact nullify this advantage.

The thallium transitions investigated are shown in Figure 3 where the pertinent partial atomic energy level scheme for the element is given. The results achieved with several one-wavelength excitations are collected in Table III. As shown, the best results were obtained with the excitation set at 276.787 nm, despite the fact that the laser energy at that wavelength was the lowest with respect to all the wavelength tested. As stated before, the comparison presented here has not be regarded as a quantitative verification of the theory but simply as a quick indicative approach to the choice of the most suitable excitation transition to be used in order to obtain the largest ionization signal. As an example, for the two transitions involving the ground state, i.e., 377.572 and 276.787 nm, the absorption oscillator strengths are known to be 0.3 and 0.7, respectively (*9*). It can therefore be predicted from eq 6 that in the linear approximation, the ionization signal after excitation at 276.787 nm would be approximately 17 times larger than that obtained after exciting at 377.572 nm, while this factor would increase to ~250 in the case of complete saturation. From the experimental data reported in Table III, it seems evident that saturation was not achieved at the lower excitation wavelength. Moreover, the theoretical considerations strictly assume the same homogeneous excitation volume in the flame which can certainly not be the case when comparing different dyes, especially in their fundamental and frequency doubled outputs. The steady-state conditions

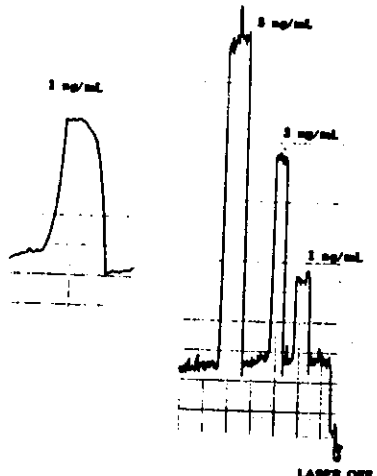

Figure 4. Recorder tracings obtained by using ground-state single-wavelength excitation at 276.787 nm. Thallium concentrations are as indicated. Laser wavelength is fixed.

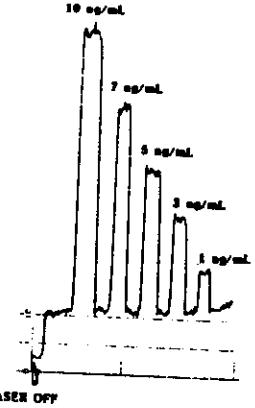

Figure 5. Recorder tracings obtained by using excited-state single-wavelength excitation at 291.832 nm. Thallium concentrations are as indicated. Laser wavelength is fixed.

might be warranted, however, by the high collision rate typical of the air–acetylene flame (*9*, *10*).

Figures 4 and 5 show the ionization signals obtained for low concentrations of thallium in slightly acidified aqueous solutions. The comparison between ground-state excitation (Figure 5) results in a factor of 2 difference in the size of the signal, as reported in Table III. A common important feature borne out in these figures is the laser-induced background ionization signal which clearly disappears when the laser beam is blocked. This wavelength-independent background signal, which can originate from several sources, including multiple photon ionization (*1*), needs to be taken into account for accurate analysis. One could then determine this background by tuning the laser at a fixed position off-resonance or, better, by scanning the laser excitation throughout the analyte absorption profile in the flame. One can also see from the figures that, as expected, the linearity of the technique at these low

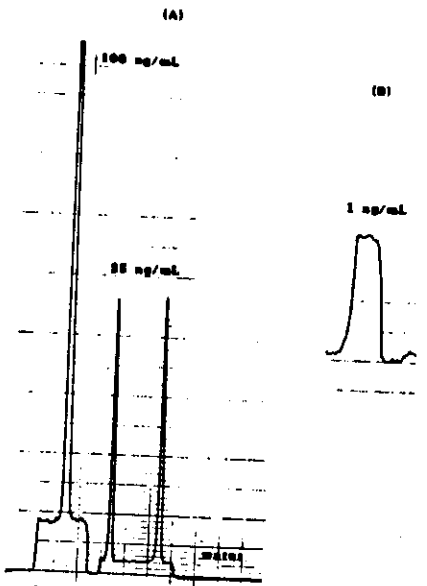

Figure 6. Recorder tracings obtained by using two-wavelength stepwise excitation at 377.572 nm and at 291.832 nm: (A) laser excitation at 291.832 nm fixed, laser excitation at 377.572 scanned throughout the absorption profile; (B) typical signal at the 1 ng/mL level, laser wavelengths fixed.

Table IV. Determination of Thallium in Commercial Lead Metal Samples

sample type	Tl content, μg/g: this work[a]	Tl content, μg/g: av value[b]
electrolytically refined	2.39 ± 0.23	2.61 ± 0.12
thermally refined	0.78 ± 0.09	0.73 ± 0.05
lead with added impurities	2.33 ± 0.22	2.27 ± 0.11

[a] Mean value of three independent determinations. [b] As obtained from eight independent laboratories.

concentration levels is acceptable, apart from a blank problem in the preparation of the solutions. As an illustration of the detection limit achievable with single-wavelength excitation, Figure 4 shows an example of the ionization signal obtained by increasing the time constant of the detection system to approximately 10 s. A statistical evaluation of the noise in the blank results in a 3σ detection limit of approximately 0.02 ng/mL. However, this time constant is not practical for analytical work due to the large sample consumption in the flame.

As reported by Turk et al. (*6*), the two-wavelength excitation scheme is most attractive not only because of the enhancement in the signal level and in the spectral selectivity but also because of the corresponding relative decrease in the spurious background signal. In the case of thallium, the enhancement predicted in the theoretical consideration was demonstrated by tuning one laser at 377.572 nm and the other at 291.832 nm, i.e., taking advantage of the increased population of the metastable level $^2P_{3/2}$ caused by both radiative and collisional decay processes (see Figure 3). In this way, an enhancement factor of 38 was experimentally observed. This enhancement was not accompanied, however, by a similar increase in the

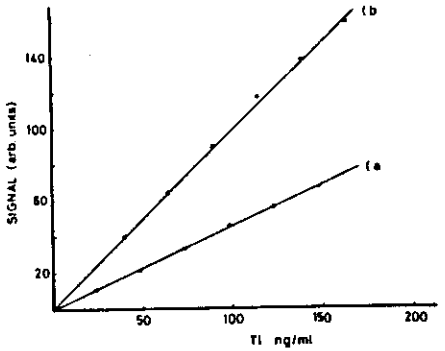

Figure 7. Calibration graphs obtained by positioning the measuring gate (50 ns duration) at the peak of the ionization pulse: (a) aqueous thallium solutions; (b) thallium in the matrix solutions.

signal to noise ratio. In addition, it was noticed that by scanning one laser in the immediate vicinity of the absorption transition, an off-resonance background could still be measured, the signal being proportional to the concentration of thallium (see Figure 6A). This result is likely due to the single-wavelength ionization process occurring since one laser remains tuned at 291.832 nm. In this case, no background correction would be necessary. A typical signal-to-noise ratio obtained for 1 ng/mL of thallium with this excitation scheme is shown in Figure 6B. Here the repetition frequency of the laser was increased to 50 Hz so that the overall time constant of the measurement was maintained within approximately 1 s. By a careful optimization of the laser parameters and of the amplifier-detection system, at detection limit of 8 pg/mL could be calculated. This limit not only improves the limit of 90 pg/mL previously obtained by flame laser enhanced ionization (3) but is considerably better than the value of 100 pg/ml quoted for electrothermal atomization by introducing 100 μL of solution into the furnace (*14*).

The experimental results achieved for aqueous thallium solutions allow us to conclude that, for single- as well as for two-wavelength excitation, the sensitivity achieved in the air–acetylene flame does indeed rival that typical of electrothermal atomization techniques.

Determination of Thallium in Commercial Lead Samples. The applicability of the above-mentioned features was checked in the direct determination of thallium at the submicrogram-per-grams level in three commercial metal lead samples, BCR candidate reference materials, to be certified for a number of trace elements, and specially pepared in the form of chips for the analytical round robin. More detailed information on these samples, their preparation and the certification procedure can be obtained from the Community Reference Bureau, Commission of the European Communities, DG XII, 200, rue de la Loi, Bruxelles, Belgium. Because of its high ionization potential, lead is not expected to create any serious electrical interference when a 1% solution is aspirated in the flame. The sample (1 g) was dissolved in high-purity nitric acid, diluted to 100 mL, and then aspirated in the flame. Because of the difficulty of obtaining lead samples free of thallium and because of the high solid content of the solutions aspirated into the flame, the standard addition method was chosen in order to obtain accurate results. These are collected in Table IV.

The analysis was performed by a two-wavelength excitation scheme using as a first step the transition at 377.572 nm, since this wavelength was available without the necessity of frequency doubling the dye laser output and therefore could be easily scanned by rotating the grating with a stepping motor. The second laser photon was tuned at 291.832 nm. The distance between the burner head and the cathode was set at 20 mm.

When a boxcar averager is used to process the ionization pulse, it is worth stressing here that the relative widths of the gate and of the ionization pulse must be accurately known and controlled during the measurements. Indeed, it is known that the pulse shape modifies when the aqueous analyte solutions are replaced by the matrix solutions, the effect being dramatic for easily ionizable matrices (*9*, *11*, *15*). Even in the case of our lead matrix, some effect is present and the pulse shape becomes narrower when the aqueous thallium solution is replaced by the lead matrix solution. If the width of the gate is smaller than that of the ionization pulse (which is approximately 200 ns), then different signals (and consequently different slopes of the calibration graphs) will be obtained for different positions of the gate under the signal pulse. This is clearly borne out experimentally in Figure 7 where a graph obtained for aqueous thallium solutions is compared with that obtained in the presence of the lead matrix. In both cases, the gate (50 ns) position was optimized to obtain the maximum signal. It is therefore clear that, in order to obtain accurate results, the gate position should be kept constant in time during the measurements. The alternative would be to use a gate width large enough so to average the entire ionization pulse.

CONCLUSIONS

Several conclusions can be derived from the study presented here and are summarized below:

(i) The laser-enhanced ionization technique is extremely sensitive for the determination of thallium in the air–acetylene flame, the detection limit obtained being better than that given by electrothermal atomization techniques.

(ii) The two-wavelength excitation scheme can be effectively used even when the two transitions do not share a common level.

(iii) Because of the existence of a wavelength-independent ionization background, which can vary with the composition of the matrix, a background correction procedure is mandatory. This can be performed by scanning the laser excitation throughout the atomic absorption profile.

(iv) The modification of the ionization pulse due to the presence of the matrix in the flame requires rigorous control of the measuring gate width and position under the pulse in order to obtain accurate results.

(v) The direct determination of thallium in high ionization potential matrices is indeed feasible with remarkable good accuracy in an air–acetylene flame at concentration levels of 0.02 μg/g.

Registry No. Tl, 7440-28-0; Pb, 7439-92-1.

LITERATURE CITED

(1) Travis, J. C.; Turk, G. C.; Green, R. B., *Anal. Chem.* **1982**, *54*, 1006A–1018A.
(2) Travis, J. C. *J. Chem. Educ.* **1982**, *59*, 909–914.
(3) Travis, J. C.; Turk, G. C.; DeVoe, J. R.; Schenck, P. K.; Van Dijk, C. *A. Prog. Anal. At. Spectrosc.* **1984**, *7*, 199.
(4) Chaplygin, V. I.; Zorov, N. B.; Kuzyakov, Yu. Ya. *Talanta* **1982**, 505–508.
(5) Camus, P., Ed. *J. de Phys.* **1983**, *44*, "Optogalvanic Spectroscopy and Its Applications"; Colloque C7, supplément au no. 11.
(6) Turk, G. C.; DeVoe, J. R.; Travis, J. C. *Anal. Chem.* **1982**, *54*, 643–645.
(7) Travis, J. C.; Schenck, P. K.; Turk, G. C.; Mallard, W. G. *Anal. Chem.* **1979**, *51*, 1516–1520.
(8) Axner, O.; Berglind, T.; Heully, J. L.; Lindgren, I.; Rubinaztein-Dunlop, H. *J. Appl. Phys.* **1984**, *55*, 3215.
(9) Alkemade, C. Th. J.; Hollander, T.; Snelleman, W.; Zeegers, P. J. Th. "Metal Vapours in Flames"; Pergamon Press: New York, 1982.
(10) Omenetto, N.; Winefordner, J. D. *Prog. Anal. At. Spectrosc.* **1979**, *1–2*.

(11) Berthoud, T.; Lipinsky, J.; Camus, P.; Stehle, J. L. *Anal. Chem.* **1983**, *55*, 959.
(12) Omenetto, N.; Berthoud, T.; Cavalli, P.; Rossi G. *Appl. Spectrosc.*, in press.
(13) Turk, G. C. *Anal. Chem.* **1981**, *53*, 1187–1190.
(14) Perkin-Elmer commercial literature, Jan 1982.
(15) Havrilla, G. J.; Schenck, P. K.; Travis, J. C.; Turk, G. C. *Anal. Chem.* **1984**, *56*, 188–193.

RECEIVED for review October 26, 1984. Accepted January 28, 1985.

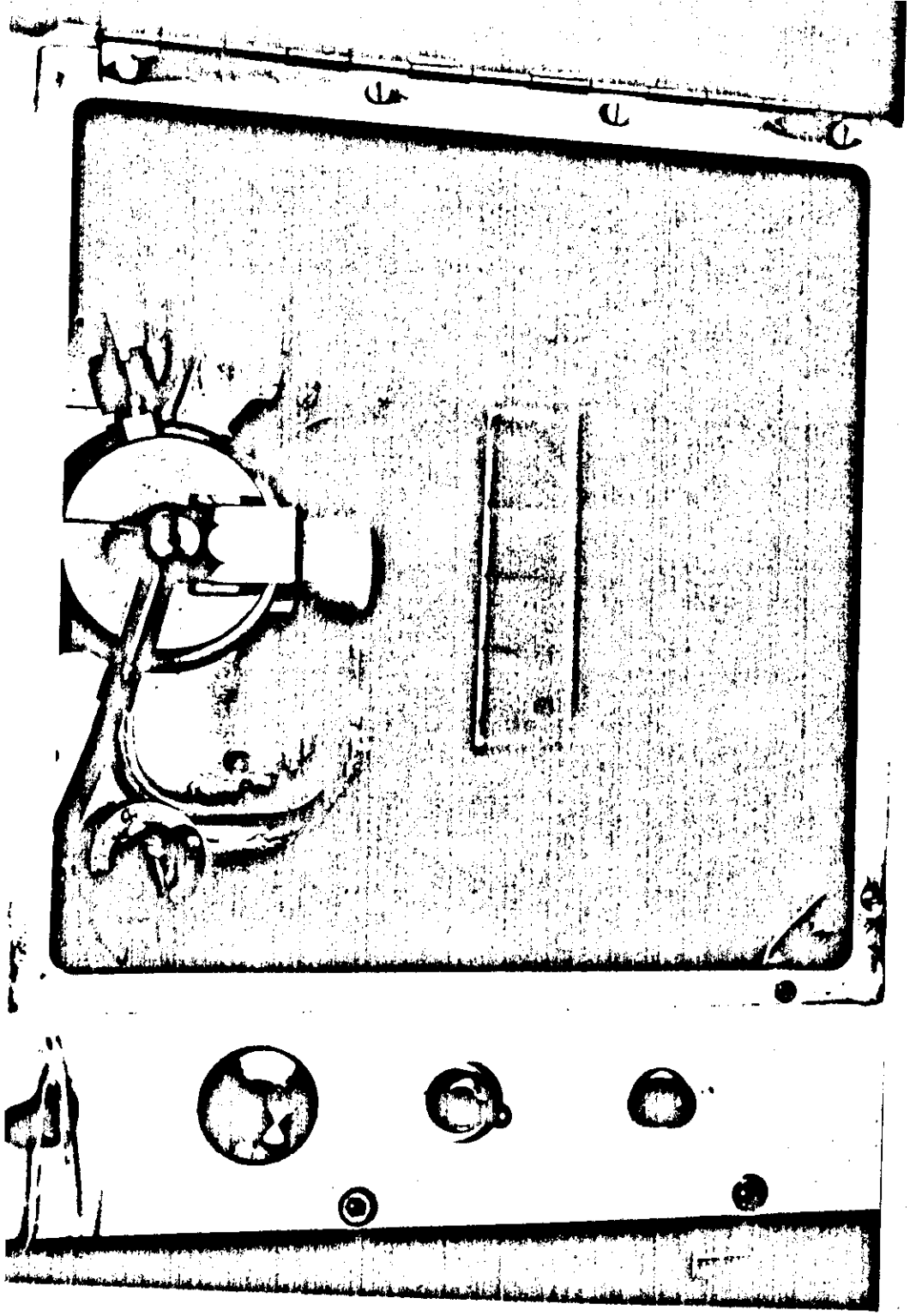

Spectrochimica Acta, Vol. 40B, Nos 10–12, pp. 1637–1649, 1985.
Printed in Great Britain.

0584–8547/85 $3.00 + .00

Laser induced stepwise and two-photon ionization studies of strontium in the air acetylene flame

L. P. HART,* B. W. SMITH* and N. OMENETTO
Joint Research Centre, Chemistry Division, Ispra, Varese, Italy

(*Received April* 1985; *in revised form July* 1985)

Abstract—Using strontium atoms present as a trace constituent in an air–acetylene flame as an example, a rich laser enhanced ionization spectrum was obtained. One pulsed tunable dye laser was tuned to a transition originating from the ground state (460.73 nm) and another scanned over different spectral regions. The lines obtained were spectroscopically characterized as to the type of absorption process, which included non-resonant processes as well as single wavelength, two-wavelength, and two-photon resonant processes.

With a maximum irradiance of 100 MW cm^{-2}, two-photon transitions resulting in collisionally assisted ionization included the 5*sns* and 5*snd* Rydberg series (up to 37*s* and 15*d*) together with a strong auto-ionizing transition at 431.10 nm. The complexity of the observed ionization spectrum when the irradiance is high indicates that spectral interferences need to be carefully considered in analytical applications.

1. INTRODUCTION

LASER enhanced ionization (LEI) spectroscopy in atmospheric pressure flames has been the subject of many investigations [1, 2]. A major emphasis has been on the analytical potential of the technique, as characterized by detection limits in aqueous solutions; for a significant number of elements these equal or are better than those achieved by optical techniques with electrothermal atomization. Stepwise excitation, followed by collisional ionization has extended the analytical application of the technique to elements of high ionization potential, and also improved its spectral selectivity [3, 4]. The wavelength of one laser beam is resonant with a transition from the ground state; the other beam, temporally and spatially coincident with the first, and tuned to a resonant transition from the level populated by the first beam, can efficiently promote atoms to electronic levels close to the ionization potential. These levels are then subject to rapid collisional ionization in the flame with a spectacular increase in the sensitivity compared to single wavelength ionization.

When the laser spectral irradiance is sufficiently high, multi-photon ionization can also occur. In that case, an excited, bound state is reached by the simultaneous absorption of two (or more) laser photons via an intermediate virtual level(s). The difference between the two-step double resonance or two wavelength absorption and the two photon absorption process is shown in Fig. 1. The second step in the two step process can originate from the same level as reached by the first step, or from nearby levels collisionally populated. The two-photon process has different angular selection rules [5]. In the case of the strontium atom the initial state has $J = 0$, and the linearly polarized laser used here can populate final states with $J = 0$ or $J = 2$ with two-photon absorption [6]; the two-step process proceeds through one or more intermediate levels, for which $\Delta J = \pm 1$ for the optical transition.

In the analytical application of stepwise ionization in flames the enhancement of the

This paper is dedicated to Professor V. A. Fassel.
*On leave from the Department of Chemistry, University of Florida, Gainesville, FL, U.S.A.

[1] J. C. TRAVIS, G. C. TURK, J. R. DE VOE, P. K. SCHENCK and C. A. VAN DIJK, *Prog. Anal. Atom. Spectrosc.*, 7, 199 (1984), and references therein cited.
[2] P. CAMUS (ed.), Optogalvanic spectroscopy and its applications, *J. Physique*, Colloque C7, Suppl. au No. 11. Les Editions de Physique, Les Ulis Cedex, France (1983).
[3] G. C. TURK, J. R. DE VOE and J. C. TRAVIS, *Anal. Chem.* 54, 643 (1982).
[4] C. A. VAN DIJK, F. M. CURRAN, K. C. LIN and S. R. CROUCH, *Anal. Chem.* 53, 1275 (1981).
[5] R. B. BIRGE, One photon and two-photon excitation spectroscopy, in Ed. D. S. KLIGER, *Ultrasensitive Laser Spectroscopy*, Chap. 2. Academic Press, New York (1983).
[6] P. ESHERICK, *Phys. Rev.* 15A, 1920 (1977).

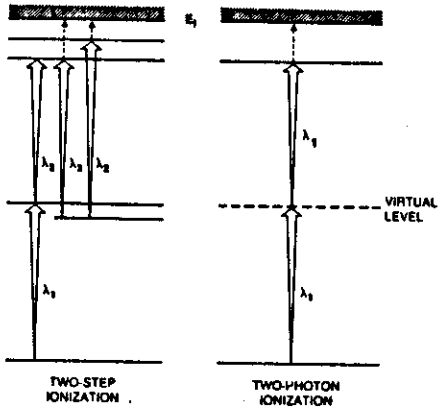

Fig. 1. Energy schemes for the two-step and two-photon absorption processes. Collisionally assisted ionization is indicated.

analytical signal and the consequent improvement of the detection limits attainable has been considered [3, 4, 7, 8]; only in the case of sodium was the ionization spectrum characterized [9]. During our study of stepwise ionization of several elements in the air–acetylene flame [10], many transitions were observed which were not among those listed in standard references [11]. Some of the lines observed could be attributed to a two-photon rather than a stepwise excitation process. It was therefore felt important to better characterize the ionization spectrum and to identify the important ionization processes in the flame when using two wavelength excitation. The ionization spectrum of Sr was studied since the stepwise and multiphoton processes [12–19], as well as the stepwise fluorescence [20, 21], have been well characterized for Sr vapour at 300°C in 1 torr of noble gas.

For purposes of clarity, the ionization process can be named according to the different types of the primary absorption processes. Three types of processes have been distinguished in analytical LEI spectroscopy [1, 7–9, 22]:

(i) *Double resonance* or *two-step* (*two-wavelength*) ionization, resulting from the absorption of photons at two different wavelengths, provided by two different lasers;

(ii) *Two-photon* ionization, resulting from the simultaneous absorption of two identical photons, provided by a single laser, of energy equal to (1/2) E_{exc}, where E_{exc} is the excitation energy of the level. Excitation proceeds via a *virtual* level located at (1/2) E_{exc};

[7] N. OMENETTO, T. BERTHOUD, P. CAVALLI and G. ROSSI, *Anal. Chem.* 57, 1256 (1985).
[8] F. M. CURRAN, K. C. LIN, G. E. LEROI, P. M. HUNT and S. R. CROUCH, *Anal. Chem.* 55, 2382 (1983).
[9] C. A. VAN DIJK, Two-photon excitation of higher sodium levels and population transfer in a flame Ph.D. Dissertation, University of Utrecht, (1978).
[10] N. OMENETTO, B. W. SMITH and L. P. HART, *Fresenius Z. Anal. Chem.*, in press.
[11] C. H. CORLISS and W. R. BOZMAN, Experimental transition probabilities for spectral lines of seventy elements, NBS Monograph 53, Washington, D.C. (1962).
[12] P. EWART and A. F. PURDIE, *J. Phys.* 9B, L437 (1976).
[13] W. E. COOKE, T. F. GALLAGHER, S. A. EDELSTEIN and R. M. HILL, *Phys. Rev. Lett.* 40, 178 (1978).
[14] C. H. SKINNER, *J. Phys.* 13B, 55 (1980).
[15] W. R. S. GARTON and K. CODLING, *J. Phys. B*, Ser. 2, 1, 106 (1968).
[16] W. E. COOKE and T. F. GALLAGHER, *Opt. Lett.* 4, 173 (1979).
[17] S. L. CHIN, D. FELDMANN, J. KRAUTWALD and K. H. WELGE, *J. Phys.* 14B, 2353 (1981).
[18] C. J. LORENZEN and K. NIEMAX, *Opt. Comm.* 43, 26 (1982).
[19] C. BRECHIGNAC and P. CAHUZAC, *Opt. Comm.* 43, 270 (1982).
[20] W. GORNIK, *Z. Physik* 283A, 231 (1977).
[21] A. L. OSHEROVICH, Y. F. VEROLAINEN, S. A. PULKIN, V. I. PRIVALOV and S. M. LUPEKHIN, *Opt. Spektrosk.* 46, 243 (1979).
[22] C. TH. J. ALKEMADE, *Proc. XX CSI and 7th ICAS, Praha, Czekoslovakia* (1977).

(iii) *Single-step* (*single-wavelength*) ionization, resulting from the absorption of a photon from the ground state to a resonant bound level.

All the above processes involve collisional transfer of the atoms from an excited electronic level to the ionization limit. Collisions may also further contribute to the ionization signal either directly by the thermal population of a higher energy level from which a resonant photon is absorbed [1, 7] or by a collisionally induced absorption, in which a non-resonant photon is absorbed in the collisionally broadened wings of a transition and a second photon absorbed from that shifted broadened level [9, 22, 23]. In the air–acetylene flame, we observed lines in the ionization spectrum attributed to these absorption processes, as well as lines involving processes (i–iii) above.

2. APPARATUS AND TECHNIQUE

2.1. *Apparatus*

The laser enhanced ionization was observed using a cylindrical, water cooled, molybdenum electrode immersed in an air–acetylene flame supported on a three-slot burner head fitted on a conventional premix chamber with penumatic nebulization [7]. The optical system with two dye lasers pumped by one XeCl excimer laser, and the signal processing, with the boxcar amplifier connected to the output of the transimpedence pulse amplifier [7], were similar to that used for the study of double-resonance fluorescence in an ICP [24]. Signals reported correspond to the output of that fixed gain pulse amplifier. Laser energy was measured w th a volume absorbing calorimeter.

2.2. *Techniques*

For all measurements, the electrode was at −1300 V with respect to the burner head. A 5-mm aperture was used on either side of the flame for alignment purposes. For the two wavelength measurements, an aqueous solution of 100–500 ng ml^{-1} was aspirated into the flame and the single photon ionization signal used to tune one dye laser to the 460.733-nm line. This line was selected on the basis of its high transition probability relative to other resonant transitions from the ground state and suitability of use with a second visible wavelength to reach an energy level close to the ionization limit. The other dye laser was then scanned over the wavelength of interest using the appropriate dye. The optical delay line [24] was adjusted so that the pulses from the two beams, nearly co-linear and counter-propagating, were coincident temporally at the flame.

For the single wavelength measurements the laser used was focussed into the flame, using a 30-cm focal length lens, and reflected back using a convex mirror, to increase the irradiance. In this case, a 5 μg ml^{-1} solution was used because of the weaker signals.

Detection limits were obtained by dilution of the above solutions and calculated on the basis of twice the standard deviation of the blank signal.

Lines were identified using prominent tabulated lines as wavelength references [11], interpolating from the recorded spectrum to obtain the wavelength of the desired line, and comparing the corresponding energy with those one and two photon transitions observed at 10 torr and below, and reported by ESHERICK [6] and by EWART and PURDIE [12]. Good agreement was found between the wavelengths observed and those reported in the *MIT Tables* [25] as well those calculated from the available energy levels for the transitions identified [26], generally less than 0.3 Kaysers. The wavelengths given in the figures are either those observed in the d.c. arc [11] or calculated from the energy levels, for air.

3. RESULTS AND DISCUSSION

3.1. *Two-wavelength absorption spectra*

The results of scanning the second dye laser over several regions of interest are given in Figs 2–10. In these figures, most predominant lines are identified together with the corresponding excitation process shown in the partial energy level diagrams also given. As expected, the strongest laser enhanced ion zation signals correspond to transitions directly coupled to that

[23] N. OMENETTO, L. P. HART and B. W. SMITH, to be published.
[24] N. OMENETTO, B. W. SMITH, L. P. HART, P. CAVALLI and G. ROSSI, *Spectrochim. Acta B* 40B, 1411 (1985).
[25] G. R. HARRISON, *MIT Wavelength Tables*. Wiley, New York (1960).
[26] C. E. MOORE, *Atomic Energy Levels*, Volume II, NSRDS-NBS 35, Washington, D.C., (1971).

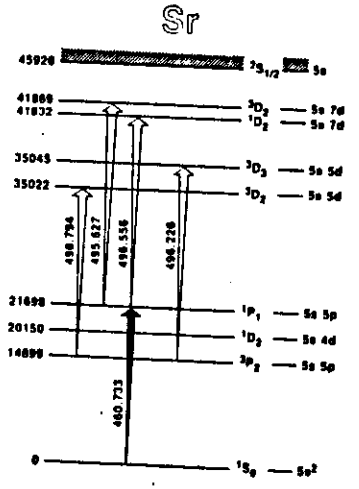

Fig. 2. Partial energy level diagram of the two-step absorption processes leading, via collisional excitation to the continuum, to the ionization spectrum shown in Fig. 3.

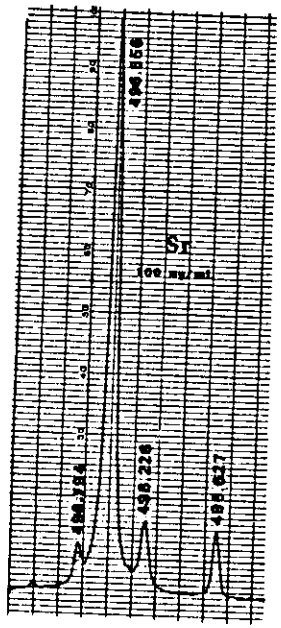

Fig. 3. Ionization spectrum with one laser at 460.733 nm and the other laser scanned over the transitions identified in Fig. 2. Sensitivity: 1V/full scale.

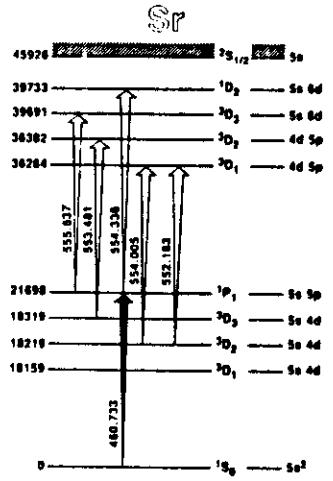

Fig. 4. Partial energy level diagram of the two-step absorption processes leading, via collisional excitation to the continuum, to the ionization spectrum shown in Fig. 5.

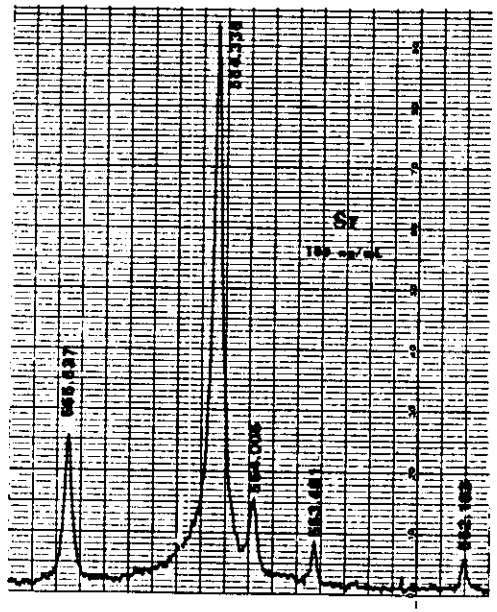

Fig. 5. Ionization spectrum with one laser at 460.733 nm and the other laser scanned over the transitions identified in Fig. 4. Sensitivity: 0.25 V/full scale.

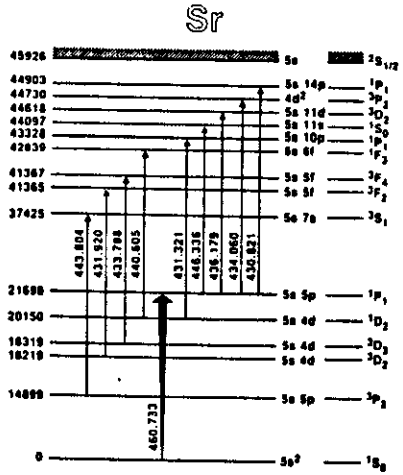

Fig. 6. Partial energy level diagram of the two-step absorption processes leading, via collisional excitation to the continuum, to the ionization spectrum shown in Figs 7 and 8.

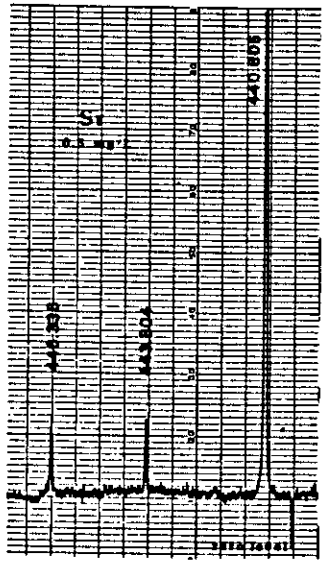

Fig. 7. Ionization spectrum with one laser at 460.733 nm and the other laser scanned over the transitions identified in Fig. 6. The Sr concentration is fivefold greater than in Figs 3 and 5. The difference in the underlying background continuum and the "zero level" is due to single-wavelength ionization at 460.733 nm. Sensitivity: 0.2 V/full scale.

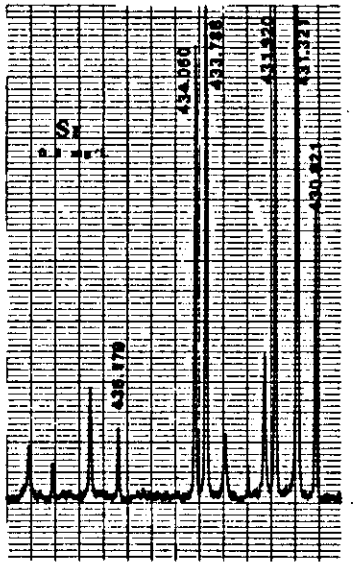

Fig. 8. Ionization spectrum with one laser at 460.733 nm and the other laser scanned over the transitions identified in Fig. 6. Only some of the more intense lines have been labeled. Sensitivity: 0.2 V/full scale.

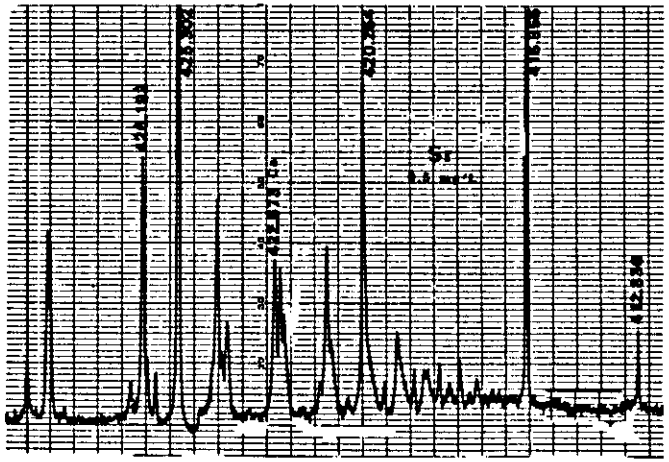

Fig. 9. Ionization spectrum with one laser tuned at 460.733 nm and the other laser scanned from 410 to 430 nm. Only some of more intense lines have been labeled. Sensitivity: 0.2 V/full scale.

level pumped by the other laser at 460.733. However, in the air–acetylene flame, even during the 5-ns duration of the second laser pulse, nearly coincident temporally with the first, there is sufficient collisional-coupling of the 5*p* singlet level with nearby levels to observe second-step

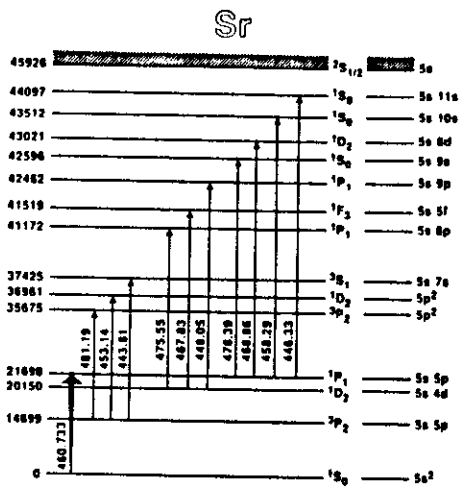

Fig. 10. Partial energy level diagram of the two-step absorption processes leading, via collisional excitation, to ionization. The relative intensities of the ionization signals observed for the transitions indicated here are reported in Table 1.

ionization signals from the 4*d* and the 5*p* triplet levels (see Figs 3, 5, 7, 8). Under these concentration and irradiances, *no signals were observed* when there was no 460.733 excitation step. Also, as expected and as indicated in Fig. 7, a background signal due to single-step ionization at 460.733 nm was always present.

As the shorter, higher energy, wavelengths are used for the second step, and the higher lying states, of which there are a larger number and which are closer to the ionization limit, are reached, many lines appear in the ionization spectrum, as shown in Figs 6–9. The signal at 422.673 nm in Fig. 9 was due to a calcium impurity in our solution and it was the only signal left when the same spectral scan was repeated without the 460.733-nm excitation step.

The relative intensities of the ionization signals obtained with the two-step excitation transitions schematized in Fig. 10 are reported in Table 1, together with the measured laser energies. On the basis of the energy diagram reported in Fig. 10, and assuming linearity in the interaction process, the line at 446.33 nm was expected to give the largest signal since it is directly coupled with the level reached by the first excitation step and it is closer than the other transitions shown to the ionization potential. However, the signal from this line was 1/2 of that for the 468.86-nm line with the same laser pump irradiance. These results then provide a qualitative indication of the relative absorption strength of the transitions identified in Fig. 10.

3.2. *Two-photon absorption spectra*

When only one laser is used, focussed and retroreflected, the maximum irradiance at the beam waist (~ 0.5 mm) is estimated to vary, depending upon the dye used, from 20 to 100 MW cm^{-2}, in which range two-photon transitions are easily observed. The line in the ionization spectrum resulting from the two-photon absorption at 459.513 nm, corresponding to the 5*s* to 10*s* transition, is close to that from absorption at 460.733 nm, corresponding to the 5*s* to 5*p* transition. Figure 11 clearly shows the differences between the two signals; the two-photon line is considerably narrower due to the square-law dependence on energy over the absorption width. A plot of the ionization signal vs laser energy, which was varied with neutral density filters, indeed shows the square-law dependence (Fig. 12).

In addition to the $J = 0$ transitions, for transitions from the 5*s* level to the 6*s* level up to 11*s*, shown in Fig. 13, additional lines in the wavelength range from 530 to 550 nm and from 410

Table 1. Relative intensity of two-step two-wavelength ionization signals for 100 ng ml^{-1} of strontium obtained with λ_1 fixed at 460.733 nm (500 μJ/pulse; transition saturated), and λ_2 scanned (440–490 nm)

Wavelength λ_2 (nm)	Transition and levels	Laser energy (μJ/pulse)	Ionization signal (mV)
443.81	$5s5p$–$5s7s$ $^3P_1$–$^3S_1$	240	26
446.33	$5s5p$–$5s11s$ $^1P_1$–$^1S_0$	390	58
448.05	$5s4d$–$5s9p$ $^1D_2$–$^1P_1$	500	176
453.14	$5s5p$–$5p^2$ $^3P_2$–$^1D_2$	800	67
458.29	$5s5p$–$5s10s$ $^1P_1$–$^1S_0$	1000	120
467.83	$5s4d$–$5s5f$ $^1D_2$–$^1F_3$	914	202
468.86	$5s5p$–$5s8d$ $^1P_1$–$^1D_2$	810	219
475.55	$5s4d$–$5s8p$ $^1D_2$–$^1P_1$	530	129
478.39	$5s5p$–$5s9s$ $^1P_1$–$^1S_0$	345	82
481.19	$5s5p$–$5p^2$ $^3P_2$–$^3P_2$	190	32

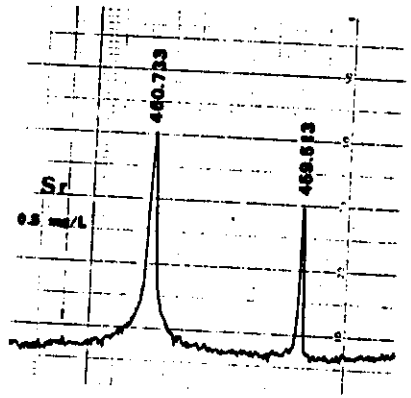

Fig. 11. Single-step vs two-photon excitation processes. The ionization signals shown are obtained by scanning a single laser focussed in the middle of the flame. Sensitivity: 0.2 V/full scale.

to 450 nm were observed and are shown in Figs 14–16. Some of the possible $J = 0$ and $J = 2$ two-photon transitions belonging to the Rydberg *ns* and *nd* series [6, 12] are labeled. As shown, the two-photon spectrum can be quite complex as the energies approach the ionization limit. The most striking spectral feature of Fig. 16 is the broad line at 431.10 nm, occurring *above* the ionization limit of the atom as indicated in the figure. As reported by ESHERICK [6] this line is due to a strong autoionizing resonance corresponding to a $J = 2$ state. Autoionizing resonances occur when both electrons are excited and the state reached is above the first ionization limit of the atom. This line is broad (~ 0.8 nm FWHM) when

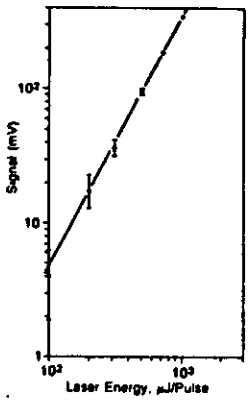

F g. 12. Double-logarithmic plot of the two-photon ionization signal vs laser energy at 459.513 nm, fcr a Sr concentration of 500 ng ml⁻¹. Error bars (one standard deviation) are also indicated. The slope of the line is 1.92 and the correlation coefficient is 0.998.

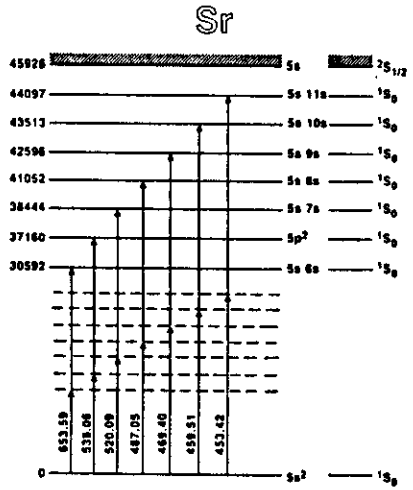

Fig. 13. Two-photon absorption transitions for the 5s-ns series, with $n = 6$–11. These transitions obey the angular selection rule $\Delta J = 0$.

compared to the other bound-state resonances, indicating a very short lifetime of the level associated with it.

3.3. *Additional single-wavelength observations*

During the identification process of the two-photon absorption transitions reported in the previous paragraph, several lines were observed which could not fit a two-photon scheme involving the ground state and a virtual level at $(1/2)E_{exc}$. Instead, the wavelengths calculated

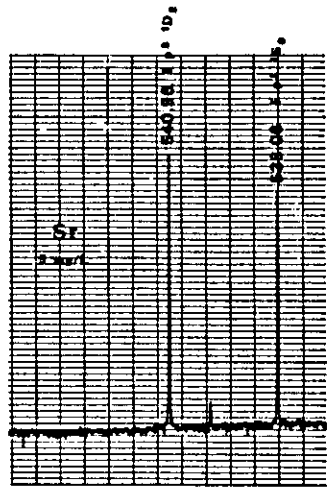

Fig. 14. Ionization spectrum resulting from the two-photon absorption process. A single laser, focussed in the middle of the flame, was scanned from 532 to 550 nm. The excited levels reached are indicated. Sensitivity: 0.25 V/full scale.

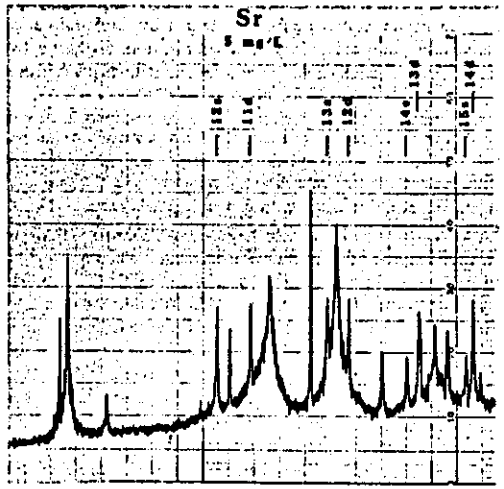

Fig. 15. Ionization spectrum resulting from scanning a single laser, focussed in the middle of the flame, from 456 nm (left) to 442 nm (right). The Rydberg levels *ns* and *nd* (with $n = 12, \ldots, 15$ for the *s*-series and $n = 11, \ldots, 14$ for the *d*-series) reached by two-photon excitation are indicated. Sensitivity: 0.25 V/full scale.

corresponded to resonance energies between excited states close to the ionization potential, and two lower energy levels, i.e., the $^1P_1$ and the $^1D_2$ levels, lying 21 698 cm^{-1} and 20 150 cm^{-1} above the ground state, respectively. These lines, together with the energy levels

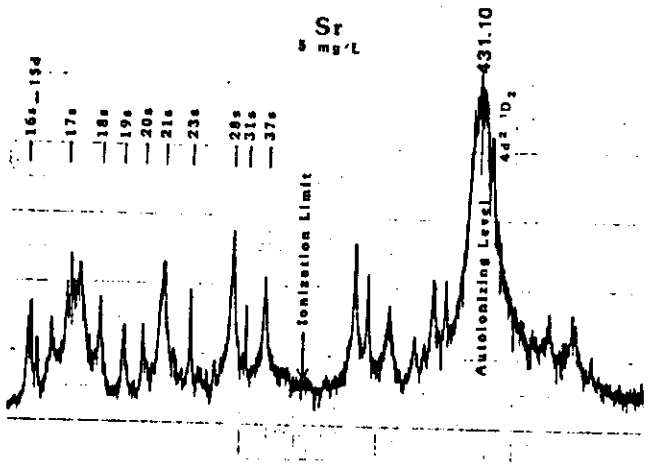

Fig. 16. Ionization spectrum resulting from scanning a single laser, focussed in the middle of the flame, from 442 nm (left) to 437 nm (right). The Rydberg levels *ns*, with $n = 16, \ldots, 37$, and 15*d* reached by two-photon excitation are indicated, as well as the ionization limit of the atom and the large autoionizing resonance at 431.10 nm. Sensitivity: 0.25 V/full scale.

involved, are collected in Table 2. Since these lines were observed at high photon irradiances, it is believed that their origin cannot be fully explained by single-step absorption from a thermally populated level followed by collisional ionization. Rather, a two-step process involving as a first step a collisionally assisted, non-resonant absorption process, leading to a population of the $^1P_1$ or $^1D_2$ levels is operative.

These processes, together with the experimental spectra obtained, are considered in detail in another paper [23].

3.4. *Analytical considerations*

The spectra shown in Figs 14–16 were obtained using an order of magnitude greater concentration, due to weakness of the signals; they are small compared to the two-wavelength signals. However, they may be of importance analytically, when a high energy density is desired to maximize the signal from the analyte, and when a matrix element has a two-photon absorption within the linewidth of the laser. The complexity of the resulting spectrum would be particularly significant when the level reached by the matrix element is close to the ionization limit. Therefore, in addition to *wavelength independent* ionization interferences, which can vary with the matrix, but which can be corrected for by scanning the laser excitation over the absorption profile [1, 3, 7], other *spectral* interferences will result from multiphoton excitation of concomitant species in the flames [4, 27].

The detection limit calculated with the two-photon transition at 459.513 nm for a signal-to-noise ratio of 2 was 10 ng ml^{-1}. This limit compares favorably with the single-step 460.733 nm detection limit of 4 ng ml^{-1} reported for flash-lamp pumped dye laser excitation and a $S/N = 3$ [1]. The two-step non-resonant transitions collected in Table 2 are expected to give results similar to the two-photon transitions since the magnitudes of the signals at the same concentration were comparable. Two-step two-wavelength excitation (460.733 and 554.336 nm, see Figs 4 and 5) gave the best detection limit of 0.2 ng ml^{-1}.

[27] F. M. CURRAN, C. A. VAN DIJK and S. R. CROUCH, *Anal. Spectrosc.* 37, 385 (1983).

Table 2. Two step non resonant transitions observed with 5 μg ml^{-1} of strontium while scanning a single dye laser focussed in the flame (440–490 nm)

Wavelength (nm)	Transitions and levels
444.847	5*s*5*p*–5*s*8*f* $^1P_1$–$^3F_2$
446.336	5*s*5*p*–5*s*11*s* $^1P_1$–$^1S_0$
447.406	5*s*5*p*–5*s*11*s* $^1P_1$–$^3S_1$
458.293	5*s*5*p*–5*s*10*s* $^1P_1$–$^1S_0$
467.781	5*s*5*p*–5*s*8*d* $^1P_1$–$^3D_2$
468.860	5*s*5*p*–5*s*8*d* $^1P_1$–$^1D_2$
475.548	5*s*4*d*–5*s*8*p* $^1D_2$–$^1P_1$
478.392	5*s*5*p*–5*s*9*s* $^1P_1$–$^1S_0$

The analytical potential of he two-step excitation and the importance of several parameters, e.g. the duration, and power density of the laser excitation pulse, in the case of the strontium as well as several other atoms are discussed in detail in another paper [10].

4. CONCLUSIONS

Our study has shown that the technique of two-step laser enhanced ionization is an extremely efficient tool for the characterization of many transitions which are not reported in standard wavelength tables and are normally not observed in flames by conventional absorption, emission and fluorescence methods. In the case of strontium atoms present as trace constituents in an air–acetylene flame, many transitions were identified from the ionization signals observed after populating, with two lasers, levels close to the ionization continuum. In addition, it has been shown that, when the laser irradiance is high, optical flame spectroscopy can easily expand into the realm of multiphoton processes. Two-photon absorption increases the diagnostic capabilities of the technique allowing transitions to occur between states of the same parity.

From the analytical point of view, the two-step process with short laser pulses (~ 5 ns) gives very low detection limits which are more than an order of magnitude better than those published so far. However, when the energy density in the flame is very high, the ionization spectra observed are very complex, because of the occurrence of multiphoton excitation in addition to single-step and two-step excitation. In this case, the technique should be considered as being subject to additional matrix interferences, i.e. ionization of concomittant species through either resonant or non-resonant processes.

Acknowledgements—L. P. HART and B. W. SMITH would like to thank the Joint Research Centre authorities and in particular the Education Training Service of Ispra for the grant of visiting scientist fellowships.

Reprinted from Analytical Chemistry, 1986, 58, 2147.

Measurement of the Laser-Induced Ionization Yield for Lithium in an Air–Acetylene Flame

B. W. Smith,[1] L. P. Hart,[2] and Nicoló Omenetto*

Joint Research Centre, Chemistry Division, Ispra (Varese), Italy

Single-step excitation and two-step excitation, followed by collisional ionization, have been used to measure the ionization yield of lithium atoms produced in a separated air–acetylene flame. The excitation is provided by two pulsed, tunable dye lasers, pumped simultaneously by an excimer laser and tuned to two connected transitions of the atom. The ionization signal is taken simultaneously with the fluorescence signal, which is measured with a monochromator and a photomultiplier placed at 90° with respect to the laser beams. The ionization yield for a single-step excitation at 670.784 nm was found to be 0.26%, increasing to 58% for two-step excitation (670.784 + 460.286 nm). By use of these values in a simplified theoretical treatment of the ionization process, it is shown that one can obtain order of magnitude estimates of the effective collisional ionization rate coefficients of the process(es) assumed.

The techique of laser-enhanced ionization or optogalvanic spectroscopy is now well established in atmospheric pressure flames as a very sensitive analytical tool and a most versatile diagnostic method (*1–6*). Several types of lasers have been used to provide the primary excitation step, i.e., flash lamp pumped dye lasers, nitrogen, Nd·YAG, or excimer-pumped dye lasers, and continuous wave lasers. The duration of the interaction between the atoms and the radiation field was therefore widely different, being in the microsecond range for flash lamp pumped lasers, in the nanosecond range for the gas discharge pulsed lasers, and in the millisecond range for the continuous wave (CW) lasers. In the last case, the interaction time is the dwell time of the atoms in the laser beam, which is in turn dictated by the rise velocity of the flame gases. The ability to achieve a significant ionization clearly depends, among other parameters, upon the length of the laser pulse. As it has been shown from simple theoretical considerations (*1–3*), the ionization yield, i.e., the ratio between the number of ions created during the laser pulse and the total number of neutral (ground state) atoms present in the laser volume, will approach unity when an optically saturating laser pulse has a duration that significantly exceeds the reciprocal of the effective ionization rate of the laser populated excited state (see below). The fact that the excitation produced in ~5 ns by a single laser beam to a level lying some electronvolts below the ionization potential would result in a significant ionization yield can then be questioned, since in this case the collisional ionization rate from that level is believed to much lower than the radiative and quenching rates. A second laser can therefore be used to populate in a stepwise manner (*6–9*) excitation levels much closer to the ionization potential of the atom. In this way, the ionization yield should increase appreciably. Although such considerations are clearly stressed in several papers, there appears to be no experimental measurement of the absolute value of the ionization yield in the case of single-step or two-step excitation with pulsed or CW lasers. A neutral depletion of 60% and 75% for sodium atoms and for laser pulses longer than 100 μs was reported in the air–hydrogen and air–acetylene flame, respectively (*10, 11*). However, laser-induced chemistry (*12*) was also considered to be partially responsible for the observed depletion.

The aim of this work is to describe the experimental evaluation of the absolute ionization yield of the lithium atoms in the air–acetylene flame. Single-step and two-step excitation is provided by two laser beams tuned at appropriate bound transitions of the atoms. The duration of the laser pulses is 4.4 ns. The temporal wave forms of the laser have been experimentally measured and are reported elsewhere (*13*). The total number of lithium atoms in the laser volume has been measured by an absolute absorption method (*14*) and the ionization detection system is calibrated in terms of output voltage per electron produced.

The results obtained have been used in connection with a simplified excitation–ionization model to derive order of magnitude estimates of the effective ionization rate coefficients. Due to the simplified nature of the model, especially regarding the temporal shape of the laser pulses, assumed to be rectangular, quantitative accuracy cannot be claimed nor was this in the scope of the present investigation. It is believed, however, that the absolute measurement of the ionization yield for short laser pulses represents an essential step in any further modeling of the ionization mechanism in flames.

[1] Permanent address: Department of Chemistry, University of Florida, Gainesville, FL 32611.
[2] Present address: Oregon State University, Department of Chemistry, Corvallis, OR 97331.

0003-2700/86/0358-2147$01.50/0

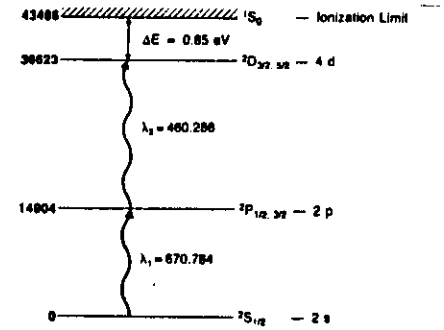

Figure 1. Simplified partial energy level diagram of the lithium atom pertinent to the experiment described in this work. Laser transitions are indicated in nanometers; energies (left) in cm^{-1}.

THEORETICAL CONSIDERATIONS

The ionization yield, IY, is defined here as the number of ions (electrons) produced during the laser excitation time divided by the total number of atoms present in the laser volume. When two lasers are used, it is assumed that their pulse duration is strictly the same and that the spatially uniform excitation volumes in the flame overlap perfectly.

If the signal obtained by integrating the electron current pulse is representative of the total charge created by the laser (*15*), the yield is given by

$$\mathrm{IY} = \frac{n_e}{n_T} = \frac{(\text{voltage pulse})/e(\Delta t_p)^{-1}\xi}{n_e b \pi r_l^2} \qquad (1)$$

In this equation, n_e is the number of electrons produced in the ionization process, n_T is the total number of atoms in the laser volume, e is the charge of the electron (coulomb), Δt_p is width of the electron pulse (seconds), ξ is the calibration factor of the detection system ($V\ A^{-1}$), n_e is the number density of the atoms in the flame (cm^{-3}), b is the laser interaction length in the flame (cm), and r_l is the radius of the laser(s) beam(s) in the flame (cm).

The energy level diagram for lithium pertinent to our experiment is shown in Figure 1. In the single-step excitation acheme, one laser is tuned to the resonance transition at 670.784 nm, involving the excited 2p doublet, and subsequent collisional ionization occurs in the flame. With this simple scheme, the fraction of the total number of atoms ionized during an optically saturating laser pulse, i.e., the ionization yield, will be given by (*1–3, 13*)

$$\frac{n_i}{n_T} = 1 - \exp\left[-\left(\frac{g_2}{g_1 + g_2}\right)k_{2i}\,\Delta t_l\right] \qquad (2)$$

In this equation, g_1 and g_2 are the statistical weights of the ground state (here indicated as level 1) and of the excited doublet (here indicated as level 2), k_{2i} (s^{-1}) is the coefficient describing the *effective* collisional ionization rate (*14*), and Δt_l (s) is the duration of the (rectangular) laser pulse. As stated before, Δt_l must be (much) greater than the ratio $(g_1 + g_2)/(g_2 k_{2i})$ in order to attain unity ionization yield.

In the two-step excitation scheme, the second laser is tuned to 460.286 nm (see Figure 1) and populates the 4d doublet, which lies 0.85 eV below the ionization limit. If this last level is indicated as level 3 and if both transitions are now optically saturated, the ionization yield is given by (*13*)

$$\frac{n_i}{n_T} = 1 - \exp\left[-\left(\frac{g_3}{g_1 + g_2 + g_3}\right)k_{3i}\,\Delta t_l\right] \qquad (3)$$

where now g_3 is the statistical weight of the 4p doublet and k_{3i} becomes the effective ionization rate coefficient.

From these simple considerations it can be deduced that, provided that the ionization yield can be measured experimentally under saturated conditions, order of magnitude estimates can be inferred from eq 2 and 3 for both k_{2i} and k_{3i}.

As seen in eq 1, the number of absorbing atoms in the laser volume needs to be measured. This number can safely be identified with n_T (see eq 2 and 3) since this last number in the air–acetylene flame at 2500 K represents, within less than 0.1%, the lithium ground-state population. In order to accurately evaluate n_T, it was decided to adopt the well-known absorption method (*14–17*). In our case, the laser can be considered to be a quasi-continuum excitation source, since its spectral bandwidth exceeds approximately 10 times the absorption profile of the lithium atoms in the flame.

Finally, to check that the transitions used were optical saturated, atomic fluroescence was simultaneously recorded with a conventional monochromator–photomultiplier setup.

EXPERIMENTAL SECTION

A block diagram of the experimental arrangement is shown in Figure 2. An excimer laser (Model EMG-102, Lambda Physik, Göttingen, FRG) operated with XeCl pumped two dye lasers (Jobin Yvon, Longjumeau, France) that were located on either side of a commercially available flame ionization system (SOPRA, Bois Colombes, France), which was modified for this experiment. A hole was drilled at the rear of the burner housing to allow the observation of fluorescence and the long path burner head normally used for flame ionization was replaced by a homemade capillary-type burner fitted with an argon sheath. This burner, which has been used in our laboratory in several emission and fluorescence experiments (*18*), was mounted on a standard mixing chamber with pneumatic nebulization. Gas flows were accurately measured with calibrated rotameters. As shown in Figures 1 and 2, the first laser provided the excitation of lithium atoms from the ground state (λ_1 670.784 nm) and was adjusted to be temporally coincident with laser 2, tuned at 460.286 nm. With this scheme, the final level was 0.85 eV below the ionization limit. Both laser beams were expanded and then reduced in size with apertures to provide spatially homogeneous beams of about 0.3 cm diameter. Figure 3 shows the geometry of the beams in the flame and their positions with respect to the burner surface and the high-voltage electrode.

The energy of the lasers was measured with a volume absorbing calorimeter (Model 38-0101, Scientech, Boulder, CO). The temporal coincidence of the two beams was ascertained by examining their respective temporal positions with a fast photodiode (Electrooptical Products Division ITT, Fort Wayne, IN, Type F-4000, S-5 response). The high-voltage electrode (molybdenum around a water-cooled glass tube) was biased at −1800 V and the electrons produced via laser excitation were collected at the burner, converted to a voltage, and processed by a boxcar integrator

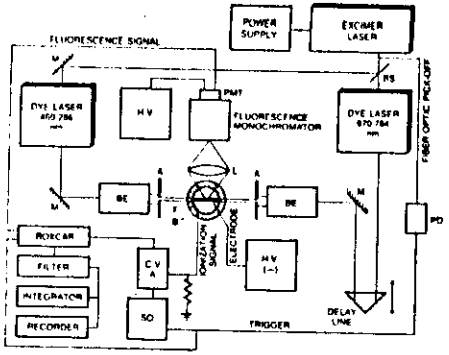

Figure 2. Experimental setup: BS, beam splitter; PMT, photomultiplier tube; PD, photodiode; H.V., high voltage; BE, beam expander; M, mirror; L, Lens; A, aperture; F, flame; B, burner; C-V A, current-to-voltage amplifier; SO, storage oscilloscope. See text for description.

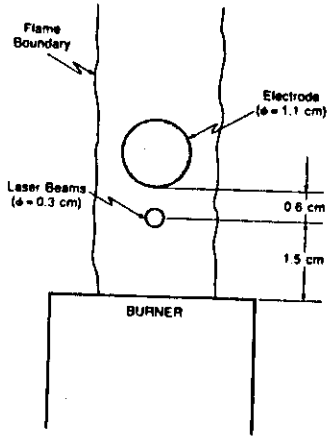

Figure 3. Geometrical arrangement of the exciting laser beams, high voltage electrode and burner for the experiment described.

(Stanford Research Corp., Palo Alto, CA). The dc flame ionization background was blocked by an ac coupling capacitor. Some characteristics of the signal processing electronics have been discussed by Berthoud et al. (*19*). The resonance fluorescence signals are collected at 90° with respect to the excitation axis with a lens and a high luminosity monochromator (Model H-10, Jobin Yvon, Longjumeau, France). The signal from the photomultiplier (Type R928S, Hamamatsu Corp., Japan) is then fed to the boxcar integrator.

RESULTS AND DISCUSSION

As stated before, the calculation of the ionization yield requires the determination of two parameters: the number of electrons produced per laser pulse and the number of ground-state atoms present in the region of excitation. These will be discussed separately.

The electrons collected at the burner head produce a current pulse of approximately 200 ns width (*1*, *19*). In our experiment the pulse is stretched by the current to voltage converter and arrives at the input to the boxcar integrator as a voltage pulse of 800 nm fwhm and full base width of 1.8 μs. In order to determine the number of electrons produced at the burner head, it is necessary to measure the total integrated voltage pulse at the boxcar and to know the gain of the current to voltage preamplifier at the frequency of the measurement. This gain was calibrated by injecting current pulses of the same shape and duration of those produced by the laser ionization in the flame at the burner head and measuring the time integrated input to the current to voltage preamplifier. The response to a current pulse was 2.913×10^5 V A^{-1} (±3%). The dc gain was also measured by injecting signals from a precision dc current source directly at the input at the amplifier. The dc response was 5.4×10^5 V A^{-1}. The output of the current to voltage preamplifier was integrated with a 2.0-μs boxcar gate width. The response of the boxcar and digital readout were also calibrated against known voltage sources.

In the absence of the excimer firing, the limiting noise was that of the boxcar and had a standard deviation of 10 μV (referred to the boxcar input, 20 Hz repetition rate, 30 laser shots), which corresponded to about 500 electrons at the burner. When the excimer laser was firing, the radio frequency noise increased the background noise to a standard deviation of 14 mV, which corresponded to 6×10^5 electrons at the burner. This noise was much larger than that reported when the overall system was optimized for analytical measurements (*9*).

An aqueous solution of 1 μg/mL of lithium was aspirated into the flame. The resulting current pulse, integrated over the 2.0-μs boxcar gate, was measured with laser excitation set at 670.784 nm only and subsequently with the additional excitation at 460.286 nm. The spatial coincidence of the beams was ascertained by visual alignment at the burner head and subsequently by maximizing the ionization signal by a small adjustment of one beam. The energy of the lasers was 62 μJ per pulse for the 670.784-nm beam and 51 μJ per pulse for the 460.286-nm beam, corresponding to peak excitation powers close to 200 kW/cm^2.

The number of ground-state atoms present in the beam volume was determined by carrying out several measurements, namely, the measurement of the laser diameter and spectral bandwidth, the total fraction of radiation absorbed, and the absorption interaction length in the flame. The diameters of the laser beams in the flame (after the beam expanders and the apertures) were measured by translating with a stepping motor a photodiode with 0.1 mm × 0.5 mm aperture across the center of the beam and recording the resulting intensity profile. An estimate was also obtained by recording an image of the beams at the burner on the photographic paper. The beam had a nearly rectangular intensity profile with ±20% reproducible fluctations in the maximum intensity. The diameter was taken as that of a perfectly rectangular profile having the same area as the measured profile. The radius determined in this way, 0.129 ± 0.013 cm, agreed with that estimated from the image on photographic paper within 7%.

The spectral width of the laser was measured in three different ways: (i) the beam was directed into a 1.29-m focal length grating monochromator (Model 1269, Spex, Metuchen, NJ) equipped with 10-μm slits whose instrumental function was 0.006 nm; (ii) a fluorescence excitation profile was recorded with the high luminosity fluorescence monochromator by slowly scanning the laser throughout the absorption profile of the atoms; and (iii) the laser output was directly monitored in absorption during a spectral scan with a photodiode with and without lithium atoms in the flame. The procedures followed agreed with each other satisfactorily and a value of 0.0526 ± 0.005 nm was found.

The measurement under (iii) was indeed performed to evaluate the fraction of the incident laser radiation absorbed in the flame. The photodiode (Type PIN 10 DP/58, United Detector Technology, Santa Monica, CA) fitted with a diffuser was positioned to detect the laser after it traversed the flame.

Table I. Parameters Used in the Calculation of the Curve of Growth

parameters	value	source
$\Delta\lambda_I$	0.0526 ± 0.005 nm	measured
a	0.6 ± 0.2	ref 21–23
k_0/n	$(3.136 \pm 0.094) \times 10^{12}$ cm^2	ref 24
$\Delta\lambda_D$	0.0090 ± 0.0002 nm	calculated (T = 2450 K)

$^a(k_0/n) = ((4 \ln 2)^{1/2} e^2 \lambda_0^2 / mc^2)(f_{abs}/\Delta\lambda_D)$. Here, e is the electronic charge, m is the electron mass, c is the velocity of light in vacuum, and f_{abs} is the absorption oscillator strength.

It was necessary to avoid saturation effects and to ensure linearity in the photodiode response, to attenuate the laser with a stack of neutral density filters of total (nominal) density 5.3. With these filters, the residual energy of the laser was approximately 300 pJ per pulse. The current pulse from the photodiode was converted to a voltage and measured with the boxcar averager and a 10-s integrator. Five 10-s integrations were taken on each of eight alternating aspirations of water and a 10 μg/mL lithium solution.

From the theory of absorption of radiation with continuum and line sources (*14–17*) the *product* of the absorbing atoms and the absorption path, i.e., $(n_a b)$ in eq 1, can be directly evaluated from the *curve of growth* obtained as the double logarithmic plot of the fraction of radiation absorbed α, vs. this product. A curve of growth was calculated for lithium for this particular experiment. The calibration was carried out by numerical integration using the approach of Hui et al. (*20*). Table I lists the necessary parameters used. These parameters either have been directly measured, e.g., the source half width, or were taken from the literature or calculated. Curves of growth were calculated for the range of damping parameter values from 0.5 to 0.7. Because the measured source width, 0.0526 nm, is rather wide compared to the absorption width of the atoms in the flame (~0.01 nm), the curve of growth in the low density region is not sensitive to changes in the damping parameter (*14–17*). The experimental value of α obtained for a 10 μg/mL solution is slightly outside the linear region of the curve of growth and therefore a ±20% variation in the damping parameter introduces a small (±1%) error in the value of the product $(n_a b)$ calculated. The absorption coefficient in Table I has been calculated from the absorption oscillator strength given in the literature (*24*) and is believed to be accurate to within ±3%. The Doppler width has been calculated for a temperature of 2450 K and varies by no more than 2% over a range of ±100 K. This particular flame and burner have been well characterized during several years in our laboratory (*18*, *25*). A plot of the curves of growth calculated for three values of the damping parameters is shown in Figure 4.

The value of $\alpha = 0.215$ corresponds to a product $(n_a b) = (6.34 \pm 0.06) \times 10^{11}$ cm^{-2}. From the value of η measured (0.129 cm), the number of atoms in the beam volume for the aspiration of a 10 μg/mL solution is therefore 3.31×10^{10}. It is safe to assume that a 1.0 μg/mL solution will introduce exactly 10 times fewer atoms into the flame, and as a result, a value of 3.31×10^9 atoms was taken for the calculation of the yield.

As said before, simultaneous fluorescence and ionization measurements were performed. Firstly, it was checked that the resonance transition at 670.784 nm was optically saturated. This was done in the usual way, i.e., by attenuating with calibrated filters the laser output and monitoring the resulting fluorescence signal. A typical saturation curve obtained is shown in Figure 5. A simultaneous monitoring of the ionization and fluorescence signals is reported in Figure 6. Here, it is clearly shown that the ionization enhancement obtained when the second laser step is spectrally tuned into

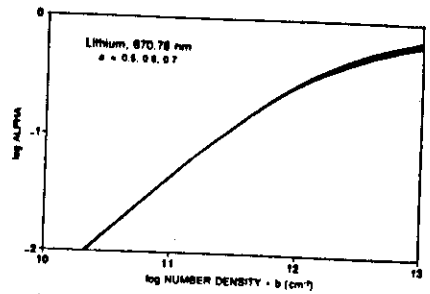

Figure 4. Calculated curves of growth for the fraction of radiation absorbed by increasing values of the product $(n_a b)$, for the different values of the damping parameter, a, indicated in the insert: upper curve, a = 0.5; intermediate curve, a = 0.6; lower curve, a = 0.7.

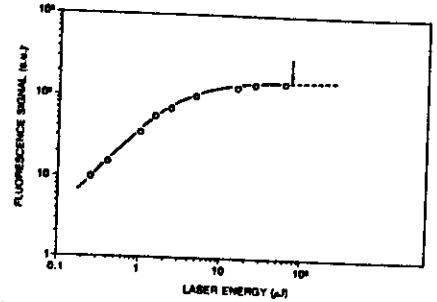

Figure 5. Saturation curve obtained by aspirating 1 μg/mL of lithium in the flame. The arrow indicates the laser energy pertinent to the experiment.

resonance with the 460.286-nm line is accompanied by a decrease in the resonance fluorescence signal at 670.784 nm, indicating the depletion in the population of the 2p doublet.

Table II summarizes all the measured parameters and the values of the ionization yield calculated for single-step and two-step excitation. With the pertinent values in eq 2 and 3, k_{2i} and k_{3i} are calculated as 0.78×10^8 s^{-1} and 3.55×10^8 s^{-1}, respectively. As repeatedly pointed out, no quantitative accuracy can be claimed for these values, due to the simplifying assumptions of the theory (*15*). However, our values seem to be consistent with those calculated by Smyth et al. (*26*) for their *global* rate constants (s^{-1}) and for principal quantum number $n = 4$.

CONCLUSION

The results described in this paper can be extrapolated to several other atoms present in a similar flame environment and excitation conditions. If the level excited by a single laser pulse lies several electronvolts below the ionization potential and the pulse duration does not exceed a few nanoseconds, the ionization yield will not be significant. Two interesting observations can then be derived:

(i) A resonance fluorescence measurement obtained under optically saturated conditions can indeed be related to the total number density of the atoms in the two levels connected by the laser excitation. In other words, during the short excitation, no significant losses are expected for the atoms interacting with the laser field. This has important consequences in flame and plasma diagnostics.

(ii) The *analytical* sensitivity and detection limit that can be obtained by the ionization technique under these excitation conditions are still very good, despite the low ionization yield.

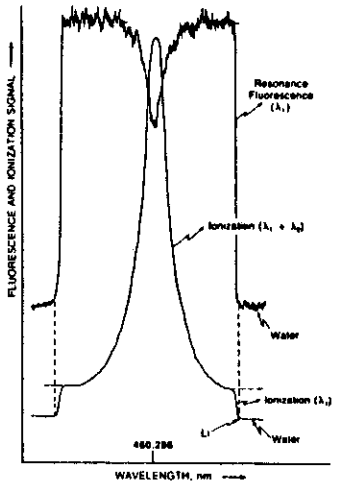

Figure 6. Simultaneous recording of the fluorescence and ionization signals for both single-step and two-step excitation. The wavelength of the second laser, which is spectrally scanned, is indicated in abscissa. Lithium concentration was 0.2 μg/mL. Laser energy was 1 mJ/pulse for both lasers. The explanation of the labeling in the figure is as follows: water, the background level due to the aspiration of water in the flame; Li, the aspiration of the lithium solution into the flame. This results in the ionization signal due only to λ_1 and in the resonance fluorescence signal, also excited at λ_1. Ionization (λ_1 + λ_2) indicates the enhancement in the ionization signal, and the corresponding dip in the fluorescence signal, when λ_2 is tuned to resonance with the second step (460.286 nm). The two-step ionization signal (λ_1 + λ_2) resulted in the saturation of the detection system, and therefore the enhancement cannot be calculated from this figure.

Table II. Parameters Measured and Ionization Yield for Single-Step and Two-Step Laser Excitation

parameters	value	error
$\Delta\lambda_1$ (nm)	0.0526 nm	±0.005
α	0.215	±0.0032
r_1 (cm)	0.129	±0.013
$n_a b$ (cm^{-2}) (10 μg/mL)	6.34×10^{11}	±0.063
ξ (V A^{-1})	2.91×10^{8}	±0.087 × 10^{8}
Δt_1 (s)	4.4×10^{-9}	±0.5 × 10^{-9}
Δt_p (s)	8×10^{-7}	±0.2 × 10^{-7}
electrons (λ_1) (1 μg/mL)	8.61×10^{6}	±2 × 10^{6}
electrons (λ_1 + λ_2) (1 μg/mL)	1.93×10^{8}	±2 × 10^{7}
I.Y. (λ_1)	0.0026	±0.0006
I.Y. (λ_1 + λ_2)	0.58	±0.12

This can be easily seen for the lithium case investigated from the following considerations. The number of atoms in the laser volume for a solution of 1 μg/mL was 3.31×10^{9}. With a 0.26% ionization yield, 8.61×10^{6} electrons are formed (see Table II). If the collection efficiency is unity, this number corresponds to a total charge of 1.4×10^{-12} C. For a 800-ns pulse, this will give a current of 1.75×10^{-6} A, or a voltage pulse of 510 mV, by taking into account the calibration of our detection system. If the root-mean-square noise of 1.2 mV is now used (9), 1 μg/mL will result in a signal-to-noise ratio of 425 or in a detection limit, for $S/N = 2$, of 4.7 ng/mL. This calculation stresses once again the extremely high sensitivity of the laser-enhanced ionization technique.

When two lasers are used, energy levels close to the ionization limit can be efficiently populated and the ionization yield increases considerably. This scheme is therefore the choice for the best analytical sensitivity. It is recalled that the two-step excitation described here for lithium gave a detection limit of 0.2 pg/mL (*13*).

The errors reported in Table II have been calculated from several repeated measurements of the parameters involved. As far as the accuracy of the values of the ionization yield is concerned, one should take into account the dependence of the current pulse on the position of the laser beam relative to the electrode. In our case, this position was fixed at 0.6 cm (see Figure 3). When the laser beam is aligned near the cathode, the magnitude of the signal should not vary by more than 20% (*15*). However, this correction factor should be kept in mind since the values of the ionization rate coefficients should be modified accordingly. A study of the dependence of the integrated pulse signal on the laser position in the flame is therefore warranted.

Finally, it would be interesting to study the dependence of the ionization yield upon the duration of the laser pulse. For single-step excitation, larger yields (and lower detection limits) should be achieved. It is therefore hoped that similar measurements, along the lines described in this work, will be performed with other types of lasers and for several other elements.

ACKNOWLEDGMENT

The authors are grateful to G. C. Turk for the critical reading of the manuscript and useful suggestions. B. W. Smith and L. P. Hart wish to thank the Joint Research Centre and in particular the Education Training Service of Ispra for the grant of Visiting Scientist Fellowships.

Registry No. Li, 7439-93-2.

LITERATURE CITED

(1) Travis, J. C.; Turk, G. C.; DeVoe, J. R.; Schenck, P. K.; Van Dijk, C. A. *Prog. Anal. At. Spectrosc.* **1984**, *7*, 199–241.
(2) Travis, J. C.; Turk, G. C.; Green, R. B. *Anal. Chem.* **1982**, *54*, 1006A–1018A.
(3) Travis, J. C. *J. Chem. Educ.* **1982**, *59*, 909–914.
(4) Schenck, P. K.; Hastie, J. W. *Opt. Eng.* **1981**, *20*, 522–528.
(5) Camus, P., Ed. *J. Phys.* **1983**, *44*, Suppl. 11.
(6) Turk, G. C.; DeVoe, J. R.; Travis, J. C. *Anal. Chem.* **1982**, *54*, 643–645.
(7) Axner, O.; Lindgren, I.; Magnusson, I.; Rubinsztein-Dunlop, H. *Anal. Chem.* **1985**, *57*, 776–778.
(8) Van Dijk, C. A.; Curran, F. M.; Link, C.; Crouch, S. R. *Anal. Chem.* **1981**, *53*, 1275–1279.
(9) Omenetto, N.; Berthoud, T.; Cavalli, P.; Rossi, G. *Anal. Chem.* **1985**, *57*, 1256–1261.
(10) Schenck, P. K.; Travis, J. C.; Turk, G. C.; O'Haver, T. C. *Appl. Spectrosc.* **1982**, *2*, 168–171.
(11) Schenck, P. K.; Travis, J. C.; Turk, G. C., National Bureau of Standards Washington, DC, unpublished results, 1982.
(12) Muller, C. H., III; Schofield, K.; Steinberg, N. In *Laser Probes for Combustion Chemistry*; Crosley, D. R., Ed.; American Chemical Society: Washington, DC 1980; ACS Symp. Ser. No. 134, pp 189–194.
(13) Omenetto, N.; Smith, B. W.; Hart, L. P. *Fresenius' Z. Anal. Chem.*, in press.
(14) Alkemade, C. Th. J.; Hollander, Tj.; Snelleman, W.; Zeegers, P. J. Th. *Metal Vapours in Flames*; Pergamon Press: New York, 1982; Chapter IX.
(15) Havrilla, G. J.; Schenck, P. K.; Travis, J. C.; Turk, G. C. *Anal. Chem.* **1984**, *56*, 186–193.
(16) Mitchell, A. C. G.; Zemansky, M. W. *Resonance Radiation and Excited Atoms*; Cambridge University Press: London, 1961.
(17) De Galan, L.; McGee, W. W.; Winefordner, J. D. *Anal. Chim. Acta* **1967**, *37*, 436–444.
(18) Rossi, G.; Benetti, P.; Omenetto, N., EUR External Report, (1971) No. 4598e.
(19) Berthoud, T.; Lipinsky, J.; Camus, P.; Stehlé, J. L. *Anal. Chem.* **1983**, *56*, 959–963.
(20) Hui, A. K.; Armstrong, B. H.; Wray, A. A. *J. Quant. Spectrosc. Radiat. Transfer* **1978**, *19*, 509–516.
(21) Hinnov, E.; Kohn, H. *J. Opt. Soc. Am.* **1957**, *47*, 156.
(22) Holmann, F. W.; Kohn, H. *J. Opt. Soc. Am.* **1961**, *51*, 512.
(23) Lovett, R. J.; Parsons, M. L. *Appl. Spectrosc.* **1977**, *31*, 424.
(24) Wiese, W. L.; Smith, M. W.; Glennon, B. M. *Atomic Transition Probabilities, Vol. 1 Hydrogen through Neon*; National Bureau of Standards: Washington, DC, 1966; NSRDS-NBS-4.
(25) Omenetto, N.; Benetti, P.; Rossi, G. *Spectrochim. Acta, Part B* **1972**, *27B*, 453–461.
(26) Smyth, K. C.; Schenck, P. K.; Mallard, W. G. In *Laser Probes for Combustion Chemistry*; Crosley, D. R., Ed.; American Chemical Society: Washington, DC, 1980; ACS Symp. Ser. No. 134, pp 175–181.

RECEIVED for review February 18, 1986. Accepted May 1, 1986.

VI.53

Lifetime Measurements of Metastable Levels of Thallium and Lead in the Air-Acetylene Flame by Laser-Enhanced Ionization Spectrometry

N. OMENETTO,* T. BERTHOUD,† P. CAVALLI, and G. ROSSI

Joint Research Center, Chemistry Division, Ispra (Varese), Italy

Laser-enhanced ionization spectrometry with two-step excitation has been used to evaluate the collisional lifetime of the metastable P levels of thallium and lead in an air-acetylene flame burning at atmospheric pressure and supported by a three-slot burner head fitted on a conventional nebulizing chamber. A water-cooled molybdenum electrode immersed in the flame was maintained at high negative potential with respect to the burner body. The ionization current resulting after the two-step excitation was amplified and measured with a digital storage oscilloscope and a boxcar averager. The two excimer lasers were triggered externally with two trigger pulses, one being delayed in time with respect to the other one. In this way the second laser photon, tuned at a transition starting from the metastable level under study, could be correspondingly delayed from the first photon tuned at a transition starting from the ground state. The lifetimes measured were found to be 81 ns and 360 ns for Tl and Pb, respectively.

Index Headings: Flame spectroscopy; Spectroscopic techniques.

INTRODUCTION

Laser-enhanced ionization (LEI) or optogalvanic effect in flames at atmospheric pressure is gaining an increasing popularity as a very sensitive technique for trace analysis.[1,2] Several photoexcitation schemes involving one and two laser photons have been used and identified in the literature as "resonance," "nonresonance," and "stepwise" ionization modes of LEI spectrometry. With a two-step excitation scheme, both sensitivity and spectral selectivity are enhanced.[3] Here, the lower level of the transition reached with the second photon is usually the same as the upper level of the transition reached with the first photon. Moreover, both excitation beams are made spatially and temporally coincident in the flame.

Clearly, by delaying in time the second photon with respect to the first one, one can, in principle, obtain the lifetime of the common level. The same reasoning holds even if the excited level reached by the first photon and the starting level of the second transition are not the same, provided that they are strongly collisionally and/or radiatively coupled. This can be the case with elements, such as lead and thallium, with metastable levels lying above the ground state, i.e., levels not radiatively coupled with the ground state. The importance of these levels has been amply recognized in saturation studies

Received 5 August 1984.
* Author to whom correspondence should be sent.
† Present address: DCAEA/SEA/SEACC, Fontenay-aux-Roses, France.

0003-7028/85/3903-0500$2.00/0

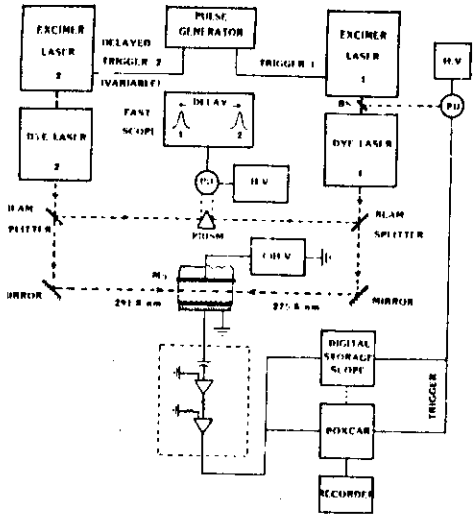

FIG. 1. Schematic diagram of the experimental set-up. The wavelengths indicated for the two laser beams (291.8 nm and 276.8 nm) refer to the thallium atom. H.V. = High Voltage Supply; PD = Photodiode.

volving laser-induced fluorescence for flame and plasma diagnostics. In fact, the metastable level can act as trap, modifying considerably the value of the parameter known as steady-state saturation spectral irradiance.[4-7] It is therefore important to evaluate the lifetime such levels.

The aim of this paper is to describe a measuring procedure based on the observation of the decay of the ionization signal when the two laser photons, tuned at appropriate transitions in the flame, are suitably delayed th respect to each other. From the lifetime obtained, value for the collisional mixing cross-section between e P levels, at a given flame condition, can also be rived.

KPERIMENTAL

The experimental set-up used for the two-step ionation studies is schematically depicted in Fig. 1.

The trigger pulses for the operation of the two excimer sers were derived from two pulse generators (Model H-137A, EH Research Lab., Oakland, CA, USA, and odel 100A, Data Pulse, Culver, CA, USA). Both excier lasers (Lambda Physik, Göttingen, Germany, Model EMG-102 and EMG-50E) were operated on XeCl (308) at a repetition rate of 15 Hz. The two dye lasers are anufactured by Jobin-Yvon (Instruments S.A. Division Jobin Yvon, Longjumeau, France). One laser consts of the eight-cell oscillator-amplifier system deibed by Bos,[8] which allows a quick change of dye and associated spectral range, while the second laser has normal one-cell oscillator-amplifier configuration. th lasers are equipped with holographic gratings (3000

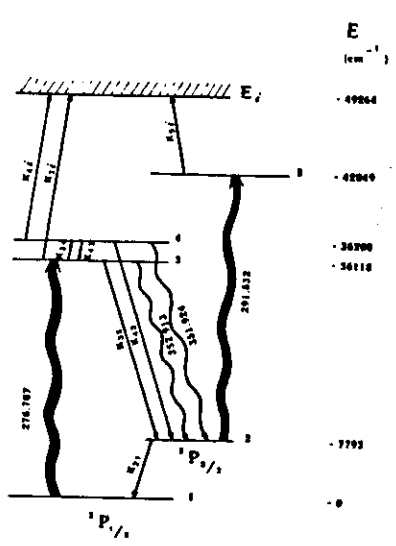

ENERGY LEVEL SCHEME for Tl

FIG. 2. Simplified energy level diagram for thallium. The two wavy lines correspond to laser excitation. The rate coefficients between levels are indicated as well as the two radiative transitions at 352.913 nm and 351.924 nm. Thermal ionization from levels 3, 4, and 5 is also indicated.

groove/mm) and frequency doubling crystals to cover the wavelength range from 217 nm to 360 nm.

Two fractions of the dye laser beams were sampled with two beam splitters and then recombined by a prism onto a fast photodiode (Type F-4000, S-5 response, Electrooptical Products Division, ITT, Fort Wayne, IN, USA) whose output was read directly on a 500-MHz oscilloscope (Model 7904, Tektronix Inc., Beaverton, CO, USA). In this way the optical delay between the two excitation pulses could be accurately monitored. The jitter in the laser firings under external triggering was found to be slightly less than 10 ns. Although this jitter had no pronounced effects on our measurements, because of the long lifetime of the metastable levels investigated, it would clearly negate the possibility of measuring the fast decays characteristic of the excited states reached in conventional two-photon ionization experiments.[9]

The optogalvanic system was made by SOPRA (Société de Production et de Recherches Appliquées, Bois Colombes, France). A water-cooled molybdenum electrode as described by Turk[10] was immersed in the air-acetylene flame supported by a three-slot Perkin Elmer burner. The electrode was maintained at high negative potential (−1600 V) with respect to the burner body. The ionization current induced by the laser, after amplification by a combination of current and voltage amplifiers, was read on a digital storage oscilloscope (Model 468, Tektronix, Beaverton, CO, USA) and its output was

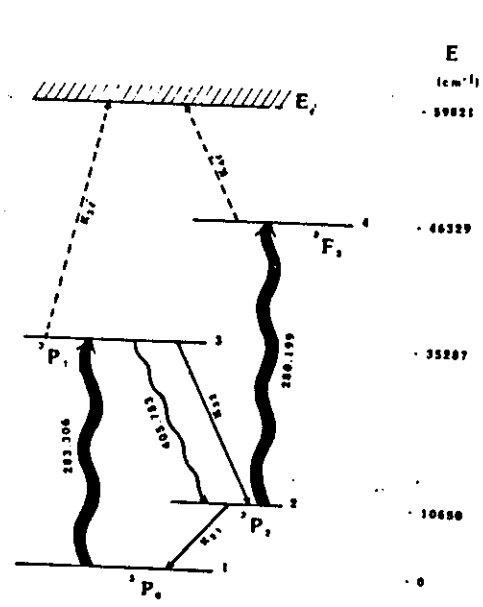

ENERGY LEVEL SCHEME for Pb

FIG. 3. Simplified energy level diagram for lead. The two wavy lines correspond to laser excitation. Radiative transition at 405.783 nm and collisional rate coefficients are indicated. Thermal ionization from levels 3 and 4 is also indicated.

then fed into a boxcar averager (EG&G, P.A.R., Princeton, NJ, USA, Models 165 and 162) and displayed on a strip chart recorder.

For both thallium and lead, a solution of 100 ng/mL, slightly acidified with nitric acid, was aspirated into the flame, whose exact composition was not known. The dyes, Rhodamine 590 chloride and Coumarine 540A, were supplied by Exciton (Dayton, OH, USA) and were dissolved in methanol at the concentration suggested by Bos.[8]

RESULTS AND DISCUSSION

The pertinent simplified energy level diagrams for thallium and lead are shown in Figs. 2 and 3. As one can see, for thallium, the metastable $^2P_{3/2}$ level lies 7793 cm^{-1} above the ground state and is expected to be somewhat thermally populated at the flame temperature (~2500 K). Indeed, analytical studies have been performed with the use of the 291.832 nm as a single excitation step before collisional ionization. For lead (see Fig. 3), the $^3P_2$ level should be less populated than in the case of Tl since the energy difference with the ground state exceeds 1 eV. Single-photon ionization occurs after pumping at 280.199 nm.

The following discussion refers to the thallium atom

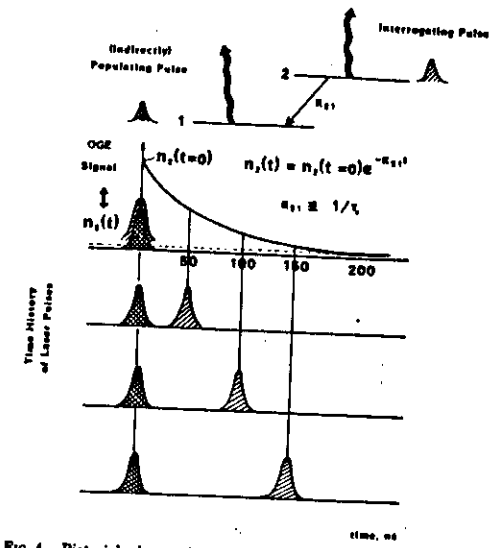

FIG. 4. Pictorial scheme of the measuring principle for the evaluation of the lifetime of level 2. Four successive laser pulses are indicated.

but it could equally well refer to the case of lead, due to the similarity of the two energy schemes. The $^2P_{3/2}$ level is populated from the excited states (3 and 4 in Fig. 2) by collisional and radiative deexcitation. Levels 3 and 4 are considered to be strongly coupled at the flame temperature because of their exceedingly small energy difference. If one therefore enhances the population of level 3 by optical pumping of the 276.787-nm transition, and if the lifetime of this level is short (nanosecond scale) due to downwards collisional quenching and radiative emission, then the (thermal) population of the metastable level will correspondingly be increased. The only decay considered for the metastable level is by collisions with flame molecules which bring the atoms back to the ground state (mixing collisions). It can therefore be predicted that during the irradiation pulse of the resonance transition at 276.787 nm a significant fraction of the excited atoms will decay to the $^2P_{3/2}$ level, where they can be further excited by the second laser photon tuned at 291.832 nm and subsequently ionized by collisions. A two-step enhancement in the ionization signal is therefore expected to occur. If the second photon is now temporally delayed with respect to the resonant one, the decay of the ionization signal would reflect the decay of the population of the $^2P_{3/2}$ level.

The time history of the overall process is pictorially shown in Fig. 4. Here the two laser photons are identified as the indirectly populating pulse (the resonant

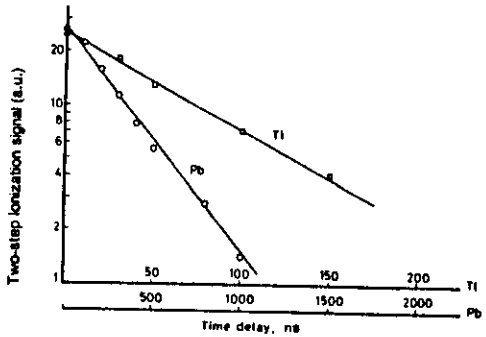

FIG. 6. Time decay plots of the two-step ionization signals for thallium and lead as a function of the time delay of one photon with respect to the other. The experimental error (one standard deviation) is approximately 10%.

photon) and the interrogating pulse. Assuming that the mixing collisions of atoms between the P levels is the dominant deexcitation process, the reciprocal of the decay time of the decreasing ionization signal represents the collisional rate coefficient, k_{21}, of the process

$$Tl(6^2P_{3/2}) + Z \rightarrow Tl(6^2P_{1/2}) + Z \qquad (1)$$

where Z represents a flame collision partner. It is known that k_{21} is related to the effective cross-section of the deactivation process by the relationship

$$k_{21} = \sum_j n_j \sigma_j \bar{v}_j \qquad (2)$$

where n_j (cm^{-3}) is the density of particles of kind j, σ_j (cm^2) is the effective cross-section, $\bar{v}_j$ ($cm\ s^{-1}$) is the mean relative velocity of atoms and colliding particles, and the summation extends over the various types of colliding partners in the flame at atmospheric pressure.

The predicted two-step enhancement was easily observed for both thallium and lead. The corresponding semilogarithmic plots of the decays of the ionization signal vs. time are shown in Fig. 5. From the slope of the graphs, a lifetime of 81 ns and 360 ns is calculated for Tl and Pb, respectively.

To the authors' knowledge, no previous measurements of these lifetimes in flames have been reported in the literature. However, for thallium, an extremely low value ($<10^{-3}$ Å^2) of the cross-section for collisional mixing has been measured in a cell at 600 K by Bellisio and Davidovits[11] for nitrogen, which is the main constituent of our flame. According to our results, by inserting in Eq. 2 the values $n_j = 10^{18}\ cm^{-3}$, $\bar{v}_j = 10^5\ cm\ s^{-1}$ and $k_{21} = 1.64 \times 10^7\ s^{-1}$, one can calculate that $\sigma(N_2)$ would be approximately 1 Å^2. However, as found by the same authors, the cross-section for O_2 at 600 K is of the order of 30 Å^2. It is therefore clear that, as suggested by Alkemade,[12] if the flame used in our experiment has a noticeable concentration of free oxygen molecules, which are very efficient in this mixing process, the large difference in the values of the cross-sections can be easily explained. In our case, a 5% volume concentration of oxygen would indeed give approximately 30 Å^2 for the mixing cross-section. In addition, the water contribution should also be taken into account.[12]

From the above considerations, it is clear that the measurements should be carried out in a flame of known and variable composition and temperature. In this way one could perhaps derive specific cross-sections for some major flame constituents. Work is now in progress in this direction on the elements Tl, In and Ga.

1. J. C. Travis, G. C. Turk, J. R. DeVoe, P. K. Schenck, and C. A. Van Dijk, Progress Anal. Atom. Spetroscopy 7, 199 (1984).
2. J. C. Travis, J. Chem. Educ. 59, 909 (1982).
3. G. C. Turk, J. R. DeVoe, and J. C. Travis, Anal. Chem. 54, 643, (1982).
4. C. Th. J. Alkemade, T. Hollander, W. Snelleman, and P. J. Th. Zeegers, *Metal Vapours in Flames* (Pergamon Press, Oxford 1982).
5. N. Omenetto, C. A. Van Dijk, and J. D. Winefordner, Spectrochim. Acta 37B, 703 (1982).
6. M. A. Bolshov, A. V. Zybin, V. G. Koloshnikov, and K. V. Koshelev, Spectrochim. Acta, 32B, 279 (1977).
7. J. D. Bradshaw, N. Omenetto, G. Zizak, J. N. Bower, and J. D. Winefordner, Appl. Opt. 19, 2709 (1980).
8. F. Boe, Appl. Opt. 20, 3553 (1981).
9. T. Berthoud, J. Lipinsky, P. Camus, and J. L. Stehle, Anal. Chem. 55, 959 (1983).
10. G. C. Turk, Anal. Chem. 53, 1187 (1981).
11. J. A. Bellisio and P. Davidovits, J. Chem. Phys. 53, 3474 (1970).
12. C. Th. J. Alkemade, personal communication.

Optical Detection of Laser-Induced Ionization: A Study of the Time Decay of Strontium Ions in the Air-Acetylene Flame

G. C. TURK* and N. OMENETTO†
Joint Research Center, Chemistry Division, Ispra (Varese), Italy

Strontium atoms in the air-acetylene flame are directly photoionized in two steps provided by one dye laser tuned at the resonance ground-state transition (460.733 nm) and by the excimer pump beam at 308 nm, partially split from the amplifier section of the dye laser. The ions produced are then monitored by a third laser beam, colinear and counterpropagating in the flame, tuned to an ionic fluorescence transition and delayed in time with respect to the ionizing beams. In this way a fast decay, which is not affected by variations in the electron number density in the flame and therefore attributed to ion chemistry, and a slow decay, due to recombination, could clearly be observed. The fast decay is affected by variations in the flame stoichiometry and the slow decay by the number density of electrons in the flame, as shown by the addition of varying concentrations of an easily ionized element like caesium. The advantages of this optical probing of the laser-induced ionization in flames are discussed.

Index Headings: Flame spectroscopy; Fluorescence; Pulsed dye lasers; Spectroscopic techniques; Time-resolved spectroscopy; Laser-enhanced ionization; Optogalvanic spectroscopy.

Received 18 April 1986.
* On leave from: Center for Analytical Chemistry, National Bureau of Standards, Gaithersburg, MD.
† Author to whom all correspondence should be sent.

INTRODUCTION

Laser-enhanced ionization (LEI) spectroscopy utilizes direct electrical detection of element-specific ionization induced as a result of resonant laser photoexcitation. This detection is accomplished by using electrodes to pass an electrical current through the laser-irradiated region of the flame and measuring the increased current caused by the enhanced ionization.[1] We report here on experiments in which we have combined the ion-production aspects of LEI with ion detection by laser-induced ionic fluorescence. This optical detection of LEI offers a number of advantages for the study of the fundamental processes which control ionization in flames.[2] The specific example presented here involves the laser-induced ionization of strontium by means of an excimer pumped dye laser tuned at the 460.733-nm Sr line. Enhancement of the Sr ionization signal was observed to occur when the dye laser beam was combined with a fraction of the pumping excimer laser beam at 308 nm. We detected the resulting Sr^+ ions by using laser-induced ionic fluorescence with a second excimer pumped

0003-7028/86/4008-1085$2.00/0

dye laser at 421.522 nm to excite the Sr^+ ions and observing the fluorescence at 407.771 nm. By variation of time delay between the ionizing laser and the fluorescence probe laser, the decay of the laser-produced Sr^+ ions was studied. The magnitude of the ion fluorescence when the probe beam is temporally and spatially coincident with the ionizing beam yields information regarding the ionization yield.[2] The ionization enhancement induced by the excimer laser beam is presumably the result of photoionization of the excited Sr atoms which takes place in a manner described for combined dye laser-N_2 laser beams.[3,4] Autoionizing levels may also play a role.[5,6] We used this approach in order to achieve a greater ionization yield. This differs from the normal LEI mechanism of laser-photoexcitation followed by collisional ionization.[1] In order to avoid any confusion with terminology, we will use the term laser-induced ionization as a means of stating that the ionization occurs as a result of interaction with the lasers, without implying a specific mechanism of ionization.

Although direct electrical detection of laser-induced ionization is certainly more sensitive, as shown by the very low detection limits achieved by LEI spectrometry,[1] the mechanism of signal detection is quite complex[7-10] and therefore not always suitable for fundamental studies or flame diagnostics. When pulsed lasers are used, as is normally the case, the detected signal is generated by the current induced in the detection circuit by the motion of the ions and electrons under the influence of the electric field applied between the electrodes in the flame. The magnitude and temporal profile of this signal are very much dependent on the magnitude of the electric field, which is not uniform in a flame, and which is easily perturbed. The most common perturbation of the electric field occurs when easily ionized elements are aspirated into the flame.[11,12] Also, the electrical detection method is basically nonspecific. Electrons, owing to their higher mobility, generate the more sensitive portion of the induced current signal, and obviously any elemental specificity is lost. When ion pulses are observed some degree of specificity is preserved as a result of differences in ion mobility with mass, but sensitivity for the slower ions is low, and the mass resolution is not useful except in extreme cases.[13,14] Ionic fluorescence detection is specific to a particular ion and is not subject to the same types of perturbations as is electrical detection. It is of course less sensitive and subject to variations in quantum efficiency. Studies of temporal and spatial profiles of the laser-produced ions are straightforward.

The optical detection method is particularly advantageous for the fundamental studies of laser-induced ionization processes. In such studies it is often difficult to establish cause and effect relationships because it is often unclear whether an effect on the ion-electron production mechanism is being observed or an effect on the ion-electron detection mechanism.

The present work is similar in some respects to previous work published by Schenck *et al.*,[15] where the depletion in the population of sodium atoms in a flame caused by LEI was optically measured by laser atomic absorption. By the mapping of the depleted atom population in the flame as a function of time, flow and diffusion characteristics could be studied. The present work is more direct in that the created ions themselves are detected. In the atom depletion approach it is impossible to distinguish between depletion caused by ionization and that which may result from laser-induced chemical reactions.[16] In the present work we have concentrated on study of the decay (recombination, etc.) of the laser-produced Sr^+ ions and have not pursued any spatial mapping studies.

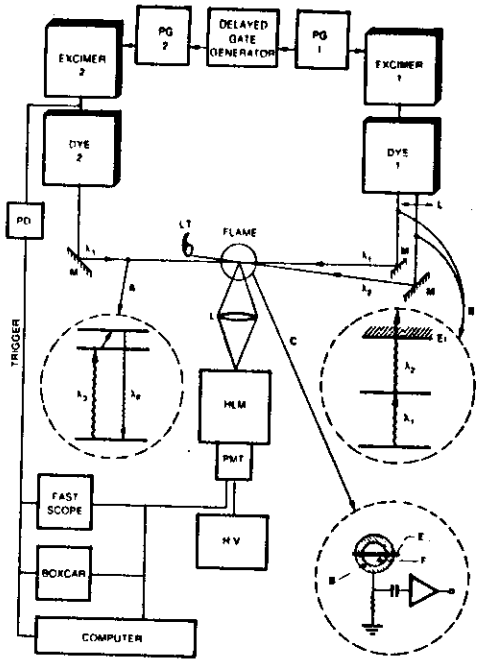

FIG. 1. Layout of the experimental setup. PG: pulse generator; PD: photodiode; Ms: mirrors; LT: light trap; L: lens; HLM: fluorescence high luminosity monochromator; PMT: photomultiplier tube; H.V.: high voltage. Insert A: excitation-detection scheme of the strontium ionic fluorescence. λ_1 = 421.552 nm, λ_2 = 407.771 nm. Insert B: two-step ionization scheme of the strontium atom: λ_1 = 460.733 nm; λ_2 = 308.2 nm; *E*, indicates the ionization continuum. Insert C: detection scheme of the laser-induced ionization current. B: burner; F: flame, E: water-cooled electrode.

EXPERIMENTAL

A schematic diagram of the experimental setup used in this work is shown in Fig. 1. An excimer laser (Lambda Physik, Model EMG 102, Göttingen, F.R.G.) operating at 10 Hz with XeCl excimer (308 nm) was used as the dye pumping source for the ionizing laser beam. Typical output energies from the excimer laser during the course of this investigation were between 25 and 35 mJ per pulse, with a pulse duration of 15 ns. The dye laser (Instruments S.A., Division Jobin Yvon, Longjumeau, France) was operated with the dye Coumarin 460 (Exciton, Dayton, OH, U.S.A.) and tuned to the Sr atom resonance at 460.733 nm (0–21,698 cm^{-1}). We modified this laser by replacing the total reflector, which directs 80% of the pumping radiation into the amplifier dye cell, with a 50% beamsplitter and allowing the unused portion of the pumping beam to exit the dye laser. The dye laser beam and the unused excimer beam were both directed into the flame, crossing at a glancing angle for maximum overlap in the flame, at a position 14 mm above the burner head. The excimer beam was partially focused by a 35-cm-focal-length lens, positioned so as to give a beam diameter of ~5 mm at the flame. The dye laser beam diameter was ~3 mm. Typical laser energy was 0.3 mJ per pulse for the 460.733-nm dye laser beam and 5.4 mJ per pulse for the excimer beam. Ionization signals for Sr were enhanced by a factor of 80 when the excimer beam was used together with the dye laser beam. No ionization signal was observed for the excimer beam alone.

A second XeCl excimer laser (Lambda Physik, Model EMG-50) was used to pump a dye laser (Instruments S.A., Division Jobin Yvon) containing the dye Stilbene 420 (Exciton Corp.) to give the Sr^+ fluorescence probing beam at 421.522 nm (0–23,715 cm^{-1}), which was directed into the flame in a path colinear with and counter-propagating to the ionizing beams. Typical output energy of the dye laser was 1.3 mJ per pulse at this wavelength.

The flame was a premixed air-acetylene flame with pneumatic nebulization of the sample solution and the use of a 1.5 cm × 1.5 cm square burner head with an argon flame separation sheath. Fuel and oxidant gas flows were as follows: acetylene: 1–3 L/min; nebulization air: 7 L/min; auxiliary air: 5–6 L/min.

We detected laser-induced fluorescence of Sr^+ at 407.771 nm (0–24,517 cm^{-1}) at a right angle to the laser beams using a 5-cm-diameter, 12.5-cm-focal-length lens to image (1:1) the flame on the entrance slit of a high-luminosity monochromator (Jobin Yvon, Model H-10). The monochromator was mounted sideways in order that the entrance slit could be placed in the same plane as the laser excitation beams. Signal averaging of the output of the photomultiplier (Type R928S, Hamamatsu Corp., Japan) was performed with a gated integrator (Model SR250, Standford Research Corporation, Palo Alto, CA, U.S.A.). Laser-induced ionization signals were optogalvanically detected with the use of the system available from SOPRA (Société de Production et de Recherches Appliquées, Bois Colombes, France) and described in Refs. 7 and 17. The water-cooled cathode was aligned 2 cm above the burner with a −1500 V potential. Except for specific experiments regarding electric field effects, no voltage was applied to the cathode when fluorescence measurements were being made. We externally triggered both excimer lasers to achieve syncronization and control of time delay between pulsing of the ionization laser and the fluorescence probe laser. We found it convenient to use the gate-scanning capabilities of a boxcar averager (Princeton Applied Research, Model 162/164, Princeton, NJ, U.S.A.) as a delay generator. The ionizing excimer laser was triggered by a pulse generator (EH Research Lab., Model EH-137A, Oakland, CA, U.S.A.) operated at an internally controlled repetition rate of 10 Hz. This pulse generator also triggered the "boxcar-delay" controller. The "gate out" pulse from this device was used to trigger a second pulse generator (Data Pulse, Model 100A, Culver, CA, U.S.A.), which in turn triggered the excimer laser pumping the fluorescence probe beam. By scanning the gate delay of the "boxcar," we could vary the time delay between the two lasers and use the time-base output as a measure of the delay. Note that this "boxcar" served only as a delay generator, not as a gated integrator. The averaged fluorescence signal, together with the time-base output of the delay generator, was connected to an analog-to-digital converter (Stanford Research Corp., Model SR245) interfaced with a computer (HP Model 9816S, Hewlett-Packard, San Diego, CA, U.S.A.) for data analysis, display, and storage. Nonlinear least-squares fitting of Sr^+ decay data was performed with the use of the regression analysis software of the Hewlett-Packard statistics library (Model HP 98820A).

RESULTS AND DISCUSSION

With the ionizing laser off, the fluorescence probe laser excites only the Sr^+ ions which are present in the flame as a result of unassisted thermal ionization of the aspirated Sr. When the ionizing laser is turned on, in spatial and temporal coincidence with the probe laser, the probe observes an increased density of Sr^+ ions and the signal increases accordingly. If the natural thermal ion fraction is known, comparison of the laser-induced ionization level with the natural ionization level gives the laser-induced ionization yield. This yield, which has been previously measured for lithium with the use of an absolute procedure,[18] is of interest in determining, among other things, the accuracy of proposed LEI mechanism models, the ultimate levels of sensitivity obtainable by LEI, and the impact of the ionization pathway on other laser-based spectroscopic methods. We have measured the natural thermal ionization fraction of Sr at a solution concentration of 10 μg/mL by observing the increase in the resonance atomic fluorescence of Sr at 460.733 nm which occurs when the thermal ionization is suppressed by the addition of 1000 μg/mL of Cs solution. In the Cs matrix the atomic Sr level was found to increase by 12% while the level of Sr^+ fluorescence decreased below the limit of detection.

This value varies considerably with flame conditions, but under exactly the same conditions the magnitude of the laser-produced Sr^+ ionic fluorescence was found to be 1.8 times that of the natural level. Defining the laser ionization yield as the fraction of available Sr atoms which undergo laser-induced ionization, a value of 25% is obtained. For comparison, we can also estimate the laser ionization yield by determining the number of electrons detected electrically from the area under the laser-induced ionization current pulse. Assuming that the pulse follows the induced current model for a point charge pair described in Ref. 8, one can calculate the number of ions created by one laser pulse. To then calculate the ion yield requires a knowledge of the number of Sr atoms in the laser beam. This can be estimated from a rough measurement of the volume of the laser-irradiated portion of the flame and from an estimate of the Sr atom density derived from the published value[19,20] of the Sr atomization efficiency (β = 0.06), estimating

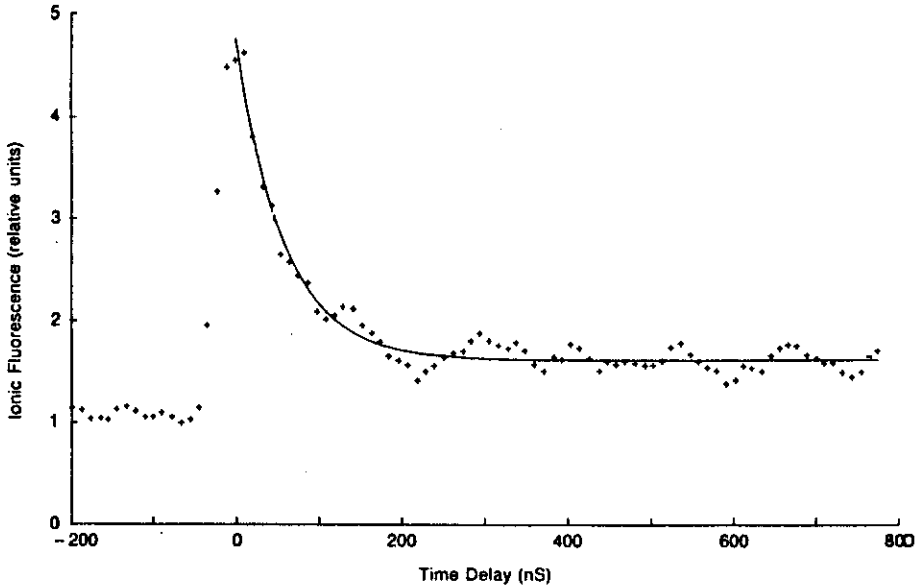

FIG. 2. Observed time decay of the strontium ionic fluorescence. The zero in the time scale (abscissa) indicates temporal coincidence between the three laser beams (see Fig. 1). The total delay indicated (1 μs) then refers to the probe laser exciting the fluorescence.

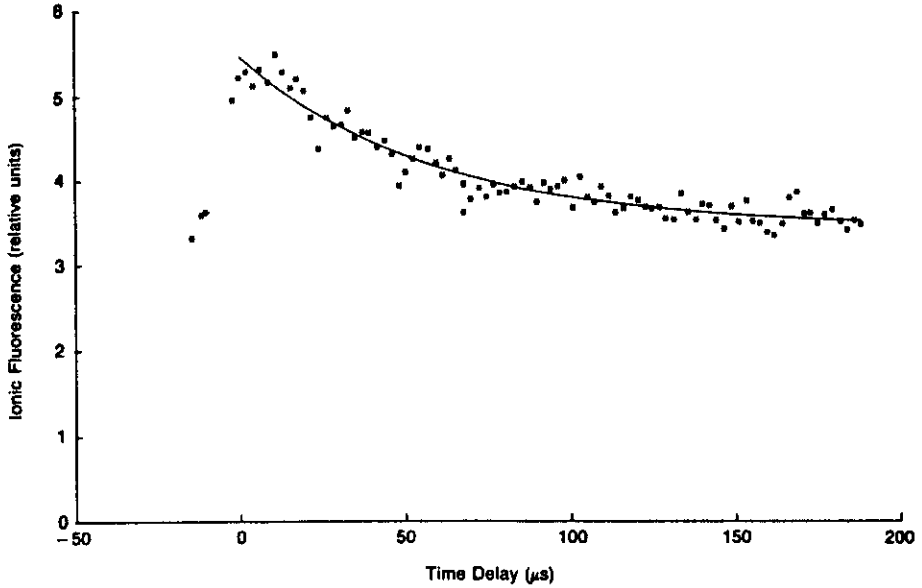

FIG. 3. Same as in Fig. 2 except for the time span in abscissa, which is increased to 400 μs.

the atom density of a completely atomized ($\beta = 1$) species to be 10^{11} cm^{-3} for a 1-μg/mL solution.[19,20] The ionization yield obtained via this procedure was 14%, which is in very reasonable agreement with the optically detected value.

As discussed earlier, by adding a variable delay time between the firing of the ionizing laser and fluorescence probe laser, we studied the time history of the laser-produced ions. Two distinctly different decay modes were observed. In Fig. 2 the Sr^+ fluorescence signal for a 10 μg/mL Sr solution is plotted as a function of time delay for a 1-μs range surrounding the moment of time coincidence. The figure includes some data collected before "time zero," where the probe laser fires *before* the ionizing laser. During this period only the natural thermally ionized Sr^+ is observed. At time coincidence we observe the laser-induced ionization, and as the delay increases we observe a fast exponential decay of Sr^+. Occurring with a time constant of 58 ns, this rapid decay consumes 85% of the laser-produced ions before reaching an equilibrium. The remaining 15% of the laser-produced ions decay at a much slower rate, as seen in Fig. 3, where the delay range has been increased to 200 μs. In this range the time resolution is too coarse to observe the fast decay. The slow decay occurs with an exponential time constant of 57 μs asymptotically approaching the natural Sr^+ level.

The slow decay occurs in a time regime where ion-electron recombination is expected to occur. In order to investigate this point further, we performed a series of time delay studies in which various levels of caesium were added to a 10-μg/mL Sr solution. The increased concentration of free electrons in the flame resulting from thermal ionization of Cs increases the rate of ion-electron recombination; this is clearly borne out in the time delay curves presented in Fig. 4. In this figure the exponential decay time constant decreases from 14.3 μs to 7.2 μs to 2.9 μs as the Cs matrix concentration increases from 100 to 300 to 1000 μg/mL. Note also that, as expected, the natural Sr ionization has been suppressed in the presence of Cs and that only laser-produced Sr ions are observed. If the rate of recombination is expressed by the relationship

$$-\frac{d[Sr^+]}{dt} = k_r[e^-][Sr^+] \qquad (1)$$

where k_r is the recombination rate coefficient and if $[e^-] \gg [Sr^+]$, then the product of $k_r[e^-]$ can be considered a pseudo-first-order rate coefficient.[19] The integrated form of Eq. 1 is

$$[Sr^+] = [Sr^+]_0 \exp(-k_r[e^-]t) \qquad (2)$$

where $[Sr^+]_0$ is the initial concentration of Sr^+. The rate coefficient $k_r[e^-]$ is the *inverse* of the time constants obtained from the delay curves. Assuming that the aspirated Cs is the principal source of electrons in the flame, then, according to the Saha ionization equilibrium,[19] $[e^-]$ should increase as the square root of Cs concentration. Therefore $k_r[e^-]$ should increase as the square root of Cs concentration, which as seen in Fig. 5 is indeed the case.

As far as the case of the slow decay in the absence of Cs is concerned (Fig. 3), it is unclear whether the ob-

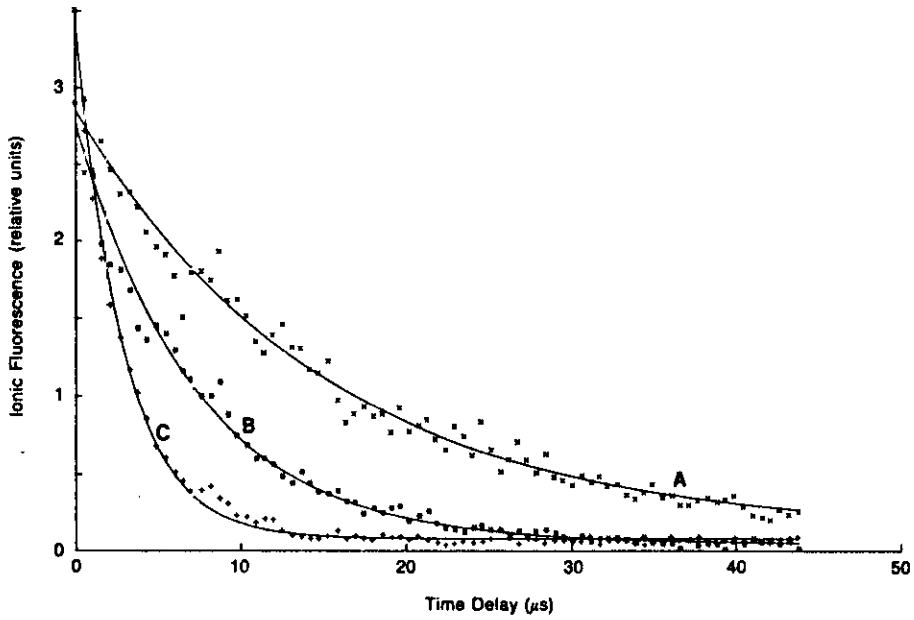

FIG. 4. Effect of varying amounts of caesium on the slow decay of the strontium ionic fluorescence. A: Cs = 100 μg/mL; B: Cs = 300 μg/mL; C: Cs = 1000 μg/mL. The concentration of strontium is 10 μg/mL.

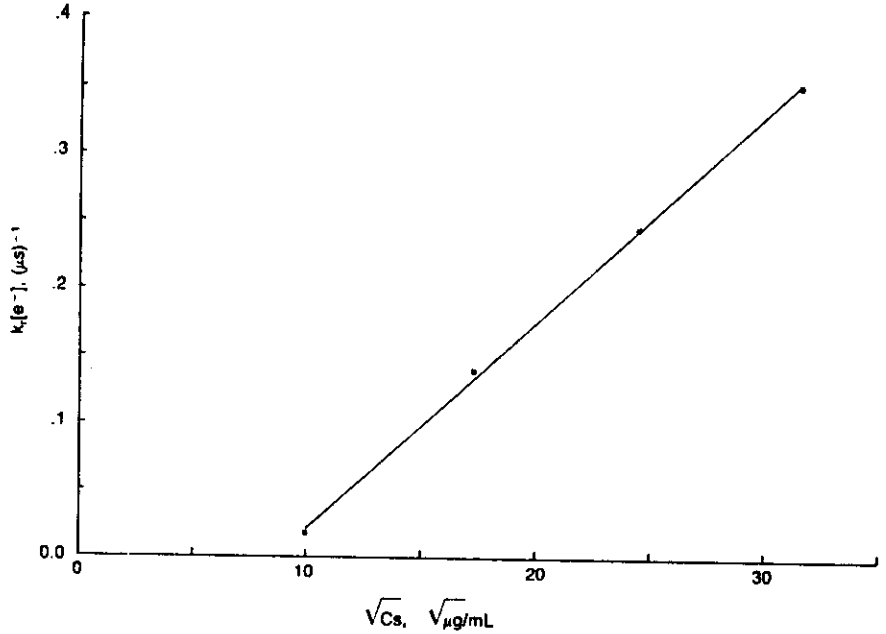

FIG. 5. Relation between the pseudo-first-order rate coefficient ($k_1 \cdot [e^-]$) and the square root of the concentration of caesium aspirated in the flame.

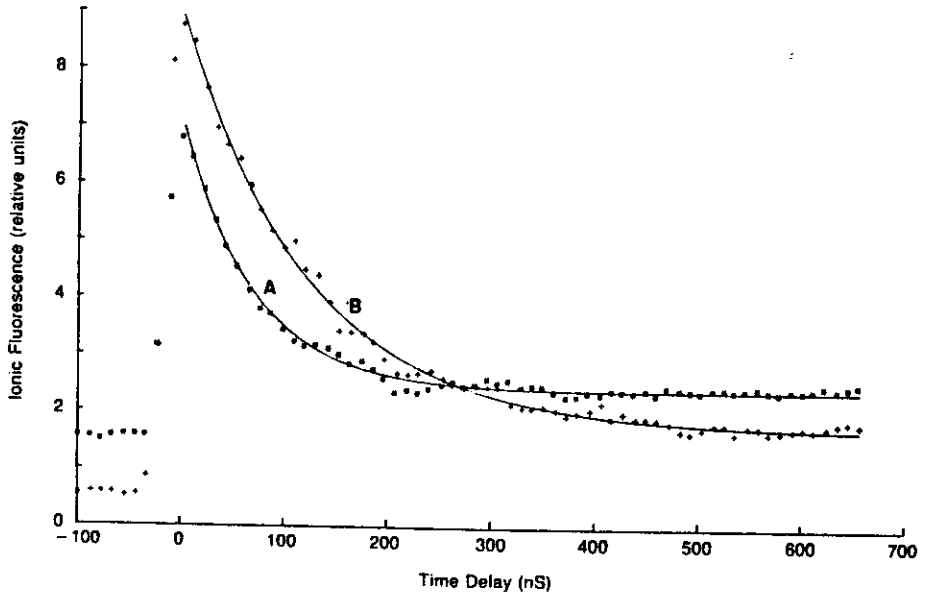

FIG. 6. Effect of flame stoichiometry on the fast decay of strontium ionic fluorescence. A: acetylene flow: 2 L t/min; B: acetylene flow: 2.75 L t/min.

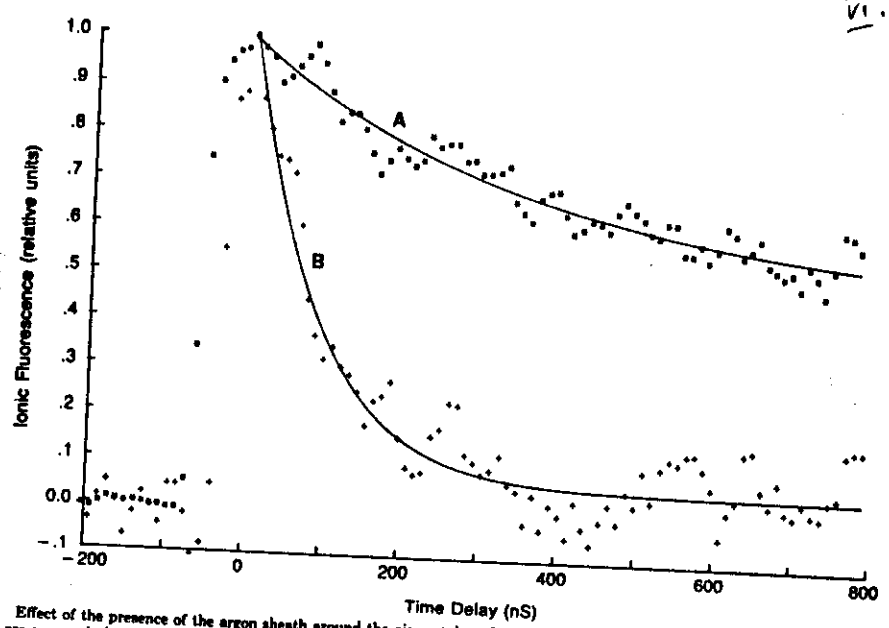

FIG. 7. Effect of the presence of the argon sheath around the air-acetylene flame on the fast decay of strontium ionic fluorescence. The laser beams are purposely located at the flame border, where the effectiveness of the sheath in separating the secondary combustion zone is more pronounced. For the clarity of presentation, the signals have been normalized to the same scale and the natural ionization level has been subtracted out. The net laser-produced ion level at time coincidence is 2.6 times greater with the sheath on. A: argon sheath on; B: argon sheath off.

served decay is due to ion-electron recombination, since the physical transport effects of diffusion and flame gas flow would also be reasonable to expect in this time range. In the presence of Cs, the slow decay is certainly due to recombination. Another interesting point of the Cs matrix study is that the magnitude of the laser-produced ionic fluorescence signal at time zero was not observed to be affected by the presence of Cs, except the normal increase in signal resulting from the increased atom population due to suppression of thermal ionization. This is relevant to ionization interferences observed in electrically detected LEI spectroscopy, and indicate that these interferences stem from the signal *detection* process, not the ion *production* process. This is in agreement with published studies of the LEI ionization interferences.[11,12]

The fast decay process (Fig. 2) is more difficult to explain. It is unaffected by the presence of a 1000-μg/mL Cs matrix, which indicates that it is not an ion-electron recombination, and it is too fast to be related to any physical transport. However, changes in the fast decay behavior were observed when the fuel-to-oxidant ratio in the flame was changed. Figure 6 shows the fast decay characteristics at two different acetylene flow rates with the use of a constant oxidant flow. A number of effects are observed, but most relevant is the increase in the decay time constant from 69 ns to 121 ns when the acetylene flow was increased from 2.0 L/min to 2.75 L/min. The implication of this observation is that the fast decay is the result of chemical reaction of Sr^+ with flame constituents which decrease in concentration under fuel-rich conditions.

We monitored the concentration of OH in the flame by measuring the fluorescence at 306 nm excited by the 308-nm excimer laser. This was found to be four times less under the richer of the two conditions presented here. More dramatic fluctuations in OH are known to occur at the edge of the flame when operated with and without an argon shield,[21] with OH levels decreasing by more than an order of magnitude with the sheath on. Figure 7 shows the very dramatic effect of the shield on the fast decay when the laser was aligned at the edge of the flame.

Although it is tempting to relate the fast decay observed to some specific reactions with flame radicals or molecules, our flame was not sufficiently characterized in terms of composition and temperature to warrant such speculations. However, it seems likely that free oxygen as well as negatively charged oxygen molecules play a major role in neutralizing the strontium ions, leaving the atoms in any excited state or taking them directly into the ground level. The role of free oxygen was clearly pointed out in a study of laser-assisted ionization of sodium.[22] In addition, water vapor could react with strontium ions by forming $SrOH^+$ through an ionic-rearrangement process.[19]

Another effect of fuel-rich conditions seen in Fig. 6 is a decrease in the level of natural Sr^+ (i.e., before time zero) and an increase in the ratio of the laser-produced to natural ionization levels. This is primarily a temperature effect which results in a lower natural ionization fraction in the cooler fuel-rich mixture. This makes the laser-induced ionization signal relatively greater, but the

ionization yield (as discussed earlier) remains essentially constant. The increase in the absolute magnitude of the laser-produced Sr^+ fluorescence signal may be the result of an improved atomization efficiency or quantum yield, although the transition was observed to be optically saturated. In the theoretical models of the LEI process which have been developed with the use of rate equation analysis,[1,23,24] the only ion loss mechanism considered has been that of recombination, which was then neglected as being too slow to have any effect on the detected LEI signal. The possibility of a very fast chemical reaction loss has never been considered, and further study will be necessary to evaluate the consequences of such fast decay. The results presented here only pertain to Sr and it would be difficult to speculate on how general this process is. Certainly, the ionic fluorescence probe technique described here is readily applicable to the other alkaline earth elements (Ca and Ba) which have strong ionic transitions at wavelengths easily accessible by dye lasers.

The authors hope that the results of this work will further stimulate the evaluation of the combination of the fluorescence and ionization techniques in the study of flame processes. Moreover, the possibility of following the fate of several ionic species created at one specific location in an inductively coupled plasma appears very attractive for the study of its complex excitation/ionization dynamics.

ACKNOWLEDGMENTS

G. C. Turk would like to thank the Joint Research Center authorities and in particular the Education Training Service of Ispra for the grant of a visiting scientist fellowship.

1. J. C. Travis, G. C. Turk, J. R. deVoe, P. K. Schenck, C. A. Van Dijk, Progress Anal. Atom. Spectrosc. 7, 199 (1984), and references therein cited.
2. G. C. Turk, O. Axnér, and N. Omenetto, paper submitted to Spectrochim. Acta B.
3. C. A. Van Dijk, F. M. Curran, K. C. Lin, and S. R. Crouch, Anal. Chem. 53, 1275 (1981).
4. F. M. Curran, K. C. Lin, G. E. Leroi, P. M. Hunt, and S. R. Crouch, Anal. Chem. 55, 2382 (1983).
5. P. Esherick, Phys. Rev. 15A, 1920 (1977).
6. L. P. Hart, B. W. Smith, and N. Omenetto, Spectrochim. Acta 40B, 1637 (1985).
7. T. Berthoud, J. Lipinsky, P. Camus, and J. L. Stenlé, Anal. Chem. 55, 959 (1983).
8. G. J. Havrilla, P. K. Schenck, J. C. Travis, and C. C. Turk, Anal. Chem. 56, 186 (1984).
9. P. K. Schenck, J. C. Travis, and G. C. Turk, *Journal de Physique*, Colloque C7, Suppl. n°11, Tome 44, C7-75, P. Camus, Ed. (Les Ulis Cedex, France, 1983).
10. J. C. Travis, P. K. Schenck, G. C. Turk, and J. Wen, in preparation.
11. R. B. Green, G. J. Havrilla, and T. O. Trask, Appl. Spectrosc. 34, 561 (1980).
12. G. C. Turk, Anal. Chem. 53, 1187 (1981).
13. W. G. Mallard and K. C. Smyth, Combust. Flame, 44, 61 (1982).
14. K. C. Smyth and W. G. Mallard, Combust. Sci. and Tech. 26, 35 (1981).
15. P. K. Schenck, J. C. Travis, G. C. Turk, and T. C. O'Haver, Appl. Spectrosc. 36, 168 (1982).
16. C. H. Muller III, K. Schofield, and M. Steinberg, in *Laser Probes for Combustion Chemistry*, D. R. Crosley, Ed., ACS Symposium Series No. 134, (ACS, Washington, D.C., 1980).
17. N. Omenetto, T. Berthoud, P. Cavalli, and G. Rossi, Anal. Chem. 57, 1256 (1985).
18. B. W. Smith, L. P. Hart, and N. Omenetto, Anal. Chem. 58, 2147 (1986).
19. C. Th. J. Alkemade, Tj. Hollander, W. Snelleman, and P. Th. J. Zeegers, *Metal Vapours in Flames* (Pergamon Press, New York, 1982).
20. N. Omenetto, and J. D. Winefordner, Progress Anal. Atom. Spectrosc. 2, 1/2, (1979).
21. D. O. Knapp, N. Omenetto, L. P. Hart, F. W. Plankey, and J. D. Winefordner, Anal. Chim. Acta 69, 455 (1974).
22. C. A. Van Dijk, *Two-Photon Excitation of Higher Sodium Levels and Population Transfer in a Flame*, Ph.D. Dissertation, Utrecht, The Netherlands (1978).
23. O. Axner, T. Berglind, J. L. Heully, I. Lindgren, and H. Rubinstein-Dunlop, J. Appl. Phys. 55, 3215 (1984).
24. N. Omenetto, B. W. Smith, and L. P. Hart, Fresenius Z. Anal. Chemie, 324, 683 (1986).

"NEAR-RESONANCE EFFECTS IN THE LASER INDUCED IONIZATION OF STRONTIUM IN THE AIR-ACETYLENE FLAME"

N.Omenetto, L.P.Hart*, B.W.Smith** and G.C.Turk***

Joint Research Centre

Chemistry Division

21020 ISPRA (Varese), Italy

*

Present Address: Radiation Centre, Oregon State University, Corvallis, OR 97331, U.S.A.

**

Present Address: Department of Chemistry, University of Florida, Gainesville, Fla. 32611, U.S.A.

***

Present Address: Centre for Analytical Chemistry, National Bureau of Standards, Gaithersburg, MD 20899, USA

ABSTRACT

Several ionization signals observed for strontium atoms in an air-acetylene flame when a single, pulsed dye laser is focussed into it are attributed to near-resonance two-step excitation followed by collisional ionization with flame species. These signals are clearly different from those obtained at exact single-photon or two-photon resonances. Other possible excitation-ionization mechanisms are also discussed.

INTRODUCTION

When an atomic vapour formed in an atmospheric pressure flame is illuminated by one or two pulsed dye lasers tuned to selected atomic transitions, efficient population of the excited levels can be achieved. Since the flame is a collision-dominated system, the excited atoms can be thermally ionized and the resulting current measured: this forms the basis of the well known laser-enhanced ionization spectroscopy technique [1].

During the course of our investigation of the characteristics of the ionization spectrum of strontium atoms in the air-acetylene flame with one and two excimer-pumped dye lasers [2], we have observed several transitions which could not fit a direct two-photon excitation scheme, i.e., a scheme involving the ground state and a virtual level at half the excitation energy of the laser photon. In addition the observed signals also showed a spectral behaviour which was different from that of other identified transitions. Figure 1 shows the ionization signals obtained by nebulizing in the flame a solution containing 5 mg/Lt of strontium and by scanning the dye laser in a narrow spectral region in the vicinity of the strontium ground state resonance transition at 460.733 nm. The five lines observed are the ground state resonance line, two lines at 459.513 and 456.70 nm which are due to two-photon absorption, a line at 458.293 nm and a small line at 460.085 nm which could not fit either scheme, i.e., resonance ground state absorption or two-photon absorption.

Several other lines in different spectral regions were observed which could also not fit a direct two-photon scheme. The aim of this paper is to present their experimental observation and to discuss their possible origin.

./...

EXPERIMENTAL

The experimental set-up is illustrated in Figure 2. The excimer laser-pumped dye laser (EMG-102 excimer laser, Lambda Physik - Fed. Rep. Germany and Jobin Yvon dye laser, France) was focussed into the flame and retroreflected with a spherical mirror so that at the beam waist the laser peak irradiance was about 100 MW cm^{-2}. The electrode configuration in the flame and the detection system, which are based on a water-cooled molybdenum electrode immersed in the flame(formed by burning acetylene and air on a conventional slot burner) and a boxcar amplifier have been described in detail elsewhere [3]. The laser spectral bandwidth in the wavelength region investigated was 0.02 nm (~30 GHz) and the spectra were obtained by scanning the holographic grating in the dye oscillator.

Strontium solutions were prepared from high purity standards and diluted with deionized and doubly-distilled water.

RESULTS AND DISCUSSION

As said before, the strongest signal shown in Figure 1 and occurring when the dye laser is tuned to 458.293 nm does not fit a direct two-photon absorption transition since no real level is reported for strontium at twice the energy of this line [4]. Instead, the wavelength calculated corresponds to a resonance energy between the $^1P_1$ excited state (5s5p) and a ^1S_o Rydberg state (5s10s) which lies only 0.3 eV below the first ionization potential of strontium (in our flame, kT = 0.215 eV). The wavelength interval (2.4 nm) between the three strong lines shown in Fig.1 was inspected in a detailed manner with the aid of the reported energy level configuration for the strontium atom [4] and all the possible excitation schemes which would result in the observation of ionization signals in that interval are collected in Figure 3.

As shown in the Figure, the signal at 458.293 nm could be due to "excited state, single step, resonance absorption" from the thermally populated $^1P_1$ level. It could however also be due to excitation of the 21814 cm^{-1} "virtual" level which is close to the real $^1P_1$ level (21698 cm^{-1}). The atom brought to this level would therefore be transferred by collisions into the real level from which resonance absorption to the ^1S_o level will occur.

By proceeding towards longer wavelengths, a two-photon absorption transition from the ground state ($5s^2\ ^1S_o$) to the 5s10s, ^1S_o state ($\Delta J = 0$) is possible and is indeed observed in the spectrum.

The existence of the $^3S_1$ level of 43428 cm^{-1} excitation energy would imply the observation of a signal of 460.085 nm which could be explained in the same manner as for the 458.293 nm signal, i.e., it could be due either to excited state absorption from the $^1P_1$ level or to excitation to the "virtual" level at 21756 cm^{-1} followed by collisional transfer to the $^1P_1$ level. However, the subsequent absorption to the $^3S_1$ level is parity forbidden and the probability of such transition would be very low. Indeed, the small signal shown in Figure 1 corresponds exactly to the calculated wavelength of 460.085 nm.

The final possibility of a two-photon absorption to the $^3S_1$ state which would occur at 460.409 nm through the intermediate level at 21714 cm^{-1} is negated by the $\Delta J = 0$ selection rule for two-photon absorption and in fact is not observed.

In conclusion, only the line at 458.293 nm could result from two different excitation-ionization schemes and we will try now to evaluate the relative importance of the two processes. It is well

known that the flame is a system very close to thermodynamic equilibrium [5] and therefore the rate of collisional excitation of level $^1P_1$ from the ground state can be calculated from the Boltzmann relationship to be approximately five orders of magnitude lower than the quenching rate, which is $\sim 10^8$ s^{-1}. On the other hand, if the laser radiation field is high, a level can be significantly broadened as a result of the strong saturation achieved. In this case, the "virtual" level reached by the off-resonance photon can be thought of as being located in the far wings of a real level, significantly broadened by collisions and by radiation. According to Van Dijk [6], in linear interaction conditions, the absorption coefficient of sodium atoms in an hydrogen flame drops by about five orders of magnitude for a detuning of $\sim$10A° form the the line centre. However, in saturated conditions, a seven orders of magnitude drop for a 200A° range reduces to two orders of magnitude. Even with such reduced absorption coefficients, it is easy to calculate that the rate of radiative excitation for a 100 MW cm^{-2} laser tuned to the off-resonance transition exceeds the collisional excitation rate of level $^1P_1$ by many orders of magnitude.

These consicerations point to the conclusion that the ionization signal at 458.293 nm is the result of the population of level 5s10s (^1S_o) in Figure 3 by two steps: (i) absorption of a photon in the far wings of the broadened $5s^2 \longrightarrow 5s5p$ transition, and (ii) resonant absorption of a photon tuned to the $5s5p \longrightarrow 5s10s$ transition. Whether the level reached by the first photon is called "virtual" or "real" seems to be irrelevant here. However, if we treat our laser as a continuum source and calculate the Rabi frequency on resonance associated with the field, we see that our detuning from resonance is larger

than two Rabi frequencies and therefore, according to Shore [7], the off-resonance level should be called "virtual".

There is ample evidence in the literature of such near-resonance processes which have been observed in ionization as well as fluorescence studies [8-19], notably also for the strontium case [11, 16]. The simultaneous observation of the resonance fluorescence signal at 460.733 nm would have been of particular relevance here to support the near-resonance excitation process.

Figures 4-6 show the ionization spectra in different spectral regions obtained under the same experimental conditions of Figure 1. Again, the strongest lines observed are believed to be due to similar near-resonance, two-step excitation processes. When the instrumental sensitivity is arranged so to have all signals on the same scale (see Figure 6) one can see that the near-resonance transitions can be up to one order of magnitude stronger than the other signals. In some cases (Figure 5) the lines observed are listed in Standard Wavelength Tables [20] as terminating to <u>metastable</u> levels lying below the $^1P_1$ level (14504 and 14899 cm^{-1} above the ground state). In this case, one would assume that the process responsible for the observed signals is the resonance excitation of the thermal population of the metastable level.

All the transitions observed in a 4 nm spectral interval and believed to be due to a two-step absorption process in the wings of the $^1P_1$ level are collected in Figure 7. The high-lying excitation levels have been named according to Moore [4]. As seen in the Figure, seven transitions were identified.

In conclusion, two considerations can be pointed out from these observations :

(i) when a single dye laser is focussed in a flame so that high photon irradiancesare achieved, the radiative absorption rate in the far wings of a real level can still exceed the collisional excitation rate by several orders of magnitude and therefore near-resonance effects can easily be observed;

(ii) for analytical applications, the resulting ionization spectrum is very complex especially when the analyte atoms are present as trace constituents in a solution containing large amounts of other concomittants As a result, the possibility of observing spectral interferences becomes severe, and there appears to be a "threshold" for the maximum laser irradiance which is analytically useful.

ACKNOWLEDGEMENTS

L. P. Hart, B.W. Smith and G.C. Turk would like to thank the Joint Research Centre authorities and in particular the Education Training Service for the grants of visiting scientist fellowships.

REFERENCES

[1] . J.C.Travis, G.C.Turk, J.R.DeVoe, P.K.Schenck and C.A. Van Dijk, Progress Anal. At. Spectrosc., 7 (1984) 199.

[2] . L.F.Hart, B.W.Smith and N.Omenetto, Spectrochim. Acta 40B (1985) 1637.

[3] . N.Omenetto, T.Berthoud, P.Cavalli and G.Rossi, Anal. Chem. 57 (1985) 1256.

[4] . C.E.Moore, "Atomic Energy Levels", Vol. II, NSRDS-NBS 35, Washington D.C., (1971).

[5] . C.Th.J.Alkemade, Tj.Hollander, W.Snelleman and P.J.Th.Zeegers, "Metal Vapours in Flames", Pergamon Press, Oxford, (1982).

[6] . C.A.Van Dijk, Opt. Commun. 22 (1978) 225.

[7] . B.W Shore, Am. J. Phys., 47 (1979) 262.

[8] . G.Mainfray and C.Manns, Appl. Opt. 19 (1980) 3934.

[9] . C.H.Becker and K.T.Gillen, J. Opt. Soc. Am. B, 2 (1985) 1438.

[10] . R.Walkup, A.Migdall and D.E.Pritchard, Phys. Rev., A, 29 (1984) 2651.

[11] . J.L.Carlsten, A.Szöke and M.G.Raymer, Phys. Rev. A, 15 (1977) 1029.

[12] . C.Chan and J.W.Daily, J.Quant. Spectros., Rad. Transfer, 21 (1979) 527.

./...

REFERENCES (to be continued)

[13] . C.A.Van Dijk and C.Th.J.Alkemade, J.Quant.Spec.Rad.Transfer, 23 (1980) 445.

[14] . R.Granier, G.Charton and J.Granier, J.Quant.Spec.Rad.Transfer, 26 (1981) 71.

[15] . J.J.Snyder, T.B.Lucatorto, P.H.Debenham and S.Geltman, J.Opt. Soc. Am. B, 2 (1985) 1497.

[16] . P.Esherick, Phys. Rev. A 15 (1977) 1920.

[17] . D.Feldmann, H.J.Krautwald and K.H.Welge, J. Phys. B 15 (1982) 4529.

[18] . G.C.Turk, F.C.Ruegg, J.C.Travis and J.R.DeVoe, submitted for publication.

[19] . G.C.Turk and R.L.Watters, Anal. Chem. 57 (1985) 1979.

[20] . C.H.Corliss and W.R.Bozman, "Experimental Transition Probabilities for Spectral Lines of seventy Elements", National Bureau of Standards, Monograph 53, Washington (1962).

LEGENDE OF FIGURES

Figure 1 : Ionization spectrum obtained by scanning the dye laser in the region 455-463 nm. The line shown at 456.70 nm results from a two-photon absorption process to the 9d level. The strontium concentration in the solution is 5 mg/Lt.

Figure 2 : Experimental set-up used. The water-cooled electrode is immersed in the flame and negatively biased at -1300V. The electrons produced are collected at the burner, converted to a voltage and processed by a boxcar integrator.

Figure 3 : Possible excitation - collisional ionization pathways pertinent to the signals shown in Figure 1 (the resonance ground state transition at 460.733 nm has been left out). The levels are given to the left and their energy (cm^{-1}) to the right [4]. Wavy lines indicate radiative excitation while straight lines indicate collisional excitation. The dashed wavy lines indicate a forbidden two-photon absorption process.

Figure 4 : Ionization spectrum obtained by scanning the dye laser in the region 443-447 nm. One line (445.710 nm) is the result of a two-photon absorption transition to a 12d level and the other three lines are attributed to a near-resonance process. The concentration of strontium in the solution is indicated.

./...

LEGENDE OF FIGURES (continued)

Figure 5 : Ionization spectrum obtained by scanning the dye laser in the region 477-484 nm. The two signals on scale are listed in the NBS Wavelength Tables [20]. The 483.208 nm line corresponds to the transition 14504 $\longrightarrow$ 35194 cm^{-1} while the 481.188 nm line corresponds to the transition 14899 $\longrightarrow$ 35675 cm^{-1}. Since the two lower levels of these transitions are metastable, the signals are believed to be due to excited state resonances from the thermally populated metastable levels. As in the other figures, the near resonance signal at 478.392 nm is at least five times more intense.The concentration of strontium in the solution is indicated.

Figure 6 : Ionization spectrum obtained by scanning the dye laser in the region 467 nm to 472 nm. Contrary to the case of Figures 1, 4 and 5, here the sensitivity was adjusted so to keep all signals on the same scale. The strongest signals at 468.860 and 467.781 nm are due to near-resonance absorption. The line indicated at 469.40 nm results from a direct two-photon absorption process while the series of lines to the left of the figure are either due to excited state resonance absorption from metastable levels or two-photon absorption to high s and p levels.

Figure 7 : Energy level scheme for the near-resonance transitions observed in this work. The real level $^1P_1$ (the resonant level) is indicated with a solid line while the virtual or far wing excitation energies are indicated ardashed lines. Energies are not drawn on scale.

Figure 1

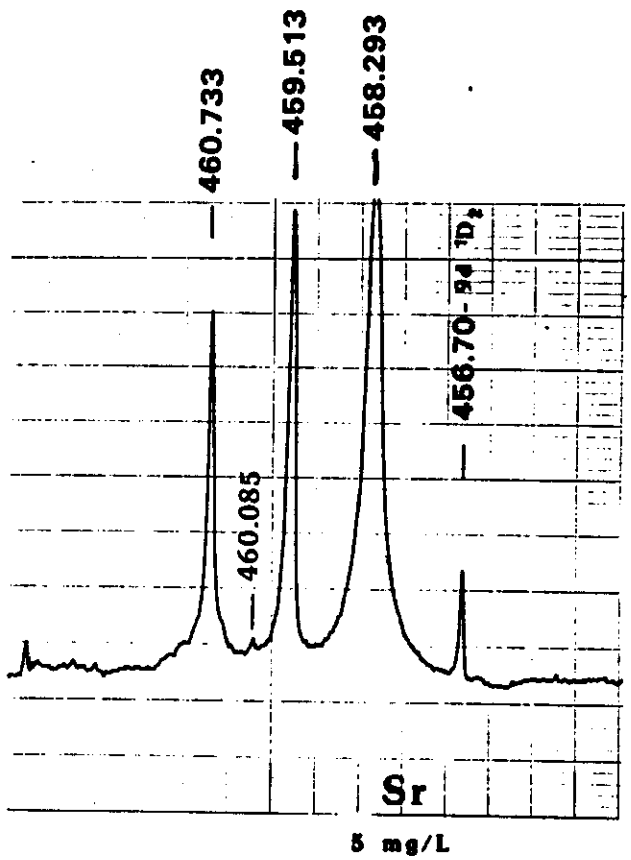

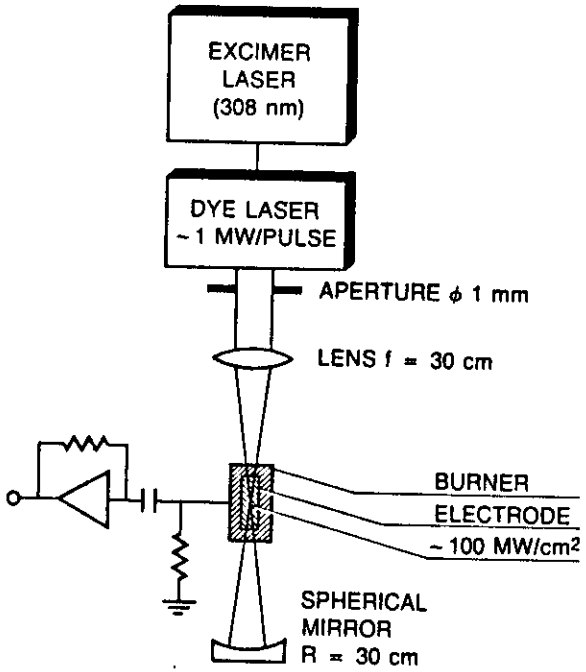
EXCIMER LASER (308 nm)
DYE LASER ~1 MW/PULSE
APERTURE ϕ 1 mm
LENS f = 30 cm
BURNER
ELECTRODE
~100 MW/cm²
SPHERICAL MIRROR R = 30 cm

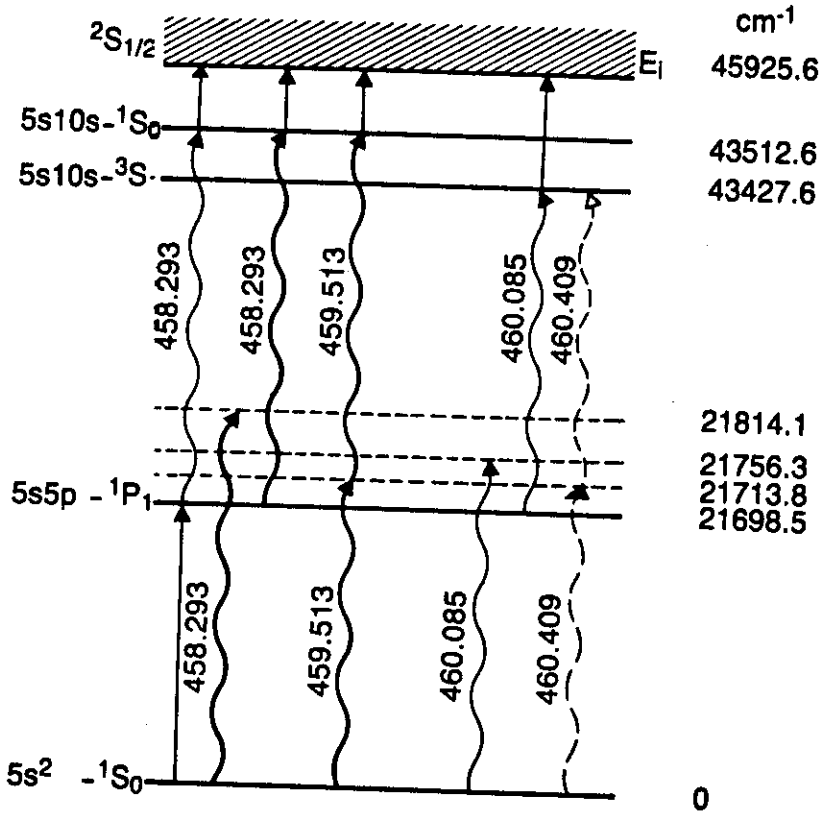
cm⁻¹
$^2S_{1/2}$
E_I
45925.6
5s10s-$^1S_0$
43512.6
5s10s-^3S
43427.6
458.293
458.293
459.513
460.085
460.409
21814.1
21756.3
21713.8
21698.5
5s5p -$^1P_1$
458.293
459.513
460.085
460.409
5s² -$^1S_0$
0

Figure 4

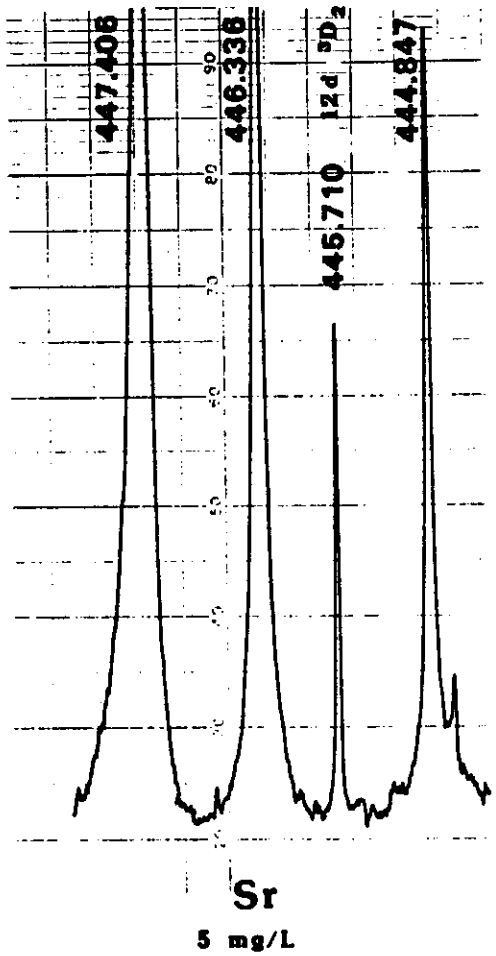

Figure 5

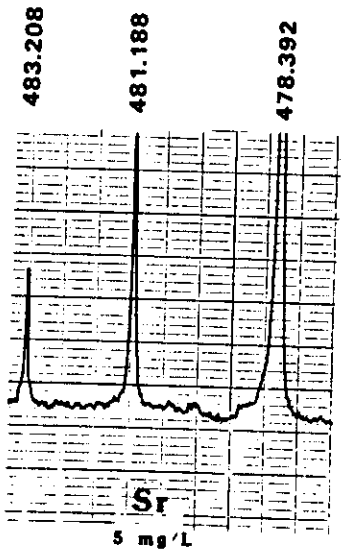

Figure 6

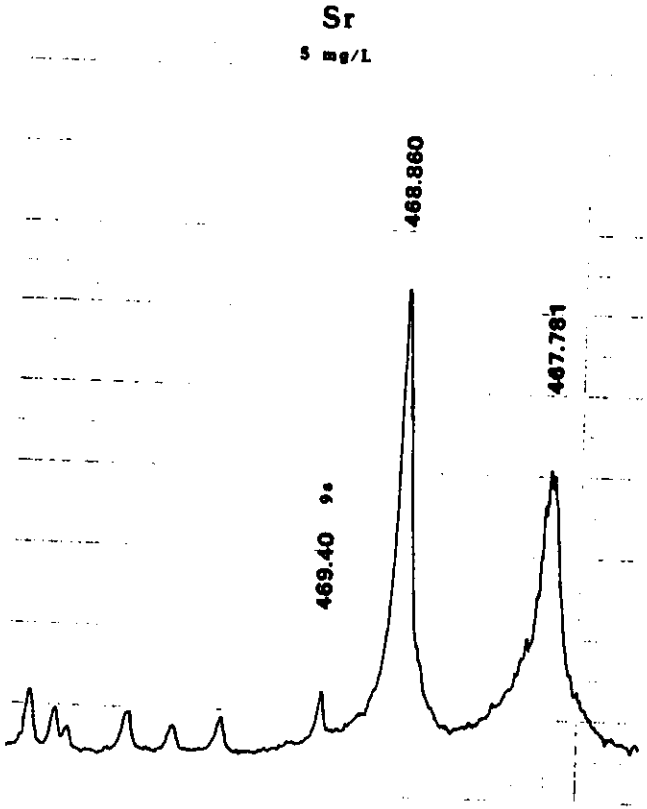
Sr
5 mg/L
468.860
467.781
469.40 9s

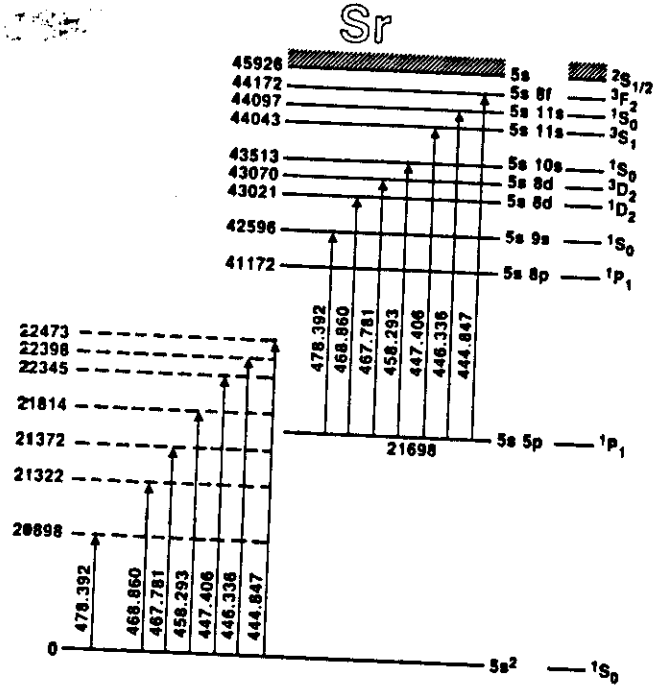
Sr
45926
44172
44097
44043
43513
43070
43021
42596
41172
22473
22398
22345
21814
21372
21322
20898
0
5s
5s 8f
5s 11s
5s 11s
5s 10s
5s 8d
5s 8d
5s 9s
5s 8p
5s 5p
21698
5s²
2S1/2
3F2
1S0
3S1
1S0
3D2
1D2
1S0
1P1
1P1
1S0
478.392
468.860
467.781
458.293
447.406
446.336
444.847

N O T E

"SOME OBSERVATIONS ON THE IONIZATION MECHANISM FOR STRONTIUM IN THE AIR-ACETYLENE FLAME UNDER RESONANT LASER EXCITATION"

G.C. Turk(*), P. Cavalli and N. Omenetto(**)

Joint Research Centre
Chemistry Division
21020 ISPRA (Varese), Italy

(*) on leave from: Centre for Anaytical Chemistry, National Bureau of Standards, Gaithersburg, MD, USA

(**) author to whom correspondence should be addressed.

The ionization spectrum of strontium atoms in an air-acetylene flame under pulsed laser excitation has been recently reported (1, 2). Single-step as well as two-step excitation were provided by an excimer-pumped dye laser tuned in the blue region of the spectrum. The collisionally assisted ionization in the flame was measured with a water-cooled electrode immersed in the flame and negatively biased (- 1300V) while the charges produced were collected at the burner, converted into a voltage signal and processed by a boxcar integrator (3).

We wish to report here a rather striking change in the excitation-ionization behaviour which occurred when the laser beam was focussed in the middle of the flame and a high irradiance was therefore achieved (~100 MW cm^{-1}). Figure 1 shows three lines which are identified as the resonance transition at 460.733 nm, a two-photon transition at 459.514 nm and a near-resonance transition at 458.293 nm. As discussed in details in reference 2, the signal at 460.733 nm is believed to be due to resonance excitation of the $^1P_1$ level, which lies 21698 cm^{-1} above the ground state, followed by collisional ionization. The signal at 459.514 nm is due to a two-photon absorption process from the ground state to the 5s10s Rydberg level (^1S_o), therefore involving a "virtual" state located at half the excitation energy of the 5s10s state. Finally, the signal at 458.293 nm is believed to be due to a two-step excitation process involving the absorption of a photon in the collisionally broadened wings of the $^1P_1$ level, followed by resonant absorption of another photon to the 5s10s Rydberg level. In the left part of figure 1, the laser beam was expanded to approximately 5 mm diameter while in the right part of the figure, it was focussed down to approximately 0.5 mm diameter. The flame length traversed by the laser beam was 1 cm. The two experiments therefore differ in two respects: (i) the irradiance is much higher in the focussed case, and (ii) the number of atoms in the laser volume is much higher (~100x) in the defocussing case.

./...

As seen by a direct comparison of the two spectra shown in Figure 1, the two-photon line and the near-resonance line decreased considerably in intensity, as one would expect from the decreased atom density in the laser volume. However, the resonance line showed practically no decrease in intensity. Moreover, its spectral behaviour changed drastically, the line wings practically disappearing, indicating the possible onset of a non linear effect.

As a further evidence that an unusual power effect was observed, the resonance fluorescence signal, i.e., the fluorescence from the $^1P_1$ level to the ground state, was measured simultaneously with the ionization signal and the laser power was varied by inserting neutral density filters in the beam. In the simultaneous fluorescence/ionization experiment, no focussing lens was used. As seen in figure 2, the fluorescence signal showed clear saturation behaviour, indicating that the maximum population of the $^1P_1$ level was attained. The curve obtained, under the same condition, for the ionization signal, is shown in Figure 3 A. Here one can see that the shape of the ionization curve differs from that of the fluorescence curve, since a full saturation plateau is not reached. Furthermore, when the focussing lens was used, a peculiar sigmoid shape resulted (curve B). It therefore appears that, for the ionization case, more saturation was achieved when comparatively lower laser powers were used.

We would like to offer a tentative explanation of this effect, with the aid of figure 4, which shows the energy levels involved in our case, as taken from standard tabulated values (4). When the laser photon irradiance is low, resonance excitation to the $^1P_1$ level is followed by collisional ionization. However, at high photon irradiance, the absorption of a second photon from the $^1P_1$ level into the wings of a collisionally broadened level, which could be either the 5s10p ($^1P_1$) or the 5s10s ($^1S_0$)

shown in the figure, might take place. Because of the small energy difference between these levels and the ionization level, the efficiency of such process is much higher than that of a simple collisional ionization process from the 5s5p level. As a result, the loss of atoms in the focussed volume is compensated by the increase in the overall efficiency of the ionization process.

This effect is similar in some respects to the process of Resonance Ionization Spectroscopy (RIS) (5), where laser excitation of a discrete atomic level is followed by absorption of a second photon which further excites the atom into the ionization continuum. The RIS experiment thus requires that the discrete atom level being excited has an energy greater than half that of the ionization potential. This is not the case for the example presented here, with the second photon excitation falling just short of the ionization limit into the Rydberg levels. Two examples of possible RIS effects using a single laser in flames and plasmas have been reported in the literature. In one case, Turk and Watters (6) postulated that in the excitation of iron in an inductively coupled argon plasma the energy of the state reached was such that a RIS mechanism could be possible. In another case, Axner etal (7) independently suggested a similar explanation for the very high sensitivity obtained for iron and magnesium in an air-acetylene flame.

Two consideration seem to be in order here. Firstly, the spatial inhomogeneity of the focussed laser beam might affect the shape of curve B in figure 3 in the same way as fluorescence saturation curves are affected (8). Although we feel that this effect alone cannot account for the significant difference between curves A and B in figure 3, it certainly deserves a careful evaluation. Secondly, it seems difficult to correctly describe the overall process occurring in laser enhanced ionization spectroscopy in flames without the simultaneous use of the fluorescence technique and a careful study of the power dependence of both the fluorescence and the ionization signals.

REFERENCES

1. L.P. Hart, B.W. Smith and N. Omenetto, Spectrochim. Acta 40B, 1637 (1985)

2. N. Omenetto, L.P. Hart, B.W. Smith and G.C. Turk, Opt. Comm., submitted

3. J.C. Travis, G.C. Turk, J.R. de Voe, P.K. Schenck and C.A. Van Dijk Progress Anal. At. Spectrosc., 7, 199 (1984)

4. C.E. Moore, "Atomic Energy Levels", Volume II, NSRDS-NBS 35, Washington, D.C. (1971)

5. Y.P. Young, G.S. Hurst, S.D. Kramer and M.G. Payne, Anal. Chem., 51, 1050 A (1979)

6. G.C. Turk and R.L. Watters, Jr., Anal. Chem. 57, 1979 (1985)

7. O. Axner, I. Lindgren, I. Magnusson and H. Rubinsztein-Dunlop, Anal. Chem. 57, 773 (1985)

8. C. Th. J. Alkemade, Spectrochim. Acta, 40B, 1331 (1985)

ACKNOWLEDGEMENTS

G.C. Turk would like to thank the Joint Research Centre authorities and in particular the Education Training Service of Ispra for the grant of a visiting scientist fellowship.

FIGURE CAPTIONS

Figure 1 : Ionization spectrum obtained by nebulizing in the flame a solution containing 10 ug/ml of strontium and scanning the dye laser from 457 nm to 461 nm. See text for discussion.

Figure 2 : Saturation curve obtained by measuring the resonance fluorescence signal at 460.733 nm. In this experiment the laser beam was defocussed in the flame and the strontium concentration was 100 ug/ml.

Figure 3 : Power dependence of the ionization signal obtained with the laser tuned at 460.733 nm. Strontium concentration: 10 ug/ml.

(A) : Laser beam defocussed as in the resonance fluorescence case (see figure 2)

(B) : Laser beam focussed in the middle of the flame with a lens.

Figure 4 : Energy level scheme for strontium pertinent to the experiment described in the text. The levels and the corresponding energies were taken from Reference 4.

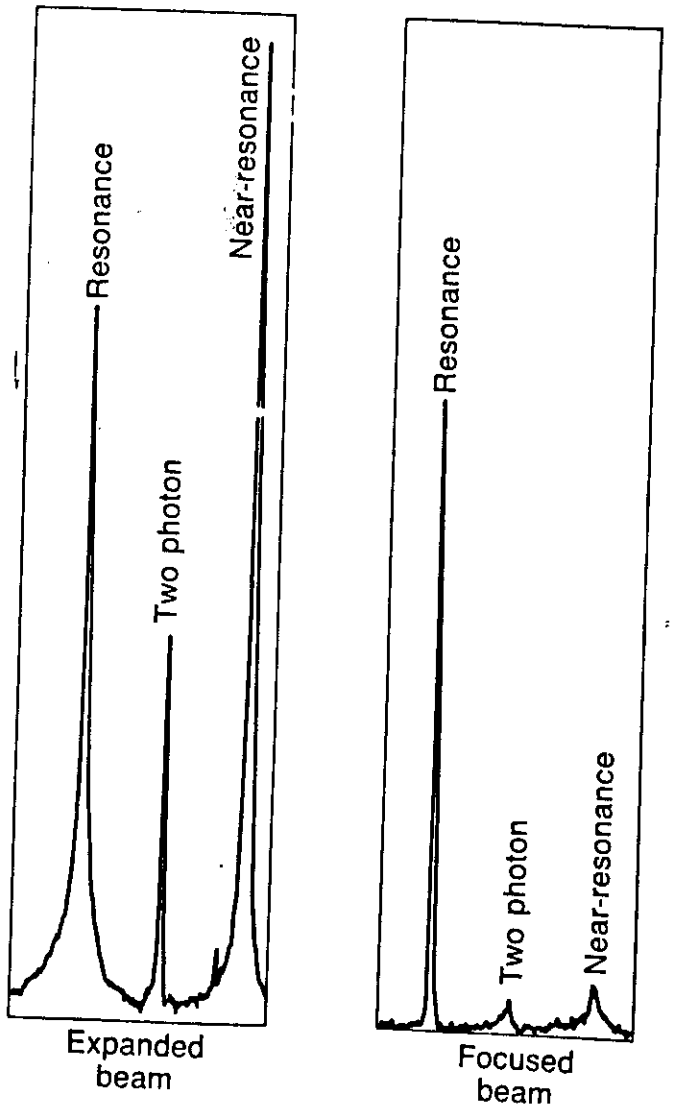
Resonance
Two photon
Near-resonance
Expanded beam
Resonance
Two photon
Near-resonance
Focused beam

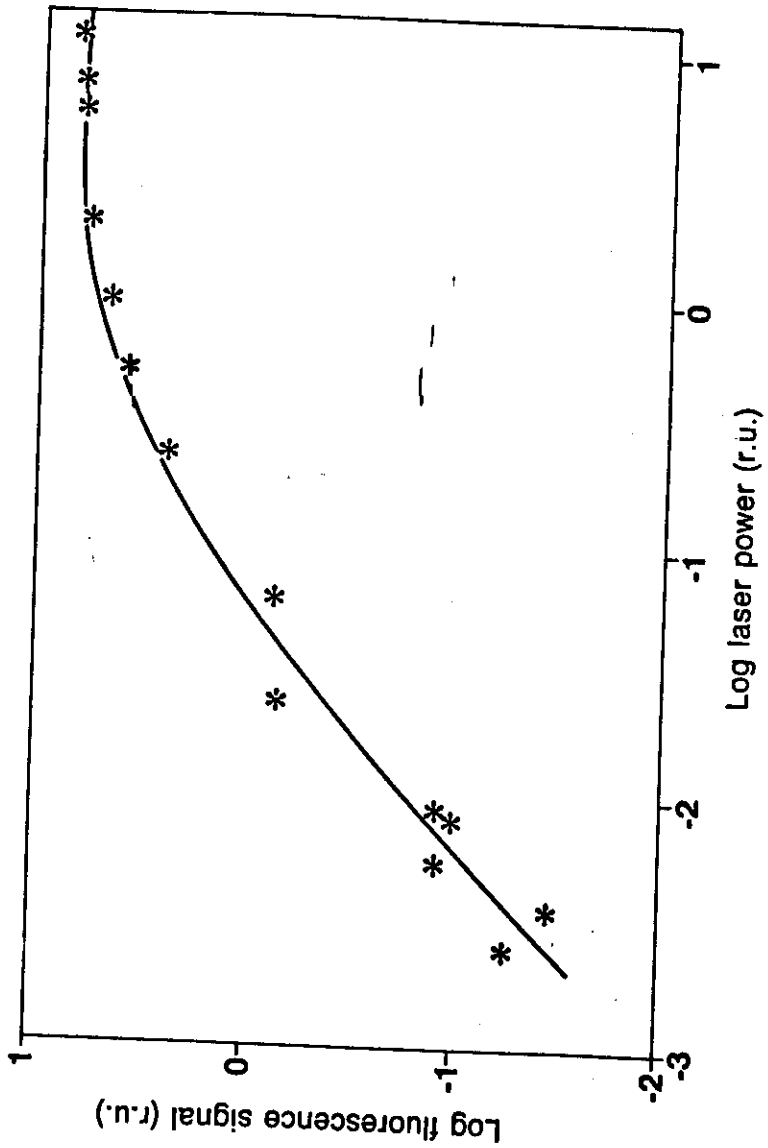
Log fluorescence signal (r.u.)
1
0
-1
-2
-3
Log laser power (r.u.)
1
0
-1
-2

Fig. 3

VI.92

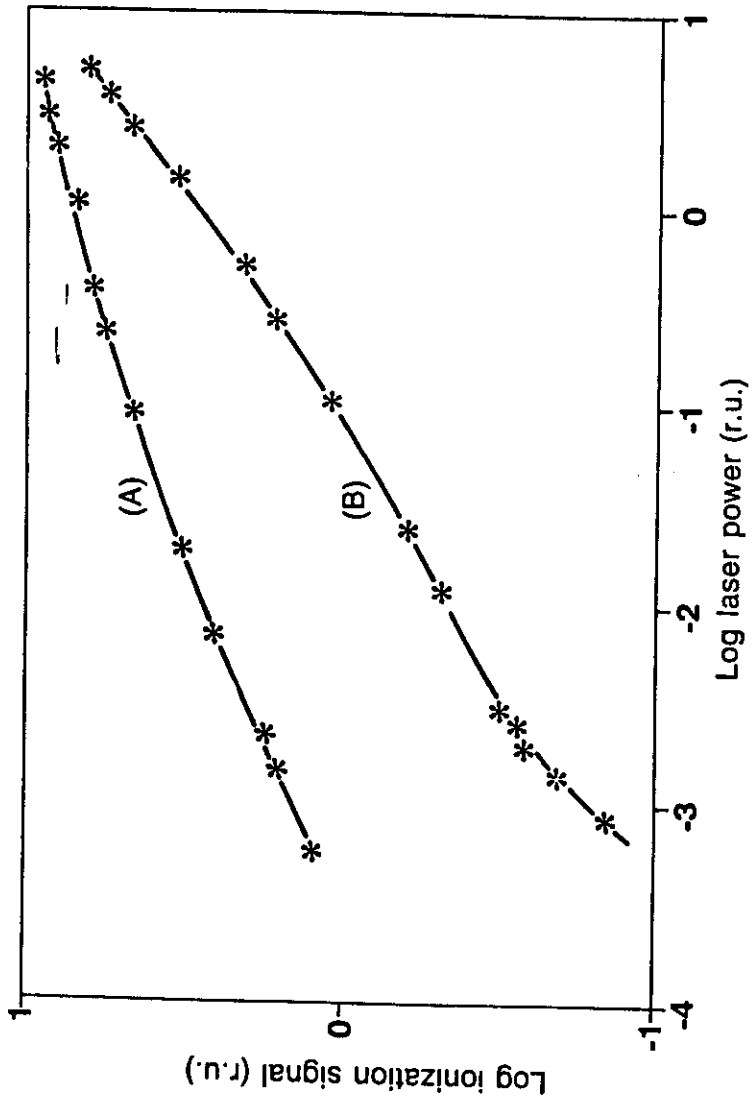

Fig. 4

VI.93